Monitoring Fluidized Bed Dryer Hydrodynamics Using Pressure Fluctuations and Electrical Capacitance Tomography

Gareth Chaplin

BScE.(ChE.), University of New Brunswick, (2001)

A thesis submitted to the

College of Graduate Studies and Research

as partial fulfillment of the requirements for the

Doctor of Philosophy (Ph.D.)

in the academic unit of Chemical Engineering

University of Saskatchewan

Permission to Use

In presenting this thesis in partial fulfillment of the requirements for a doctorate of philosophy from the University of Saskatchewan, I agree that the Libraries of this University may make it freely available for inspection. I further agree that permission for copying of this thesis in any manner, in whole or in part, for scholarly purposes may be granted by Dr. Todd Pugsley who supervised my thesis work or, in his absence, by the Head of the Chemical Engineering Department or the Dean of the College of Engineering. It is understood that any copying, publication, or use of this thesis or parts thereof for financial gain shall not be allowed without my written permission. It is also understood that due recognition shall be given to me and to the University of Saskatchewan in any scholarly use which may be made of any material in my thesis.

Requests for permission to copy or to make other use of material in this thesis in whole or part should be addressed to:

Head of the Department of Chemical Engineering
University of Saskatchewan
Saskatoon, Saskatchewan
Canada
S7N 5C5

Abstract

As part of the production of certain solid-dosage pharmaceuticals, granulated ingredients are dried in a batch fluidized bed dryer. Currently, the determination of the completion of the drying process is accomplished through measurements of product or outlet air temperatures. No quantitative measurement of hydrodynamic behaviour is employed. Changes in bed hydrodynamics caused by variations in fluidization velocity may lead to increased particle attrition. In addition, excessive desiccation of the granules caused by inaccurate determination of the drying endpoint may lead to an increase in the thermal and mechanical stresses within the granules. The activity of future high-potency or peptide based drug products may be influenced by these effects. Therefore, the quantification of hydrodynamic changes may be a key factor in the tighter control of both fluidization velocity and product moisture, which are critical for maintaining product quality.

High-frequency measurements of pressure fluctuations in a batch fluidized bed dryer containing pharmaceutical granulate have been used to provide a global, non-intrusive indication of the hydrodynamic changes occurring throughout the drying process. A chaotic attractor comparison statistical test known as the S-statistic, has been applied to quantify these changes in drying and a related unit operation, fluidized bed granulation. The S-statistic showed a sensitivity to moisture which is not seen with frequency and amplitude analysis. In addition, the S-statistic has been shown to be useful in identifying an undesirable bed state associated with the onset of entrainment in a bed instrumented for the collection of both pressure fluctuation and entrainment data.

Thus, the use of the S-statistic analysis of pressure fluctuations may be utilized as a low-cost method for determining product moisture or changes hydrodynamic state during fluidized bed drying.

Electrical capacitance tomography (ECT) has also been applied in this study to image the flow structure within a batch fluidized bed used for the drying of pharmaceutical granulate. This represents the first time that ECT has been applied to a bed of wet granulate material. This was accomplished through the use of a novel dynamic correction technique which accounts for the significant reduction in electrical permittivity occurring as moisture is lost during the drying process. The correction has been independently verified using x-ray tomography.

Investigation of the ECT images taken in the drying bed indicates centralized bubbling behaviour for approximately the first 5 minutes of drying. This behaviour is a result of the high liquid loading of the particles at high moisture. Between moisture contents of 18-wt% and 10-wt%, the tomograms show an annular pattern of bubbling behaviour with a gradual decrease in the cross-sectional area involved in bubbling behaviour. The dynamic analysis of this voidage data with the S-statistic showed that a statistically significant change occurs during this period near the walls of the vessel, while the centre exhibits less variation in dynamic behaviour. The changes identified by the S-statistic analysis of voidage fluctuations near the wall were similar to those seen in the pressure fluctuation measurements. This indicates that the source of the changes identified by both these measurement techniques is a result of the reduction in the fraction of the bed cross-section involved in bubbling behaviour. At bed moisture contents below 5-wt%, rapid divergence was seen in the S-statistic applied to both ECT

and pressure fluctuation measurements. This indicates that a rapid change in dynamics occurs near the end of the drying process. This is possibly caused by the entrainment of fines at this time, or the build-up of electrostatic charge.

The use of the complimentary pressure fluctuation and ECT measurement techniques have identified changes occurring as a result of the reduction of moisture during the drying process. Both the localized changes in the voidage fluctuations provided by the ECT imaging and the global changes shown by the pressure fluctuation measurements indicate significant changes in the dynamic behaviour caused by the reduction of moisture during the drying process. These measurement techniques could be utilized to provide an on-line indication of changes in hydrodynamic regime. This information may be invaluable for the future optimization of the batch drying process and accurate determination of the drying endpoint.

Acknowledgements

I would like to thank my supervisor Dr. Todd Pugsley. Dr. Pugsley has provided me with the freedom to pursue my own ideas and direction as a researcher. At the same time, he has provided invaluable guidance in the effective implementation of research techniques throughout this project. I am also thankful for the opportunity he gave me to participate in the Fluidization XI conference in Naples (2004).

I would like to thank Merck Frosst Canada and Co. for their financial contribution to this project as well as for granting access to the facilities at their laboratories in Montreal. I particularly would like to thank Dr. Conrad Winters for his invaluable input and support. As well, I would like to thank Helen Tanfara of Merck Frosst Laboratories for her assistance throughout this project.

The access to the x-ray tomography facilities at the Tomographic Imaging and Porous Media Laboratory (TIPM) at the University of Calgary given by the director (Dr. Apostolos Kantzas) and his staff provided critical information in this study. In particular, the assistance of Loni van der Lee of TIPM in performing the x-ray tomography experiments and the interpretation of the x-ray data is gratefully acknowledged.

The knowledge and experience of both Tivadar Wallentiny and Dragan Čekić is much appreciated for the construction of both the experimental apparatus and the electronic data acquisition system utilized at the University of Saskatchewan.

Finally, I would like to thank my family for their support. I especially would like to thank my parents who remain my greatest inspiration as educators.

Table of Contents

List of Tables

List of Figures

Chapter 1 - Introduction

1.1 Project Motivation

The production of certain solid-dosage pharmaceuticals requires the combination of a number of dry powder chemical ingredients, including fillers, binders, and disintegrants with the drug product in a granulation process. The granulation process not only achieves the mixing of these components but also increases the particle size distribution of the powder. This enhances the flowability of the powder in processing equipment such as tableting machines. One method for producing pharmaceutical granules is wet granulation. In this process, dry ingredients are mixed while they are contacted with liquid causing the growth of granules. Mixing of the dry ingredients can be accomplished through the action of an impeller in a high or low-shear granulator or a fluidized bed granulator. Before tableting, granules must be dried. Drying of the wet pharmaceutical granulate can be accomplished in a batch fluidized bed dryer. Ideally, there should be minimal batch-to-batch variation in the particle size distribution and physical properties of the granules.

A number of factors affect product quality in the fluidized bed drying of pharmaceutical granule including granule attrition and the entrainment of fines. Attrition may be related to the selection of an appropriate fluidization regime since increased superficial gas velocity leads to an increase in the number and intensity of interparticle

and wall collisions. Elevated superficial gas velocity also leads to an increase in the entrainment of fine particles from the bed surface. Entrained particles are returned to the bed through the shaking of bag filters installed at the air outlet from the unit. Since a certain percentage of the particles are trapped on the surface of these bags, entrainment is an undesirable effect because it represents a potential loss of drug product. The existence of temperature and moisture gradients within the bed also influences drug activity. Again, the operation of the bed in an optimum hydrodynamic regime is essential in order to maintain the excellent mixing characteristics of a fluidized bed. Therefore, a quantitative monitoring method for the determination of hydrodynamic changes in the fluidized bed drying process is essential for the optimization of this process.

1.2 The Drying Process

When any moist solid material is exposed to an air stream at a constant temperature and humidity, moisture is transferred to the drying air. This transfer occurs as long as the material's moisture content is in excess of its equilibrium moisture at the temperature and humidity of the drying air stream. Loss of moisture from the material is relative to the driving force for mass transfer. This driving force is proportional to both the temperature and humidity of the drying air stream and the internal resistance to mass transfer provided by the material. A schematic representation of the typical drying curve is given in Figure 1.1. In this plot, we see two distinct regions denoted as the constant rate period and the falling rate period. In the constant rate period, a continuous film of water exists at the surface of the particle. As long as this moisture is supplied to the surface at the same rate it is removed from the surface through evaporation, the material

dries at a constant rate. Once the drying process reduces the moisture content of the material to the critical moisture, surface moisture is no longer present and diffusion or capillary resistances within the material become significant. This causes the rate of moisture loss to be reduced and the total moisture decreases asymptotically towards the equilibrium moisture. In a batch fluidized bed dryer operated under a constant inlet air flow rate, the average moisture content of the particulates will follow a similar profile to that given in Figure 1.1.

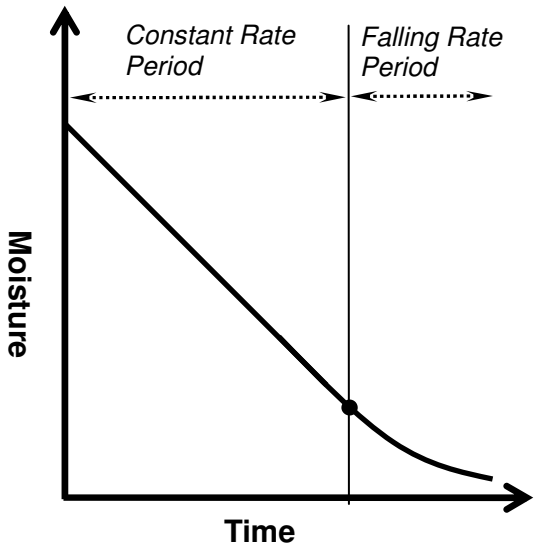

Figure 1.1 Typical drying curve for a porous material (Kunii and Levenspiel [1])

In the fluidized bed drying process, the loss of humidity is controlled by the rate of evaporation from the particles. During the constant rate period, the inlet air increases in humidity as it passes through the bed and exits the dryer as a saturated liquid. Since the dryer can be thought of as essentially adiabatic, this increase in humidity corresponds to a decrease in temperature of the air stream. The typical behaviour of the outlet temperature is given in Figure 1.2. Bed temperature follows a similar profile. It

may be noted that, at the critical moisture content, the temperature of the outlet air begins to increase above a constant temperature. This constant temperature ideally corresponds to the adiabatic saturation conditions of the incoming air stream. At moisture below the critical moisture, surface moisture is no longer present and the inlet air stream can no longer attain a saturated condition as it passes through the bed. Consequently, the heat taken up in the evaporation of the surface moisture is now transferred to the particles, causing their temperature to increase.

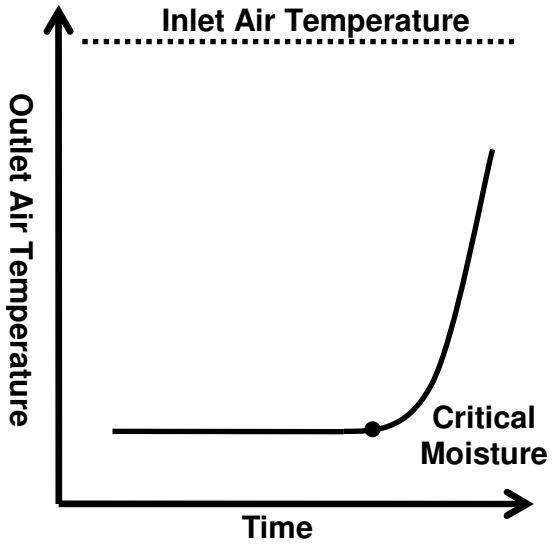

Figure 1.2 Typical behaviour of the outlet air temperature in a batch fluidized bed drying process (Kunii and Levenspiel [1]).

At fixed inlet conditions, outlet or bed temperature can be used as a control parameter to detect the endpoint of drying. Since bed temperature may be related to average bed moisture content, the attainment of a specific bed or outlet temperature can be used as the indication that drying is complete. This method of control is currently employed in the pharmaceutical industry and results in drug products of an acceptable quality. However, it provides no indication of changes in hydrodynamic regime. These

changes not only include transitions in hydrodynamic regime but also more subtle changes such those associated with variation in particle size distribution (PSD) or the distribution of the fluidizing gas. Effects detrimental to product quality associated with changes in fluidized regime may be a critical factor in the processing of future protein- or peptide-based and high-potency pharmaceuticals. Thermal stresses on the active ingredient and attrition of the granules are both effects encountered in the drying of material in a fluidized bed. Both of these effects lead to a reduction in product yield and are a concern for the production of future drug products. A monitoring technique which quantifies the hydrodynamic changes occurring in the fluidized bed is required in order to identify and minimize these effects.

1.2.1 Characterization of Fluidization Behaviour

When a group of particles is described as being fluidized, it is said that they are suspended through the drag caused by the upward flow of a fluid. As the upward flow of fluid in a packed bed of solids is increased, the pressure drop increases proportionally. At a certain velocity, the force of drag on the particles is sufficient to counteract the force of gravity. Beyond this velocity, the resistance to the flow is a maximum and bed pressure drop becomes constant with increasing flow. This velocity is denoted as the minimum fluidization velocity and is a fundamental parameter used to characterize fluidization behaviour.

Once fluidized, the hydrodynamic behaviour of a system is based on a number of factors. Two of the most important are the particle physical properties and the superficial velocity. The particle physical characteristics are a function of the granule preparation as

well as the moisture content. Bed behaviour is also a function of the residence time of the granules in the dryer. These factors all influence the hydrodynamic behaviour of the system. While particle properties depend on the initial condition of the bed and the bed moisture content, superficial gas velocity may be manipulated throughout the drying process. This control parameter can be selected in order to maintain the optimum flow patterns within the dryer, helping to alleviate the effects detrimental to product quality described above as well as minimizing drying time.

1.2.2 Classification of powders

The classification of particles based on their flow behaviour has been described by Geldart [2]. In this classification, particles are divided into four groups based on particle density and diameter. This is presented graphically in Figure 1.3.

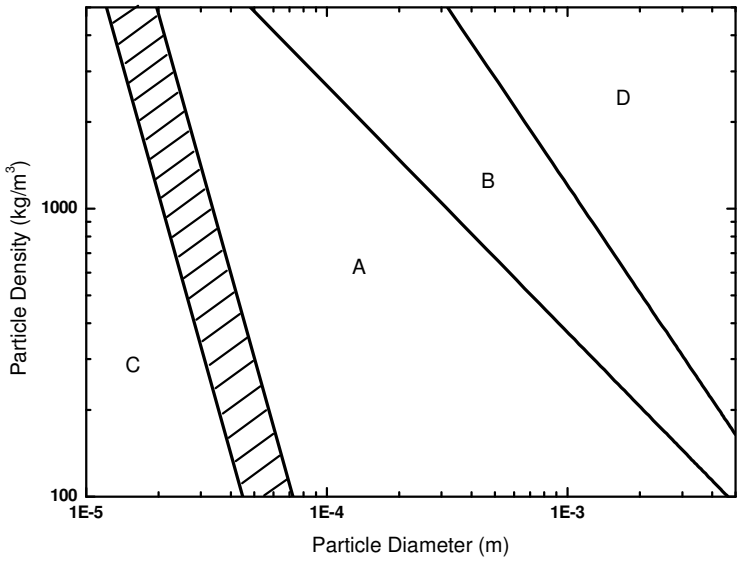

Figure 1.3 The Geldart chart for the classification of powders (Kunii and Levenspiel [1]).

To the extreme left of this diagram are the group C powders. These powders are difficult to fluidize because the cohesive forces between particles are large in comparison to the force exerted by the fluidizing air. This leads to significant channelling effects. The boundary between the group C and group A powders is shaded because of the variations in interparticle forces caused by differences in particle physical properties. Group A powders are described as aeratable. As superficial gas velocity is increased beyond the minimum fluidization velocity, a bed of Geldart A powders expands without the presence of bubbles as a smoothly fluidized bed. Bubbling only commences once a superficial gas velocity larger than the minimum fluidizing velocity, denoted as the minimum bubbling velocity, is reached. In contrast, the larger group B or sandlike particles exhibit minimal bed expansion and bubbling commences as soon as superficial velocities in excess of minimum fluidization are achieved. The final group is the large diameter, high density group D particles. These particles are generally fluidized in a spouting fluidized bed.

Geldart's classification was developed for powders having a monodisperse particle size distribution. In a polydisperse powder, variations in the particle size distribution may influence the fluidization behaviour of the bed. The behaviour of the dry pharmaceutical powders utilized in the current study was examined by Tanfara et al. [3]. In that study, it was stated that this pharmaceutical granulate belongs to the group B classification of powders, based on mean particle size of 220 μm and a density of 1100 kg/m3. However, the influence of coarse particles on the fluidization behaviour was found to be significant. Clearly, the use of Geldart's classification alone is not sufficient to describe the fluidization behaviour of this polydisperse powder.

In a drying bed, a further complication to Geldart's classification is introduced. Variation in interparticle forces will have a significant influence on bed hydrodynamic behaviour throughout the drying process. As drying progresses, the strength of the liquid bridging forces will weaken as the liquid loading is decreased. Furthermore, toward the end of drying, the effect of electrostatic forces may begin to influence the dynamic behaviour. McLaughlin and Rhodes [4] have examined the effect that the introduction of non-volatile oil into a fluidized system has on bed hydrodynamic behaviour. They showed that the bed Geldart behaviour can be manipulated by the addition of liquid. A group B Geldart powder was shown to exhibit group A and then C behaviour with increasing liquid loading. In the drying process, the decreasing liquid loading caused by the reduction of moisture will induce an opposite change in the hydrodynamic behaviour of the bed.

1.2.3 Fluidization Regimes

As mentioned above, the transition from a packed bed of particles to a fluidized system occurs at the minimum fluidization velocity. Above this velocity, a gas-solid fluidized bed exhibits a number of distinct hydrodynamic regimes with increasing superficial velocity. In Lim et al. [5] six distinct regimes are identified for gas-solids fluidization. These regimes are depicted in Figure 1.4 based on increasing superficial gas velocity.

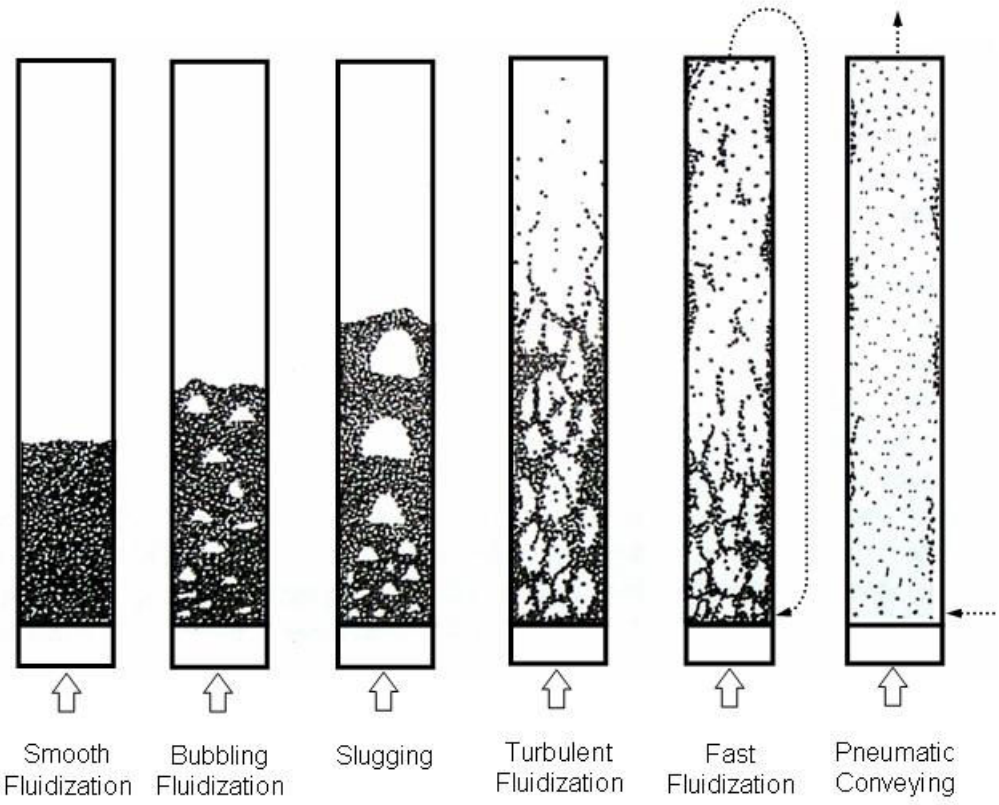

Figure 1.4 The regimes of fluidization (after Lim et al. [5])

At a superficial velocity in sight excess of the minimum fluidization velocity, the bed is smoothly fluidized and expands with increasing superficial gas velocity. This expanded bed of particles is sometimes referred to as the emulsion phase. As noted

above, a smoothly fluidized bed occurs in a bed of group A particles where group B particles transition directly to the bubbling regime from the packed state. With increasing velocity, the excess fluid begins to bypass the emulsion phase as a series of bubbles. This regime is denoted as bubbling fluidization. As superficial velocity is increased further, more gas bypasses the emulsion phase resulting in the formation of larger bubbles or more frequent bubbling depending on the particle properties. In the slugging regime, the bubbles have grown in diameter with increasing velocity until they have a diameter similar to the internal diameter of the column. Slugging behaviour is typically observed in beds having a large height to diameter ratio. Some systems do not exhibit slugging behaviour and will transition directly from bubbling to the turbulent regime. In the turbulent regime, the bubbles become distorted and eventually disappear due to the large shearing force encountered by the incoming air as it enters the bed. This causes a breakdown of the distinct two-phase characteristic of the bed and the surface of the bed becomes less well defined. Significant entrainment may be possible and the use of cyclone collectors may be required in order to return the fines to the bed surface. As superficial velocity is further increased, entrainment increases to the point where external recirculation of the particles is required in order to repopulate the bed. These regimes are denoted as the fast fluidization and pneumatic transport regimes. The distinction between these regimes is the fact that there is a certain amount of solid recirculation within the fluidizing vessel in the fast fluidization regime. In pneumatic transport, the superficial velocity is sufficient to fully suspend all particles in the gas stream and transport them upwards.

In industry, the selection of the appropriate regime is dependent on the application. When a fluidized bed is selected for gas/solid contacting, it is desirable to maximize the mass transfer between these phases. In drying, an increase in mass transfer translates into reduced drying times. The intimate contacting of the gas with the solids provided in the turbulent regime is attractive for this purpose since bypassing of the gas present in the bubbling regime is eliminated. However, the vigorous mixing provided in this regime also leads to a potential increase in entrainment and attrition of the particles. It is desirable to reduce both of these effects. Therefore, the determination of an optimum fluidization regime, controlled by the selection of an appropriate superficial gas velocity, is critical for the efficient implementation of fluid-bed technology.

1.3 Optimization of the drying process

1.3.1 Application of fluid-beds to the drying of pharmaceuticals

Because of the batch production strategy employed in the production of pharmaceutical products, a batch fluidized bed dryer is utilized. A generalized schematic of the industrial batch fluidized bed drying process examined in this study is given in Figure 1.5.

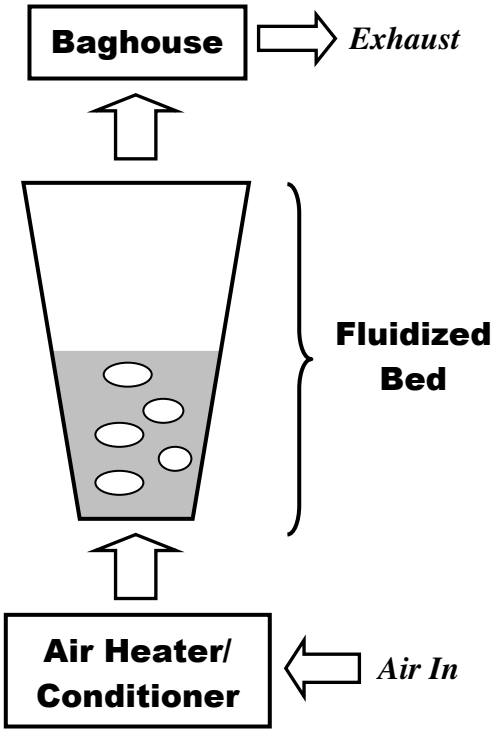

Figure 1.5 Batch fluidized bed dryer implemented for the industrial drying of pharmaceuticals

This unit is charged with wet granule from the batch high-shear granulation process immediately preceding this processing step. Atmospheric air is filtered, and heated to a predetermined temperature by a heating and conditioning unit. This unit also controls the humidity of the fluidizing air. The conditioned air introduced at the base of the conical product bowl traverses an air distributor located at the base of the unit. This

distributor ensures an even distribution of air across the product bowl cross-section. The exiting air is cleaned in a baghouse which is periodically shaken in order to return entrained fine particles to the bed.

A unique characteristic of the dryer is its conical geometry. This shape enhances mixing in a bed having high moisture content by promoting a circulation of solids in the unit. This is caused by the transport of particles by the fluidizing gas in the central region and a return of solids to the bottom of the unit near the walls. This behaviour has been described as centralized spouting by Tanfara el al. [3] and is a characteristic of the bed geometry. The regime behaviour of this geometry is not well examined in the literature. In the current work, the changes in the fluidization state resulting from the change in moisture associated with drying will be examined. The quantification of changes associated with this dynamic process is critical in developing a strategy for improved control of this process. By controlling the hydrodynamic behaviour throughout the drying process, undesirable effects such as entrainment and attrition can be reduced.

1.3.2 Measurement of Hydrodynamic Behaviour

Changes in hydrodynamic behaviour can be identified by means of pressure measurements across the bed. As described above, the absolute pressure drop can be utilized to determine if the bed is fluidized. However, the information provided by this monitoring technique may not allow for sufficient warning that changes are taking place in fluidized state. In the work of van Ommen et al. [7] absolute pressure drop proved inadequate as an early warning for defluidization occurring because of agglomeration in a fluidized bed combustor. In van Ommen et al. [6], a signal analysis technique called

the S-statistic, was applied to pressure fluctuations. The technique responded to subtle changes in the hydrodynamic state recorded in the pressure fluctuation signal resulting from the initiation of agglomeration. This early warning of agglomeration allowed for the implementation of corrective action to be taken before the onset of defluidization. The S-statistic technique has been suggested as a means of quantifying the significant changes in hydrodynamic state associated with the drying process by van Ommen [7]. The application of this signal analysis technique to the batch drying of pharmaceutical granule is the objective of the initial phase of the present investigation.

Other signal analysis techniques have been applied to pressure fluctuations in a fluidized bed. For example, the amplitude of pressure fluctuations has been utilized to determine regime transitions. An example of this is the transition to turbulence [8]. The standard deviation of the pressure fluctuations reaches a maximum intensity when plotted as a function of increasing superficial velocity, indicating the breakdown of the bubbles in the bubbling or slugging regimes into a continuous phase consistent with the onset of the turbulent regime. However, the identification of this regime transition is a source of controversy in the literature. This is partly due to variations in systems investigated and the use of differing measurement techniques. Furthermore, visual observations of the bed behaviour are often used to confirm regime changes. An extensive review of the literature discussing this controversy has been done by Bi et al. [8]. Tomographic imaging of the fluidized bed could provide a more definitive secondary technique to determine regime transitions. Tomography represents a direct measurement of the local bed behaviour and, as such may be utilized to determine the source of the dynamic changes seen in the pressure fluctuations. In the application of

this measurement technique to the drying process, this type of measurement could be utilized to optimize the gas-solids contacting patterns within the bed and enhance the drying process.

Electrical capacitance tomography (ECT) has been utilized Makkawi et al. [9] to identify regime transitions in a fluidized bed. Tanfara et al. [3] have demonstrated that ECT can be used to image a dry bed of pharmaceutical granulate. The difficulty in the application of ECT to a fluidized bed dryer is the large changes in electrical permittivity occurring as a result of the loss of moisture. This leads to a changing calibration for the device during the drying. If a correct calibration procedure could be implemented and independently verified, a dynamic analysis technique such as the S-statistic could be applied to local voidage fluctuations. This quantification of hydrodynamic behaviour could be used to control the bed condition and optimize the drying process.

1.4 Scope of this study

This dissertation is structured as a series of publications. These publications sequentially present the progress of the research from the initial investigation of the application of the S-statistic to pressure fluctuations to the dynamic analysis of the drying process using ECT. The text of these publications has been preserved in the format they have been published or been submitted for publication. Additional details outlining the author contribution, experimental apparatus and experimental procedures are included in an introductory section for each chapter. Furthermore, supplementary material to explain how the publication fits in with the research as a whole is also included.

Two bodies of work form this dissertation. The first portion deals with the application of pressure fluctuations in the monitoring of changes in fluidized behaviour throughout the drying process. The S-statistic attractor comparison technique has been applied to these measurements. Since pressure signals propagate throughout the bed, the purpose of this analysis is to quantify changes in the global bed behaviour throughout the drying process. In the second portion of the work, ECT is applied to the imaging of a drying bed of pharmaceutical granule. Here, the S-statistic has been applied to voidage fluctuations at discrete radial locations in the imaging cross-section. This allows for the determination of changes in local dynamic behaviour. From this analysis, the source of the changes identified in the pressure fluctuation measurements can be determined. This will lead to an increased knowledge about the drying behaviour of this system.

Chapters 2 and 3 present the application of the S-statistic to pressure fluctuations in a laboratory-scale industrial fluidized bed dryer at Merck Frosst research labs in Montreal. Merck Frosst Canada and Co. was a co-sponsor of this project. The motivation for performing the initial phase of the work in Montreal was to gain insight into how this process is utilized in the pharmaceutical industry. Chapter 2 demonstrates the changes in hydrodynamic state associated with the drying process as identified using the S-statistic. Chapter 3 gives further detail regarding the effects of the factorial variables of bed mass, inlet and outlet air temperature. By demonstrating that the changes in hydrodynamic state associated with drying can be discerned utilizing the S-statistic, the use of this technique as a process monitoring tool is demonstrated.

Chapter 4 is an investigation of the effect entrainment has on the state of a fluidized bed determined through use of the S-statistic. These experiments were

performed in a laboratory-scale unit at the University of Saskatchewan. The design of this apparatus was aided by the experience gained in Montreal. This apparatus has been fully instrumented for bed temperature, outlet air temperature, pressure fluctuations and fines entrainment. This investigation extends the work in chapters 2 and 3. In this chapter, the S-statistic is applied to pressure fluctuations in order to identify the undesirable fluidized state associated with fines entrainment. The successful identification of undesirable fluidization states will allow for reduction of hydrodynamic effects which lead to product degradation.

The change in state associated with moisture is also identified in Chapter 5 where the S-statistic analysis of pressure fluctuations collected in a laboratory-scale fluidized bed granulator at Merck Frosst labs in Montreal. This technical note gives a preliminary investigation of the use of the S-statistic in identifying significant changes in hydrodynamic state accompanying the addition and removal of moisture to the bed in the fluidized bed granulation process.

Chapter 6 shows the application of a correction procedure for ECT data in the laboratory-scale unit at the University of Saskatchewan which accounts for changes in moisture. Independent verification of the correction technique is given using x-ray tomography. This correction is used in chapter 7 to image the bed during the drying process. In addition, the S-statistic is applied to determine changes in localized behaviour throughout the drying process. Here, we wish to determine the location of the changes identified in the pressure fluctuations.

1.5 References

1. Kunii, D., Levenspiel, O., *Fluidization Engineering (2nd Edition)*, Butterworth-Heinemann, Toronto, 1991
2. Geldart, D. Types of gas fluidization, Powder Technology, 7, 285-292, (1973).
3. Tanfara, H, Pugsley T., Winters C., Effect of particle size distribution on local voidage fluctuations in a bench-scale conical fluidized bed dryer., Drying Technology, 20 (6), 1273-1289, (2002).
4. McLaughlin, L.J., Rhodes, M. J., Prediction of fluidized behaviour in the presence of liquid bridges, Powder Tech., 114(1-3), 213-223, (2001).
5. Lim, K.S., Zhu, J.X., Grace J.R., Hydrodynamics of gas-solid fluidization, International Journal of Multiphase Flow, 21(Suppl.), 141-193, (1995).
6. van Ommen, J.R., Coppens, M.C., van Den Bleek, C.M., Early Warning of Agglomeration in Fluidized Beds by Attractor Comparison, AIChE Journal, 46(11), 2183-2197, 2000
7. van Ommen, J.R., Monitoring fluidized bed hydrodynamics, PhD. Thesis, Delft University of Technology, (2001).
8. Bi, H. T., Ellis, N., Abba, I.A., Grace, J.R., A state-of-the-art review of gas-solid turbulent fluidization, Chemical Engineering Science, 55, 4789-4825, (2000).
9. Makkawi, Y. T., Wright, P.C., Fluidization regimes in a conventional fluidized bed characterized by means of electrical capacitance tomography, Chemical Engineering Science, 57, 2411-2437, (2002).

Chapter 2 - Application of Chaos Analysis to Fluidized Bed Drying of Pharmaceutical Granulate

The contents of the following chapter were presented at the Fluidization XI conference at Ischia (Naples), May 9-13, 2004 and a similar version has been published as part of the peer-reviewed proceedings.

Citation

Chaplin, G., Pugsley, T., Winters, C., *Application of chaos analysis to fluidized bed drying of pharmaceutical granule*, in ***Fluidization XI: Present and Future for Fluidization Engineering***, U. Arena, R.Chirone, M. Miccio and P. Salatino, eds., Engineering Foundation, New York, 419-426, (2004).

Contribution of PhD Candidate

Experiments were planned and performed by Gareth Chaplin. Todd Pugsley and Conrad Winters (Director, Formulation Development (PR&D) Merck & Co.) provided consultation regarding the experimental program. The software for all data collection and analysis was developed by G. Chaplin. All writing was done by G. Chaplin with T. Pugsley and C. Winters providing editorial guidance regarding the style content of the paper.

Contribution of this Paper to the Overall Study

The first step in implementing the S-statistic as a monitoring tool for pressure fluctuations collected in the drying of pharmaceuticals requires the determination of its sensitivity to the hydrodynamic changes resulting from the loss of moisture during the drying process. Furthermore, the applicability of amplitude and frequency analysis techniques must be considered in order to demonstrate the advantage of the S-statistic over these basic tests. The influence of variations in superficial gas velocity must also be quantified, as there is likely to be variation of this parameter in an industrial setting. These preliminary questions are addressed in this chapter. It should be noted that an 8-page limit was placed on this paper in accordance with the guidelines set for publication of the conference proceedings.

Additional Experimental Details

The production of granulate for the drying experiments in chapter 2 was performed in Fielder 25 L high shear granulator. This apparatus is diagrammed in Figure 2.01. This granulator is constructed as a cylindrical vessel having a 0.408 m diameter impeller at the bottom. This impeller spins at 261 revolutions per minute and serves to agitate and shear the particles during the granulation process. A second smaller impeller called the chopper is mounted on the walls of the vessel. This impeller serves to further agitate the bed during granulation and ensure homogeneous mixing of the granules. This impeller has a diameter of 0.081 m and spins at 1800 revolutions per minute. For each

granulation, dry ingredients were introduced into the unit and the lid closed.

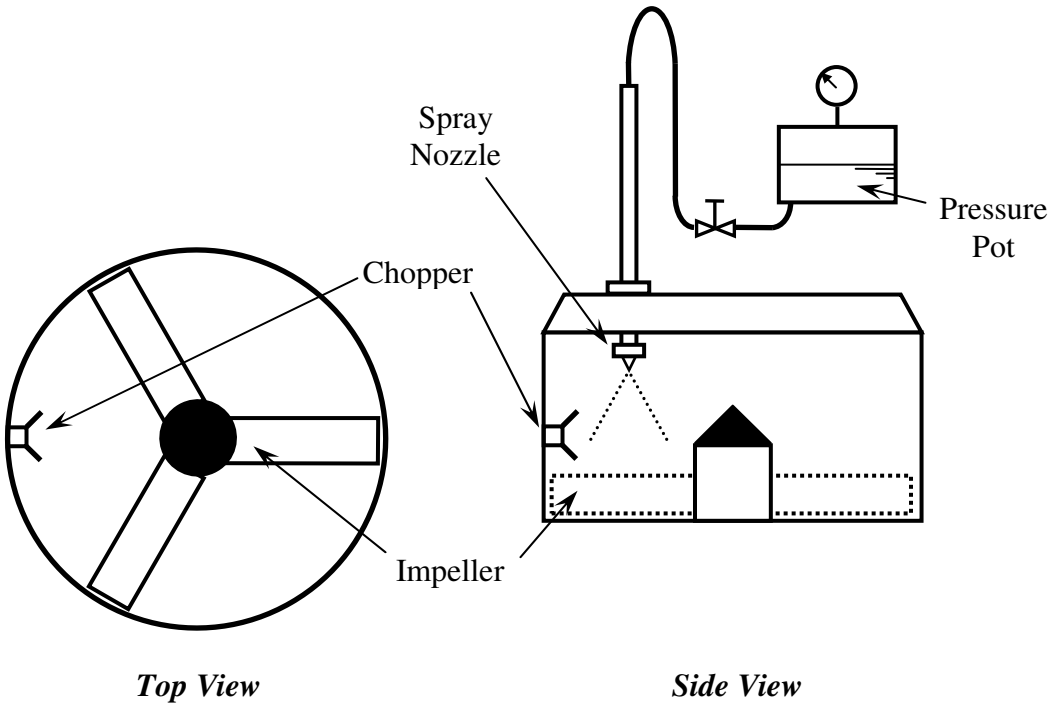

Figure 2.01 Schematic of the Fielder PM25 high-shear granulator used for the production of pharmaceutical granule in this study (not to scale).

The dry ingredients were then mixed for 2 minutes prior to granulation. After mixing of the dry ingredients, the valve at the outlet of the pressure pot, which is maintained at a pressure of 30 psi (207 kPa gauge), was opened to allow a pre-measured volume of water to drain. The addition of this water to the dry ingredients initiates the granulation process. The spay nozzle selected provided sufficient flow to complete the addition of the water over 5 minutes. Following granulation, 2 minutes of mixing was performed to insure homogeneous mixing of the granules. Each granulation produced a batch size of 5 kg. Granulations were performed in 2 batches in order to perform 2 or 3

experiments. Experiments were completed on the same day as granulation in order to conform to the practice of the pharmaceutical industry.

Following granulation, the ingredients were removed and dried in the GPCG1 (Glatt-Powder-Coater-Granulator) fluidized bed dryer from Glatt Air Technologies Inc. (Ramsey, NJ). This apparatus is diagrammed in Figure 2.02.

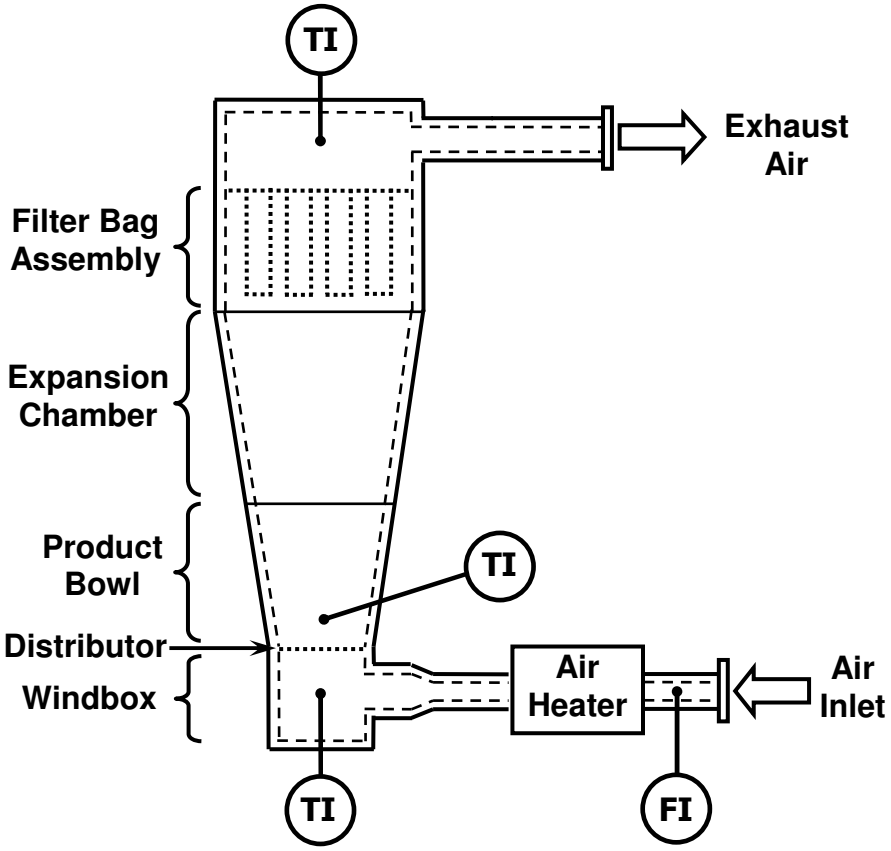

Figure 2.02 Schematic of the Glatt GPCG1 fluidized bed dryer (not to scale). The abbreviations TI and FI respectively indicate temperature and flow indicators.

This apparatus is instrumented with thermocouples to measure the temperature of both the bed and the exhaust air. This information was displayed on a digital indicator on a control panel. The temperature in the windbox is also measured using a thermocouple. This measurement is inputted into an automatic control loop for the control of air

temperature using an air heater. Both the measured temperature in the windbox and the setpoint for this parameter were displayed on the control panel. For each experiment, the dryer was pre-heated to prevent the adhesion of particles to the inner surfaces of the unit during operation. Air flow rate is measured using a pitot tube placed in the inlet duct. This measurement was also displayed on the control panel and used for the manual control of the air flow rate. The filter bag assembly was automatically shaken for 2 seconds at 30 seconds intervals throughout the drying experiment. This duration and interval was set on the control panel before the start of each drying experiment. The major difference between this apparatus and the industrial scale dryer is that no control of the inlet humidity is implemented. However, the humidity in the laboratory at Merck Frosst where these experiments were performed was measured at the beginning of each experiment and was found to be 50 ± 5% relative humidity at 20°C.

A cross-section of the PCB-106B piezoelectric pressure transducer utilized for the measurement of pressure fluctuation data from Piezotronics (Depew, NY) is given in Figure 2.03. The electrical response of this pressure transducer is governed by the piezoelectric effect. This effect is defined as a given material's electrical response to an external strain. Therefore, this effect can be used for the transduction of mechanical strain into an electrical signal. The change in thickness of the quartz plates caused by the movement of the diaphragm causes a potential to be induced across these plates. The high impedance of the piezoelectric material requires the use of amplification and signal conditioning electronics. Amplification is accomplished with an on-board integrated circuit while signal conditioning is done externally. This sensor responds only to dynamic changes in pressure and is capable of measuring high frequencies. It can

therefore be categorized as a microphone. The sensor diaphragm was flush mounted to the wall of the dryer. This ensured that pressure fluctuation measurements did not influence the dryer hydrodynamic behaviour.

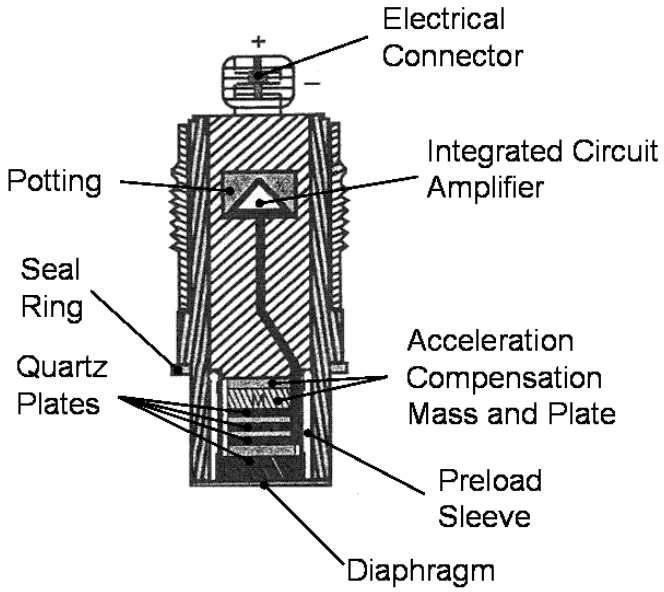

Figure 2.03 Cross-section of the Piezotronics PCB-106B piezoelectric pressure transducer used in this study †.

Pressure fluctuation data from the piezoelectric sensor was collected using an interface developed in Labview. The Matlab code used for the calculation of the S-statistic from this data is presented in Appendix A. A portion of the S-statistic algorithm code was externally compiled in C^{++} using the Matlab MEX function. The MEX function compiles and links source files into a shared library, called a MEX-file, that is executable from within Matlab significantly reducing processing time. This code is also given in Appendix A.

† Adapted from: *PCB-106B Instruction Manual*, PCB Piezotronics, Inc. Depew, NY, 2001.

2.1 Abstract

A statistical test based on attractor reconstruction has been applied to a small-scale industrial fluidized bed drier for pharmaceutical granulate. High frequency pressure fluctuation data has been collected over dryings lasting between 45 to 75 min depending on operating conditions. The data clearly shows that separate regions of slow change in fluidized state occurring at the beginning and near the end of the drying separated by a continuum of more rapid hydrodynamic change. Visual observations of the initial period of gradual change, suggests the presence of a bubble train within the central core of the contactor while the second period of gradual change, lasting 5 to 10 min, exhibits more uniform fluidization involving the entire bed. Dominant frequency and standard deviation have also been applied to the data but their connection to moisture is not clear.

2.2 Notation

d	bandwidth for the smoothing in state space (nondimensional)
H_{dry}	settled height of the dry bed of pharmaceutical granule (m)
H_{wet}	settled height of the wet bed of pharmaceutical granule (m)
L	segment length (s or nondimensional)
m	embedding dimension (data points)
Q	squared distance between two attractors
S	the test statistic (S-statistic) (nondimensional)
U_0	superficial gas velocity (m/s)
$V_C(Q)$	conditional variance of Q (nondimensional)

2.3 Introduction

In the pharmaceutical industry, the drying of pharmaceutical granulate is accomplished batchwise in a conical fluidized bed dryer. The most common method for control of this process is to monitor for changes in outlet air or product temperature. A limiting value for either one of these quantities is used to indicate the endpoint of the drying process. While this method results in an acceptable product quality for the drugs currently manufactured, there is concern that resulting non-uniform moisture content, segregation of larger granules, entrainment of finer granules, and granule attrition could impact the quality of the drug product. High potency or peptide-based drug products may be even more severely affected by these phenomena.

To assess the impact of operation conditions on product quality, a clear picture of fluidized bed dryer hydrodynamics must be resolved. It is desirable to use a non-invasive technique in order to monitor these hydrodynamic effects. An example of a non-invasive approach is analysis of pressure fluctuations. High frequency absolute pressure fluctuations have been shown to indicate changes in fluidization quality or regime transitions in a number of studies (Schouten and van den Bleek [1], van der Schaaf et al. [2]). This type of measurement has the advantage of being relatively easy to implement in lab, pilot, or industrial scale units since it can be non-intrusive and involves the logging of a single time series. Both simple statistics (Chong and O'Dea [3]) and signal analysis (Saxena et al. [4]) have been applied to such a time series of measurements to resolve changes within fluidized systems resulting from changes in

particle size distribution and gas velocity. However, investigations into the system state changes taking place during the drying process are not part of the published literature.

Recently, it has been shown that fluidized beds exhibit chaotic behaviour. The use of the Takens [5] embedding theorem has been shown to accurately represent attractors describing fluidization processes. This reconstruction has been combined with a statistical test by Diks et al. [6] in order to determine statistical changes occurring between two time series arising from differing system states. These tests have been applied to fluidized systems of dry particles by van Ommen [7] and demonstrate that subtle changes in bed hydrodynamics arising from agglomeration can be tracked. These changes can be associated with changes in bed hydrodynamics that lead to defluidization or an undesirable fluidized state.

There are no previous works involving the application of the aforementioned statistical test to fluidized bed dryers. In drying, the opposite trend to agglomeration and defluidization occurs, whereby the process progresses from a poor quality of fluidization in a wet bed to a more desirable final (dry) state signifying the endpoint of the drying process. Therefore, the objective of the present study is to apply the Diks et al. [6] test to pressure fluctuations measured in a fluidized bed dryer. Tracking bed progression using this test will allow for more precise measure of product state.

2.4 Theory

Chaos analysis of pressure fluctuation data delay vectors has been outlined by van Ommen [7]. Van Ommen uses the Diks et al. [6] test for chaotic noisy systems. The Diks test is a statistical test for the difference between reconstructed delay vector

distributions in an m-dimensional pseudo state space. Each reconstructed attractor is assumed to arise from a stationary dynamical system and the test statistic (S) represents the statistical change between these states.

$$S = \frac{\hat{Q}}{\sqrt{V_C(\hat{Q})}} \qquad [1]$$

Q is the squared distance between distributions arising from delay vectors reconstructed from 2 separate time series. These time series are referred to as the reference and evaluation time series. The test gives a measure of the statistical difference between attractors reconstructed from these time series. If S has a value greater than 3, the null hypothesis that the two reconstructed attractors compared arise from the same underlying dynamics can be rejected at the 95% confidence level. However, Diks et al. [6] has shown through numerical simulation that, since this test is one sided, this confidence level may be as high as 98 to 99%.

We also compare in the present work the information gained from the S-statistic test with two separate techniques applied to a time-series. These were standard deviation and dominant frequency. Standard deviation was calculated in the usual way for a population sample. Dominant frequency was defined as that frequency corresponding to the maximum in the power spectral density function.

2.5 Experimental

2.5.1 Product Formulation

Granulations were performed in a Fielder 25 L high shear granulator using the ingredients outlined in Table 2.1. Five minutes of ingredient pre-mixing was performed, followed by five minutes of water addition and two minutes of post water addition mixing. A Tee-Jet 9501 nozzle was used for water addition under a constant pressure of 207 kPa gauge. The nozzle was set at a height of 7.5 cm below the granulator lid.

2.5.2 Fluidized Bed Dryer

The Glatt GPCG1 fluidized bed dryer was used to dry the wet placebo granulate. This unit allows for the manipulation of inlet air temperature and air velocity. A schematic of the conical section of this unit is given in Figure 2.1. Fitted with a 12% open area wire mesh distributor, the conical section fits into the air-supply/conditioning module. Wet granule is placed in this section (product bowl). Heated air is introduced into the bottom of the conical section in order to fluidize the material. At intervals of five minutes, samples of the bed were taken with the use of a sample thief. These were later analyzed using Karl Fischer titration for moisture content. Concurrently, product and outlet air temperature measurements were read directly from the digital instrumentation panel.

2.5.3 Pressure measurement and Data Analysis

A high-frequency piezoelectric sensor (PCB-106B from Piezotronics) was used in the measurement of pressure fluctuation data. The sensor diaphragm was flush-mounted to the inside wall of the conical contactor by means of a viewing window

modified to accept the mounting of pressure transducers. This window allowed for three measurement positions at an equal spacing of 19 mm. The bottom measurement position is located at a wall distance of 90 mm above the distributor. A Keithley KPC-3101 12 bit data acquisition card was used for data acquisition. Card control and data logging was made possible by the use of a graphical user interface developed in Labview. Raw data was written at a sampling rate of 400 Hz. Raw data was filtered using a type 1 Chebychev band-pass filter design in Matlab between 0.5 Hz and 170 Hz. This was done in order to fulfill the Nyquist criterion as well as to eliminate low frequency transitory effects associated with the piezoelectric sensor. The S-statistic algorithm of van Ommen [7, 8] has been implemented in Matlab. Reference and evaluation time series were each 2 min in length for all analysis. The algorithm was calibrated as described below.

A factorial set of drying experiments was performed by varying inlet temperature, sensor position and bed mass. Drying (inlet) air temperatures were set at 55°C, 65°C, and 75°C. Wet bed masses of 2.75, 3, and 3.25 kg and sensor locations of 9, 10.9 and 12.8 cm above the distributor were examined. These values were selected to give good sensor coverage while allowing significant variation in drying times between experimental runs. A full factorial design with 3 centre point or baseline runs was implemented giving a total of 11 experiments. A constant gas velocity of 2.46 m/s was used throughout the experiment except for startup, where a slightly higher velocity of approximately 3 m/s was needed to induce homogeneous fluidization of the bed. This higher velocity was maintained for approximately 10 minutes and did not interfere with the behaviour of the test statistic. Pressure fluctuation data was logged over the entire

drying process. Completion of the experiment was signified by the attainment of a product temperature of 45°C (see Figure 2.5).

Pressure fluctuation data generated for a dry bed of pharmaceutical granule was used to quantify the response of the signal analysis techniques to changes in superficial gas velocity. To examine this effect, 2 kg of dry granule was fluidized at superficial gas velocities between 1.95 and 2.92 m/s. Pressure fluctuation data sets of 2 minutes in duration were collected in triplicate at each superficial velocity.

2.6 Results and Discussion

2.6.1 Calibration of the Test Statistic

The pressure fluctuation measurements made on different fluidized systems are a function of the system parameters such as geometry, PSD, and cohesive forces as well as the signal-to-noise ratio. Hence every signal will have slightly different characteristics and implementation of time delay embedding to a time series cannot be done according to precise rules. Rather, key parameters are optimized in order to detect the changes within the system with which one is interested. These parameters include the time window or delay vector length, embedding dimension, bandwidth and segment length. The quantity of interest in this study is the effect of moisture on bed hydrodynamics. Therefore, for the calibration, data sets collected at moisture contents of 25% and 10% were chosen as the reference and evaluation time series respectively. The reference time series was not only compared with the evaluation series, but also to two time series immediately before and after both the evaluation and reference time series. This was done to examine the reproducibility of the technique when applied to data collected

under similar conditions. The maximum value of S obtained in the calibration plots was chosen as the optimum value for each parameter selected for the S-statistic implementation. Calibration was repeated for three separate sets of drying data and the parameters obtained were identical for each calibration. A sample calibration curve for the time window parameter is given in Figure 2.2. Optimum values for all parameters are given in Table 2.2. These values are the same as those obtained by van Ommen et al. [8] except for time window and embedding dimension. The time window chosen for this work spans approximately one-third of the cycle time. Schouten [9] recommends this parameter cover the entire cycle time for chaos analysis, but the work of van Ommen [7] has shown that a lower value of one-quarter of the average cycle time is optimum for the S-statistic applied to a fluidized system. Hence, our optimum time window, though slightly different is consistent with the latter study. Embedding was chosen as the maximum value of 40. This value utilizes all the data given a time window of 0.1 s for data sampled at 400 Hz. Results of a parameter analysis (not shown here) indicate that the embedding dimension could be selected at a value as low as 10 without influencing the identification of the region of gradual hydrodynamic change (i.e. the point in time at which $S<3$ or $S>3$).

2.6.2 Dry Bed Studies

The sensitivity of a given monitoring technique to superficial gas velocity is a key issue in control implementation in fluidized beds. Slight fluctuations in gas flow were observed on the instrument panel for the fluidized bed dryer used in this study. These fluctuations likely arose from interaction of the dynamics of the gas-solid flow with the dedicated air supply to the apparatus. Such a phenomenon is not uncommon in

fluidized systems. Since it is proposed that the S-statistic may be used at some point in a control loop, it is desirable to understand if even these slight fluctuations might represent a significant disturbance to the test statistic. Hence the influence of gas velocity on the statistic must be quantified.

Figure 2.3 shows typical behaviour of the S-statistic over a range of gas velocities for the middle sensor position. The reference state is at U_0 = 2.44 m/s. It may be noted that the statistical difference between 1.95m/s and 2.44m/s is much greater than the difference between 2.92m/s and 2.44m/s. Indeed, an S value > 3 at the lowest velocity shows that a statistical change occurs between U_0 = 1.95 m/s and U_0 = 2.44 m/s. This indicates that the bed hydrodynamics at lower superficial gas velocities is less similar to the bed hydrodynamics at higher velocities or that a transition in hydrodynamics occurs within the region of U_0 = 2 m/s. A similar transition is observed in the standard deviation and dominant frequency as shown in Figure 2.4. We conclude that slight fluctuations in superficial gas velocity in the subsequent drying experiments will have negligible effect on the statistical test. We have chosen a constant superficial gas velocity of 2.46 m/s for the drying experiments in order to stay in the regime noted in Figure 2.3.

2.6.3 Drying Experiments

The drying curve, outlet air temperature, and product temperature profiles for a typical drying experiment are given in Figure 2.5. The increase in product and outlet temperatures towards the end of drying signifies the loss of surface moisture from the granules or the end of the constant rate of drying.

Using the pressure fluctuation time series measured during drying, each successive time segment of 2 minutes was transformed into a single S-statistic value. Reference time series for the statistic were chosen for two moisture contents: 26-wt% and 8-wt%, corresponding to points in time near the beginning and end of drying. Figure 2.6 shows the typical behaviour of the S-statistic when referenced to the two moisture contents. The S-statistic referenced to 26-wt% exhibits hydrodynamic consistency ($S<3$) at the start of drying and then diverges from that state as moisture is driven from the granules. The value of the statistic increases continuously before becoming constant at a later time. When the S-statistic is referenced to 8-wt% moisture, its value is initially far away from three; it gradually reaches a value less than three near the end of drying. This point in time coincides closely with the time where the S-statistic becomes constant when referenced to 26-wt% moisture, and the point at which the temperatures begin to rise in Figure 2.5. It would appear therefore, that the S-statistic is sensitive to the changes in bed hydrodynamics arising from the loss of surface moisture. This is consistent with a reduction in interparticle forces due to reduced liquid bridging. Visual observations through the viewing window provide support for this assertion. A central core of bubbles is seen in the very wet bed. This behaviour coincides with the initial region of gradual hydrodynamic change seen in Figure 2.6. After this early behaviour, the entire bed exhibited more homogeneous fluidization for the rest of the drying process. Experiments planned by our group to image the bed using a tomographic technique should reveal the details of this behaviour more clearly.

We have considered the possibility that the statistical changes noted in Figure 2.6 could simply be the response of the technique to the change in bed mass accompanying

the loss of total moisture. Figure 2.5 shows that moisture loss occurs continuously at a constant rate over the drying period. Hence the bed experiences a continuous reduction in mass throughout the drying process, and the impact on the hydrodynamic state should also occur at a constant rate. Such a continuous change in hydrodynamic state arising from a change in bed mass would manifest itself with a short period of the S-statistic below the threshold of 3 with convergence and subsequent divergence on approach and departure from the reference state. Such behaviour is noted for the S-statistic curve referenced to 20-wt% moisture (Figure 2.6) as there is a rapid change in hydrodynamic state occurring at this time. This effect is not seen when the statistic is referenced to 8-wt% moisture. Here, we see a more gradual change in hydrodynamic state. Furthermore, this effect would be most intense toward the end of drying where the change in moisture with respect to time, which is shown to be constant in Figure 2.5, represents a loss of a greater fraction of the bed's total mass. Figure 2.6 clearly shows a region of approximately 20 minutes of more consistent hydrodynamics towards the end of drying.

The consistent behaviour of the final region of gradual change in hydrodynamic state with respect to moisture provides a means for the S-statistic to be used as a process monitoring technique to track granule moisture within a drying bed. A "library" of dry bed pressure fluctuation data could be collected and compared to online data collected as drying proceeds. Thus, the S-statistic could be calculated in real time throughout the drying process to give a clearer picture of the moisture content than that currently seen in the behaviour of the product and outlet temperatures (Figure 2.5).

As expected, varying inlet air temperature only acted to change the duration of the drying experiment. When the S-statistic data collected at different temperatures were

plotted as a function of dimensionless time (time divided by total drying time), the curves collapsed onto a single curve. This demonstrates that the S-statistic is responding directly to moisture changes taking place within the drying bed. The relative influence of bed mass and sensor position on the test statistic was inconclusive based on the performed factorial experiments. For a low bed mass and high sensor position, the performance of the test was problematic as both the final and initial regions of more gradual hydrodynamic change suffered from the convergence and divergence behaviour discussed above.

The changes in bed hydrodynamics captured with the S-statistic were not detectable from the dominant frequency or the standard deviation (Figure 2.7). This shows that these methods of pressure fluctuation analysis do not adequately discern the hydrodynamic changes taking place during drying. The dominant frequency is the bubbling frequency. This frequency was nearly identical for all experiments and remained consistent throughout each experiment at approximately 3 Hz. Bed mass was the only manipulated variable impacting this frequency, with higher bed loadings slightly decreasing the dominant frequency. Elevated frequencies observed early in the data set have been found to have no impact on to the initial region of gradual change in hydrodynamic state.

Standard deviation increases throughout the experiment with no limiting value. It is possible that one could link the standard deviation to moisture content but, based on our data, this would be a vague link. Standard deviation increased more intensely at higher sensor positions and lower bed masses indicating more intense fluctuations at higher locations in the bed.

2.7 Conclusions

This study has shown that chaos analysis of pressure fluctuations is sensitive to hydrodynamic changes occurring during the drying process. The technique shows promise not only for process monitoring, but also as part of a control system. Such a control loop could make decisions on control on appropriate action based on the chaotic nature of the system, most likely by comparing the measured state of the system to a reference bank of known desired hydrodynamic states. In this way, the drying endpoint could be selected more precisely than the current method of monitoring outlet temperature allows. Furthermore, since the proposed technique provides exact quantification of the state of the system, the hydrodynamics of the fluidized bed can be controlled precisely throughout the drying process in order to prevent the undesired effects of particle attrition and non-uniform drying.

2.8 Acknowledgements

The authors would like to thank Merck-Frosst & Co. (Montreal), the Natural Sciences and Engineering Research Council of Canada (NSERC) for financial and technical assistance as well as Ruud van Ommen for consultation regarding the implementation of the S-statistic.

2.9 References

1. Schouten, J.C., Van den Bleek, C.M., *Monitoring the quality of fluidization using the short term predictability of pressure fluctuation*s, AIChE J., 44, 48-60,1998.
2. van der Schaaf, J, Schouten, J.C., van den Bleek, C.M., *Origin, propagation and attenuation of pressure waves in gas-solid fluidized bed*s, Powder Tech., 95, 220-233, 1998.
3. Chong, Y.O., O'Dea, D.P., White, E.T., Lee, P.L., Leung, L.S., *Control of the quality of fluidization in a tall bed using the variance of pressure fluctuation*s, Powder Tech., 53, 137-246, 1997.
4. Saxena, S.C., Rao, N.S., Tanjore, V.N., *Diagnostic procedures of establishing the quality of fluidization of gas-solid system*s, Exp. Ther. and Fluid Sci., 6, 56-73, 1993.
5. Takens, F., *Detecting strange attractors in turbulenc*e, Lecture notes in Mathematics, 878, Springer-Verlag, 336-381, 1981.
6. Diks, C., van Zwet, W.R., Takens, F., DeGoede, J., *Detecting differences between delay vector distribution*s, Phys. Rev. E., 53(3), 2169-2176, 1996.
7. van Ommen, J.R., *Monitoring fluidized bed hydrodynamic*s, PhD. Thesis Delft University of Technology, 2001.
8. van Ommen, J.R., Coppens, M.C., van den Bleek, C.M., Schouten J.C., *Early warning of agglomeration in fluidized beds by attractor comparis*on, AIChE J., 46(11), 2183-2197, 2000.
9. Schouten, J.C., Takens, F., van den Bleek, C.M., *Estimation of the dimension of a noisy attractor*, Phys. Rev. E. 50(3), 1851-1861, 1994.

Table 2.1 Wet Granule Formulation

Component	**Percentage by mass (dry basis)**
Lactose Monohydrate (filler)	50%
Microcrystalline Cellulose (filler)	44%
Croscarmellose Sodium (disintegrant)	2%
Hydroxypropyl Methylcellulose (binder)	4%
USP Water*	42%

*Water used conformed to the USP (United States Pharmacopeia) standard for purity.

Table 2.2 S-Statistic Parameters

Time window (delay vector length)	0.1 seconds
Embedding (m)	40
Bandwidth (d)	0.5
Segment Length (L)	3 seconds

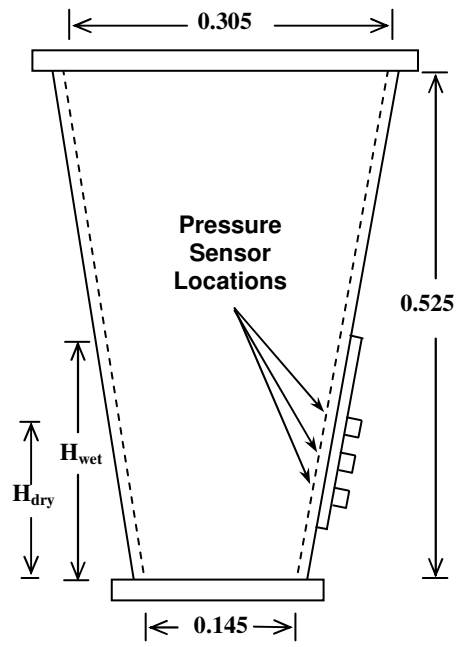

Figure 2.1 GPCG1 product bowl. Measurements are given in meters. H_{wet}, H_{dry} represent approximate settled bed heights for wet and dry beds. The three sensor positions examined were at 9, 10.9 and 12.8 cm.

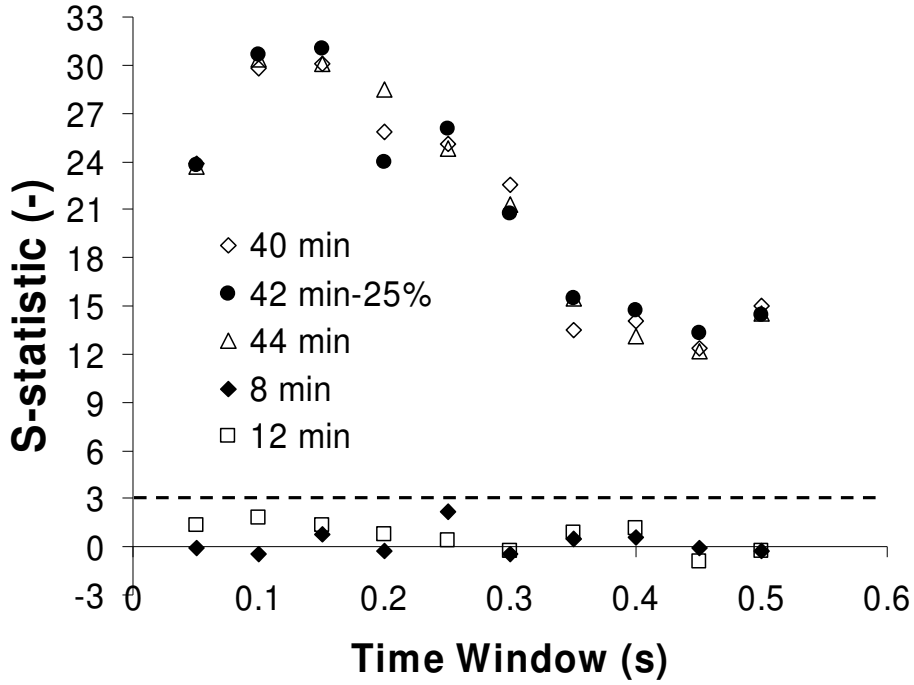

Figure 2.2 Calibration curve for the S-statistic. The optimum value for the time window is 0.1s.

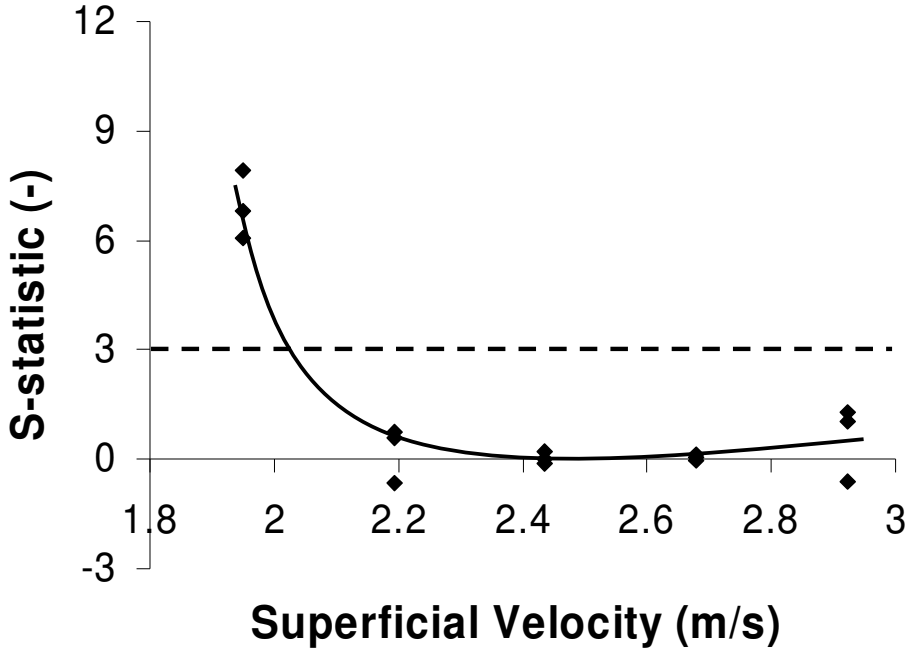

Figure 2.3 S-statistic response to changes in superficial gas velocity in a dry bed of granule. All data sets referenced to a single data set collected at 2.44 m/s.

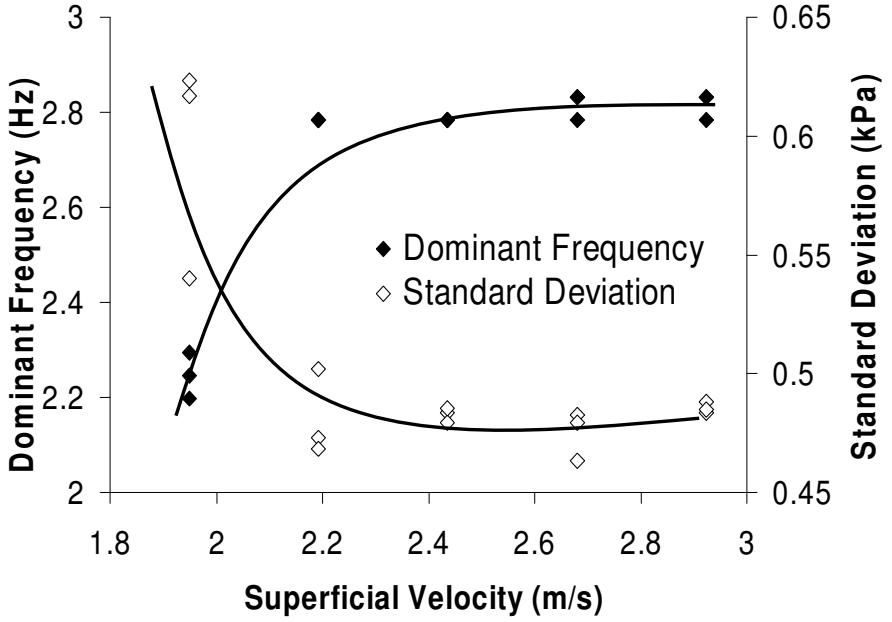

Figure 2.4 Standard Deviation and Dominant Frequency response to changes in superficial gas velocity for a dry bed.

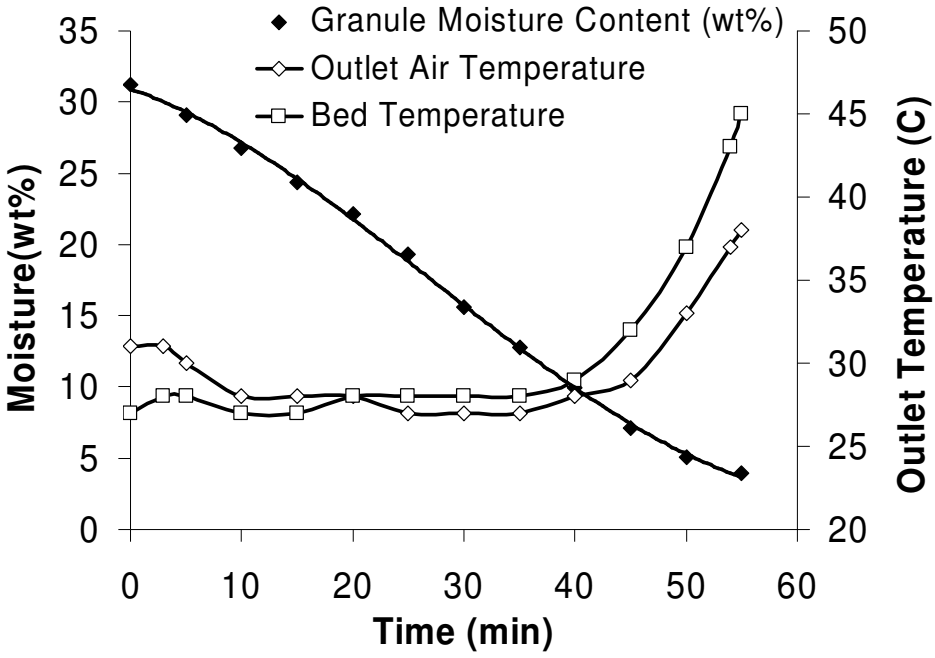

Figure 2.5 Progression of outlet air and product temperature as well as product moisture content for factorial baseline.

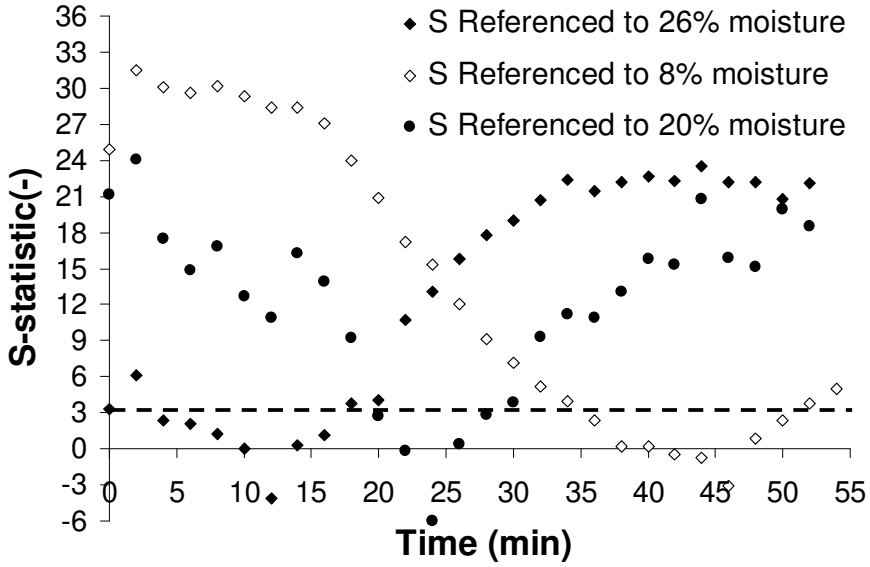

Figure 2.6 S-Statistic plot for the same drying experiment shown in Figure 2.5.

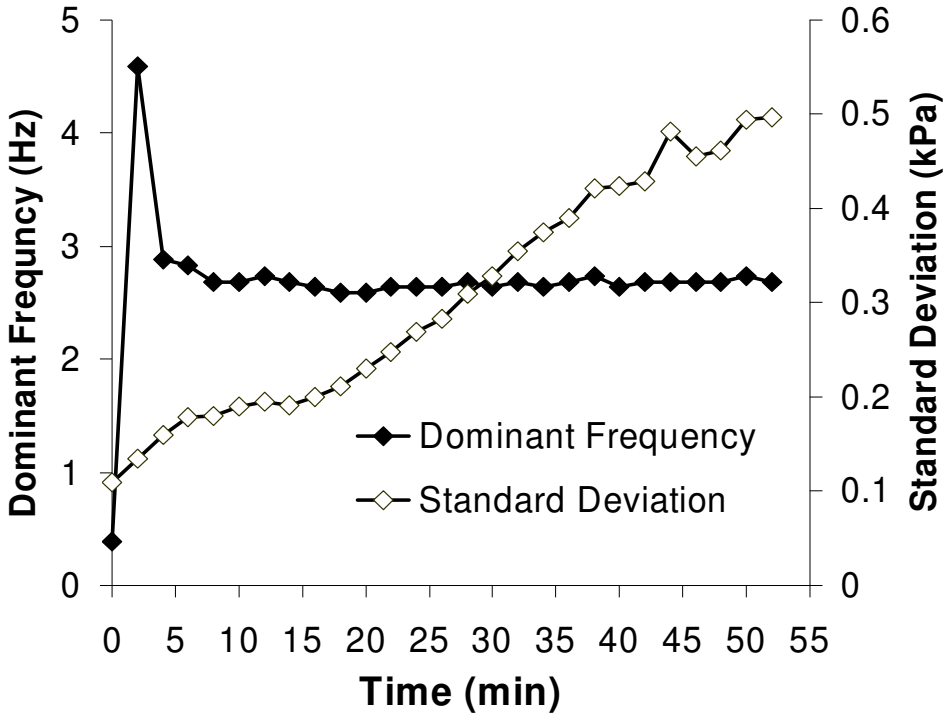

Figure 2.7 Dominant frequency and standard deviation response for the experiment given in Figures 2.5 and 2.6.

Chapter 3 - Application of Chaos Analysis to Pressure Fluctuation Data from a Fluidized Bed Dryer Containing Pharmaceutical Granule

This publication appears in the journal ***Powder Technology*** and is published in a similar version to what appears in this chapter:

Citation

Chaplin, G., Pugsley, T., Winters, C., *Application of chaos analysis to pressure fluctuation data from a fluidized bed dryer containing pharmaceutical granule*, Powder Tech. 142(2-3), 110-120, (2004).

Contribution of PhD Candidate

Experiments were planned and performed by Gareth Chaplin. Todd Pugsley and Conrad Winters (Director, Formulation Development (PR&D) Merck & Co.) provided consultation regarding the experimental program. The software for all data collection and analysis was developed by G. Chaplin. All of the writing of the submitted manuscript was done by G. Chaplin with T. Pugsley and C. Winters providing editorial guidance regarding the style and content of the paper.

Contribution of this Paper to the Overall Study

This paper extends the work in chapter 2 where it was demonstrated that the S-statistic responds to changes in hydrodynamic state resulting from the reduction in

moisture during the drying process. The 8-page limit imposed on the publication presented in chapter 2 precluded the presentation of this detailed summary. For this reason, this chapter is a definitive examination of the behaviour of the S-statistic applied to pressure fluctuations in a drying bed of pharmaceutical granule.

Additional Experimental Details

The identical apparatus and procedures presented in chapter 2 were utilized for granulation and drying. In addition, the same procedures were used for data acquisition and analysis. In this chapter, pressure fluctuation data collected in a dry bed and a drying bed of pharmaceutical granule are presented. For a dry bed of pharmaceutical granule, the influence of both particle size distribution and bed mass on the S-statistic has been quantified. These disturbances are a concern for the implementation of the S-statistic to a practical batch drying process where variations in product formulation are possible. In a drying bed, the effect of bed mass, inlet air temperature and sensor position have been quantified using a factorial experimental design. Again, these process variables are assessed in order to quantify the impact of these experimental parameters on the S-statistic. Changes in the frequency and amplitude characteristics of the pressure signals are also analyzed in order to determine the suitability, or lack thereof, of these tests as a monitoring technique for the drying process.

3.1 Abstract

The S-statistic, a statistical test between chaotic attractors for fluidized systems introduced by van Ommen et al. [1,2] has been applied to pressure fluctuations collected in a conical fluidized bed of dry pharmaceutical granule as well as a fluidized bed of wet granule as it progresses to the dry state. In a dry bed, the S-statistic has been found sensitive to the particle size distribution (PSD). Changes in bed hydrodynamics arising from PSD have been found to be most easily resolved at low gas velocities, indicating segregation at superficial velocities less than 2 m/s. In a drying bed, two regions of gradual change in hydrodynamic state have been identified. These periods correspond to visual observations of the presence of a centralized core of bubbles in a bed of high moisture content and more uniform fluidization throughout the bed cross-section toward the end of the drying process. The effect of moisture has been found to dominate the hydrodynamic changes taking place within the bed in the drying process identified with the S-statistic. The hydrodynamic changes identified by the S-statistic are not discerned by frequency and amplitude analysis techniques. Response of the S-statistic to the hydrodynamic changes associated with drying indicates the potential application of this technique to the quantification of fluidized bed hydrodynamic behaviour.

3.2 Introduction

Operation of a fluidized bed within a specific state is important for the control of particle-particle and gas-particle interactions. The former is of importance in controlling attrition effects while the latter influences the mass transfer characteristics of the bed. In the application of a fluidized bed to the drying of granular material, the rate of mass transfer influences drying time. Given the widespread application of fluidized bed dryers

in the food, biotechnology and pharmaceutical industries, quantification of fluid bed hydrodynamics throughout the drying process is of significant industrial relevance. Through the monitoring and control of this hydrodynamic behaviour, a desired fluidized state can be maintained that optimizes both product quality and drying time.

The focus of the present study is the pharmaceutical industry. In this industry, the drying of pharmaceutical granulate is accomplished batchwise in a fluidized bed dryer. The most common method for control of this process is to monitor for changes in outlet air or product temperature. A limiting value for either one of these quantities is used to indicate the endpoint of the drying process. The selection of appropriate superficial gas velocities is at the discretion of the operator and no automatic control mechanism is implemented. In typical commercial installations, the velocity will be well controlled around the desired set point input by the operator, however, manual selection of the correct velocity to operate in the optimum fluidization regime may not be possible due to subtle changes in fluidization quality not apparent in visual observations. While manual control of fluidization hydrodynamics results in an acceptable product quality for the drugs currently manufactured, there is concern that segregation of larger granules, entrainment of finer granules, and granule attrition could impact the quality of the drug product. High-potency or peptide-based drug products may be even more severely affected by these phenomena. Since attrition, segregation and entrainment arise from gas-particle and particle-particle interactions, a better understanding and control of bed hydrodynamics will lead to a lessening of these effects. Bed hydrodynamics also affect the homogeneity of the moisture within the bed at the end of drying. The good mixing characteristics of a fluidized bed can only be maximized when the proper

selection of superficial gas velocity (i.e. hydrodynamic regime) is made. Operation of the bed in an optimum fluidized state will allow for more uniform treatment of all particles within the bed. The current monitoring of bed and outlet temperatures alone does not give any indication of bed hydrodynamics.

If a clear quantification of bed hydrodynamics was possible, an automatic control system could manipulate the superficial gas velocity in order to maintain a desirable hydrodynamic state. The monitoring technique for this type of control loop should be non-intrusive so that the hydrodynamics to be quantified are not influenced. Examples of non-intrusive techniques include tomographic methods such as X-ray tomography and Electrical Capacitance Tomography (ECT). Although these techniques give direct measurements of both local and global bed behaviour, they are currently not widely implemented industrially due to cost and development limitations. However, pressure fluctuations measurements within a drying bed can be easily obtained. Since pressure fluctuations propagate throughout the bed (van der Schaaf et al. [3]), time series analysis of local measurements gives a global picture of the bed hydrodynamics. This type of measurement has the advantage of being relatively easy to implement in lab, pilot, or industrial scale units since it involves the logging of a single time series. In addition, it has the advantage of being low in cost and non-intrusive if the pressure transducer is flush mounted at the vessel wall or if differential pressure measurements are utilized.

A number of approaches may be used to analyze time-series measurements obtained during the fluidization process. The most basic of these are amplitude (Chong et al. [4]) and frequency analysis (Saxena et al. [5]). Trnka et al. [6] extended the use of frequency analysis. In their study, a fast Fourier transform method was implemented to

identify changes in a pressure time series measured in a fluidized bed. Compared to the use of total bed pressure drop, this test more clearly identified the onset of turbulence and entrainment associated with increases in superficial gas velocity. Other methods of time-series analysis applied to fluidized beds include mutual information theory (Karamavruç et al. [7]) and Kolmogorov entropy (Johnsson et al. [8]). These techniques recognize the complex nature of fluidization and provide an alternative means of identifying system state and regime transition changes not clearly identified with pure frequency and amplitude analysis.

Very few published works aimed at quantifying the dynamic behaviour of fluidized beds have considered the influence of moisture. McLaughlin and Rhodes [9] have shown that liquid bridging effects arising from the addition of a non-volatile liquid to the bed cause changes in the bed's Geldart behaviour. Dominant frequency was not affected by the presence of the liquid. Wright and Raper [10] have shown that the addition of a non-volatile oil resulted in an increase in bed pressure drop at a given superficial gas velocity compared to a dry bed. This effect was interpreted as an increase in the force resisting the fluidization of the bed caused by the presence of liquid bridges between particles. The presence of such liquid bridging effects is possible in a wet bed early in the drying process. Wright and Raper [10] also found that the standard deviation of the differential pressure drop decreased with the addition of the non-volatile oil. They reported the reason for this as being due to the formation of a stable roof of solids on the bubbles that affect the bubble rise velocity and breakage. Briens et al. [11] has utilized pressure fluctuations collected in a fluidized bed coker to identify changes leading to a loss of fluidity. Among the criteria used in this study to describe this undesirable

fluidized state denoted as 'bogging', is the presence of hydrocarbons on the particle surfaces. This surface fluid leads to liquid bridging effects resulting in an undesirable fluidized state. Clearly, the presence of surface fluid results in significant changes in fluidized state.

Recently, chaos has been observed in fluidized systems (e.g. [8, 12 – 15]). Daw et al. [12] have identified a transition to chaotic behaviour in a turbulent fluidized bed. Johnsson et al. [8] noted intermittency in pressure fluctuations collected from a fluidized bed. This intermittency is an indication of the chaotic behaviour in the system. Bai et al. [13] have shown identified two scales of behaviour utilizing the correlation dimension applied to absolute pressure fluctuations. These scales have been attributed to the particle motion causing small-scale fluctuations and the motion of voids causing large-scale fluctuations. This multi-scale nature to fluidization behaviour has also been identified through the use of Hurst's exponent by Bai et al. [14]. It was noted that the two-phase nature of the fluidized system becomes less evident with increasing superficial gas velocity. Hay et al. [15] have indicated that the Lyapunov exponent and the correlation dimension can remain constant over a wide range of operating conditions This indicates that chaotic parameters can be insensitive to certain changes in operating conditions.

The shape and dimension of attractors describing system state are one means of quantifying a system's chaotic behaviour. Time-delay reconstruction (Takens [16]) provides a means of reconstructing an attractor from regular sampling of a single variable. This reconstruction has been combined with a statistical test by Diks et al. [17] in order to determine statistical changes occurring between attractors reconstructed from

two time series collected at differing system states. This statistical test has been applied to fluidized systems of dry particles by van Ommen [1] with the test statistic being denoted as the S-statistic. This study demonstrated that subtle changes in bed hydrodynamics arising from agglomeration could be tracked. These changes can be associated with changes in bed hydrodynamics that lead to defluidization or an undesirable fluidized state [1,2]. In drying, the opposite trend to agglomeration and defluidization occurs, whereby the process progresses from a poor quality of fluidization in a wet bed to a more desirable final (dry) state signifying the endpoint of the drying process. Chaplin et al. [18] have applied the S-statistic test as presented by van Ommen et al. [1,2] to pressure fluctuations in a drying bed of pharmaceutical granule and shown the presence of two separate regions of more gradual change in hydrodynamic state near the start and toward the end of the drying process.

With the exception of our previous study [18], chaos theory has not been applied to the dynamic analysis of fluid bed dryers. The objective of the present study is to examine more closely the relationship between the regions of more gradual change in hydrodynamic state identified previously [18] and the influence of temperature, bed mass and sensor position on the S-statistic. Monitoring of bed behaviour using the S-statistic will allow for a more precise measure of product state and, consequently, moisture. This is superior to the current technique of monitoring product temperature. Therefore, a connection between bed hydrodynamic state and moisture will be made. These states and their degree of persistence may suggest a more effective mode of operation and form the basis for a control strategy. Changes in standard deviation and dominant frequency accompanying the drying process will also be examined.

3.3 Theoretical Development

As outlined by Takens [16], time delay embedding provides a means of reconstructing attractors arising from a stationary system utilizing a single measured variable. Thus, the system state can be determined from the discrete sampling of a single variable. For a fluidized bed, an obvious variable for this purpose is pressure. Fluctuations in pressure are directly related to the passage and eruption of bubbles and thus, the bed state. However, because of the noise associated with this type of measurement, a representative sample is required in order to discern the system state. Assuming that the system is stationary for a given interval, a measured pressure time series can be decomposed into a set of normalized time-delay vectors in m-dimensional space.

$$p_{ref} = \left(p_1, p_2, p_3 \ldots p_{N_P}\right) \rightarrow X_i = \left[x_{(i-1)m+1}, x_{(i-1)m+2} \ldots, x_{i \cdot m}\right]^T$$
$$x_i = \frac{p_i - \mu_{ref}}{\sigma_{P_{ref}}} \qquad [1]$$

The S-statistic provides a means of comparing this reference set of delay vectors with a corresponding evaluation data set given in Equation 2.

$$p_{eval} = \left(p_1, p_2, p_3 \ldots p_{N_P}\right) \rightarrow Y_i = \left[y_{(i-1)m+1}, y_{(i-1)m+2} \ldots, y_{i \cdot m}\right]^T$$
$$y_i = \frac{p_i - \mu_{eval}}{\sigma_{P_{eval}}} \qquad [2]$$

If these two sets arise from the same underlying physical processes, a statistical test can be performed between sets in order to determine whether a statistically significant change has taken place.

In comparing the reference and evaluation sets, it is useful to define a characteristic measure of distance between sets. The quantity Q represents the squared distance between the smoothed multi-dimensional probability distributions for the two delay-vector sets ($\rho'_x(r)$ and $\rho'_y(r)$)

$$Q = \left(2d\sqrt{\pi}\right)^m \int \left[\rho'_x(R) - \rho'_y(R)\right]^2 dR \qquad [3]$$

Smoothing of the reference and evaluation vector distributions ($\rho_x(r)$ and $\rho_y(r)$) is provided by the Gaussian kernel and is performed in order to allow for calculation of unbiased estimators in terms of sampled vectors [17]. The squared distance between smoothed distributions (Q) cannot be found directly. Therefore, an estimator for Q must be calculated. This estimator is given by Equation 4.

$$\hat{Q} = \frac{2}{N_1(N_1-1)} \sum\sum_{1 \le p < q \le N_1} h'_{pq} + \frac{2}{N_2(N_2-1)} \sum\sum_{N_1+1 \le p < q \le N} h'_{pq} - \frac{2}{N_1 N_2} \sum_{p=1}^{N_1} \sum_{q=N_1+1}^{N} h'_{pq} \qquad [4]$$

Closeness in shape between two reconstructed attractors will be proportional to the magnitude of this estimator for Q. Therefore, for reconstructed attractors of differing shape, Q will be larger than Q calculated for attractors having a similar shape.

The quantity h is calculated from distances between all possible combinations of delay vectors.

$$h\left(Z_i, Z_j\right) = e^{|Z_i - Z_j|^2 / (4d^2)} \qquad [5]$$

Here, all possible distances between X_i and Y_i are expressed through the Euclidian distance ($|Z_i - Z_j|$). Z_i represents a combination of the vectors X_i and $Y_{i\,i}$ given in Equation 6.

$$Z_i = \begin{bmatrix} Z_1 \\ \vdots \\ Z_N \end{bmatrix} = \begin{bmatrix} X_1 \\ X_2 \\ \vdots \\ X_{N_1} \\ Y_1 \\ Y_2 \\ \vdots \\ Y_{N_2} \end{bmatrix} \quad [6]$$

The quantity h_{pq}', not h, is used in Equation 4. The calculation of h_{pq}' is achieved using Equation 7.

$$h'_{pq} = \frac{1}{L^2} \sum_{i=1}^{L} \sum_{j=1}^{L} h\left(Z_{(p-1)L+i}, Z_{(q-1)L+j}\right) \quad [7]$$

This equation gives the average value of h over the segment length L. Motivation for this approach is the removal of dynamic correlations between attractor points in close temporal association. Dynamic correlations would introduce bias into the estimator for Q calculated in Equation 4. Therefore, L must be large enough to eliminate the dynamic correlations between points i and j.

To determine if a statistically significant change has taken place between reconstructed attractors, one must normalize the estimator for Q with its conditional variance. Diks [17] has calculated this variance as the following

$$V_c\left(\hat{Q}\right) = \frac{4(N-1)(N-2)}{N_1(N_1-1)N_2(N_2-1)N(N-3)} \sum\sum_{1 \le p \le q \le N} \psi_{pq}^2 \quad [8]$$

$$\psi_{pq} = H_{pq} - g_p - g_q \quad [9]$$

$$H_{pq} = h'_{pq} - \frac{2}{N(N-1)} \sum\sum_{1 \le p' < q' \le N} h'_{p'q'} \quad [10]$$

$$g_p = \frac{1}{N-2} \sum_{\substack{q \\ p \neq q}} H_{pq} \qquad [11]$$

The estimator for Q given in Equation 4 can now be normalized using its conditional variance.

$$S = \frac{\hat{Q}}{\sqrt{V_C(\hat{Q})}} \qquad [12]$$

Equation 12 is the S-statistic. If S has a value of greater than 3, the null hypothesis that the two reconstructed attractors compared arise from the same underlying dynamics can be rejected at the 95% confidence level. A more detailed description of the mathematical basis and associated algorithm for the S-statistic is given in Diks et al. [17] and van Ommen [1, 2]

3.4 Experimental

3.4.1 Product Formulation

Granule ingredients are outlined in Table 1. Granulations were performed in a Fielder high-shear granulator with a 25 L bowl and a 40.8 cm impeller having a rotational speed of 261 rpm. Five minutes of ingredient pre-mixing was performed, followed by five minutes of water addition and two minutes of post water addition mixing. A Tee-Jet 9501 nozzle was used for water addition under a constant pressure of 207 kPa gauge. The nozzle was set at a distance of 7.5 cm below the granulator lid.

3.4.2 Fluidized Bed Dryer

The GPCG1 fluidized bed dryer (Glatt Air Technologies Inc., Ramsey NJ) was used to dry the wet placebo granulate. This unit allows for the manipulation of inlet air

temperature and air velocity. The humidity of the fluidizing air was not controlled by the dryer but was measured to be approximately 50% relative humidity at an ambient temperature of 20°C. A schematic of the conical section of this unit is given in Figure 3.1. Fitted with a 12% open area wire mesh distributor, the conical section fits into the air-supply/conditioning module. For each experiment, wet granule is placed in the product bowl. Subsequently, heated air is introduced into the bottom of the conical section in order to fluidize the material. At intervals of five minutes during the drying process, samples of between 2 and 3 grams of granule were taken from the bed with the use of a sample thief. Samples were immediately stored in sealed vials and analyzed for moisture content within 24 hours of the drying experiment using Karl Fischer titration. Concurrently, product and outlet air temperature were read directly from a digital instrumentation panel. Temperature measurements were made with 1.6 mm and 1 mm type-J thermocouples placed directly within the bed and in the outlet air stream, respectively.

3.4.3 Pressure Measurement and Data Analysis

A high-frequency piezoelectric sensor (PCB-106B from Piezotronics) was used in the measurement of pressure fluctuation data. The sensor diaphragm was flush-mounted to the inside wall of the dryer by replacing the product bowl viewing window with an acrylic insert threaded to accept the mounting of the pressure transducer (see Figure 3.1). This insert allowed for 3 sensor mounting positions at an equal spacing of 19 mm, with the bottom position located at a wall distance of 90 mm above the distributor. A Keithley KPC-3101 12 bit data acquisition card was used for data acquisition. Card control and data logging was made possible by the use of a graphical user interface

developed in Labview. All raw data sets were collected at a sampling rate of 400 Hz. This data was subsequently filtered offline using a type 1 Chebychev band-pass filter design in Matlab between 0.5 Hz and 170 Hz. Filtering was performed in order to fulfill the Nyquist criterion as well as to eliminate low frequency transitory effects associated with the piezoelectric sensor.

The S-statistic algorithm of van Ommen [1] has been implemented in Matlab. Along with the S-statistic, each pressure time series was examined for changes in frequency and intensity. Only a single dominant or bubbling frequency was examined in this study. To determine this frequency, the power spectral density was calculated for each data set in Matlab. The frequency at the maximum peak of this spectrum was selected as the dominant frequency. Standard deviation was calculated in the usual way for a sample drawn from a population.

3.4.4 Experimental Conditions

Pressure fluctuation data was collected for a dry bed of pharmaceutical granule as well as a wet bed of pharmaceutical granule undergoing drying from a moisture content of 33-wt% to approximately 4-wt%. Pressure fluctuation data generated for the dry bed was used to quantify the response of the signal analysis techniques to changes in bed mass and particle size distribution (PSD). The drying experiments examine the progression of the bed state throughout the drying process.

Fluidization of the dry material was achieved with inlet air temperature of 20°C at superficial gas velocities of 1.95, 2.19, 2.44, 2.68 and 2.92 m/s. These velocities were selected to encompass the full range of possible operating velocities utilized in the

drying of pharmaceutical granules. Superficial velocity has been defined as the mean flow velocity of fluidizing air at the inlet to the product bowl (Figure 3.1). Pressure fluctuation data was collected at 400 Hz in two-minute runs repeated in triplicate at each superficial gas velocity. Variations in hydrodynamic behaviour arising from changes in bed mass were examined at dry bed masses of 1.04, 1.44 and 1.82 kg. Regarding particle size distribution (PSD), the work of van Ommen [1, 2] identifies a clear sensitivity of the S-statistic technique to changes in PSD. Since the PSD of the granule may not be consistent due to batch-to-batch variation in manufacture and formulation, it represents a potential disturbance in the implementation of the S-statistic as a system monitoring technique. To quantify the sensitivity of the S-statistic to this disturbance, pressure fluctuation measurements were made on two separate 2 kg beds of dry granule having the PSDs shown in the sieve analyses given in Table 2. PSD 1 has a wider distribution than PSD 2 and the mean diameter of PSD 1 is 281μm while PSD 2 has a mean diameter of 166 μm. For each PSD, two minutes of data was taken in triplicate at superficial gas velocities of 1.95, 2.19, 2.44, 2.68 and 2.92m/s. The middle sensor position was used for the PSD experiment.

For the wet bed, a set of drying experiments was performed where the inlet temperature, bed mass and sensor position were manipulated. Wet bed masses of 2.75, 3.00 and 3.25 kg were chosen, while drying (inlet) air temperatures were set at 55, 65, and 75°C. These factors, along with the three sensor positions outlined in Section 3.4.3, were used in a full factorial experimental design with 3 centre point runs giving a total of 11 experiments. A constant gas velocity of 2.46 m/s was used throughout the majority of a given drying experiment. This superficial gas velocity was selected based on the

results of dry bed experiments that show insensitivity of the test at velocities higher than 2.2 m/s (Chaplin el al. [18]). A slightly higher velocity of close to 3 m/s was needed at startup in order to induce homogeneous fluidization of the bed. This higher velocity was maintained for approximately the first 10 minutes of the experiment. This increased velocity did not interfere with the behaviour of the test statistic as shown by Chaplin et al. [18]. Furthermore, since experiments ranged in duration from 45 to 90 minutes, the startup period does not represent the bulk of the drying experiment. Pressure fluctuation data was logged over the entire drying process. Completion of the experiment was signified by the attainment of a product temperature of 45°C. The attainment of this temperature was selected as the experimental endpoint because it is the technique currently employed in the pharmaceutical industry to determine the completion of the drying process.

3.5 Results and Discussion

3.5.1 Determination of Test Parameters

The constant parameters in the S-statistic algorithm are the time window, embedding dimension (m), bandwidth (d) and segment length (L). The time window parameter refers to the duration of the delay vector used in the attractor comparison. Embedding is the embedding dimension or the number of data points contained by each delay vector. Bandwidth is a parameter that sets the Gaussian kernel smoothing length scale. Segment length is a parameter used to eliminate dynamic correlations between adjacent points in the state space. For each of the above quantities, optimum values were chosen that gave the largest separation between the two hydrodynamic states tested.

Results of the optimization are given in Chaplin et al. [18] and are summarized in Table 3.

The optimum values found are identical to those found by van Ommen [1, 2] except for time window and embedding dimension. The time window chosen for this work spans approximately one-third of the cycle time based on the dominant frequency of approximately 2.8 Hz (Figures 3.9-3.11). Schouten et al. [19] recommends this parameter cover the entire cycle time for chaos analysis, but the work of van Ommen [1] has shown that a lower value of one-quarter of the average cycle time is optimum for the S-statistic applied to a fluidized system. Hence, our optimum time window, though slightly different is consistent with the latter study. This slight discrepancy is due to the variable nature of the dynamics inherent in different fluidized systems. One cause of this variation is the fact that our system is has a conical geometry while the van Ommen studies [1, 2] use a cylindrical bed. In a conical bed, superficial velocity is not constant from the entrance to the exit of the bed. The increase in cross-section leads to the highest superficial velocities occurring near the inlet. This means that the fluidization conditions within the bed may be less homogenous in a conical bed. In addition, the van Ommen studies utilized sand having a particle density of 2700 kg/m^3 while our study utilizes pharmaceutical granule having a particle density of 1100 kg/m^3.

3.5.2 Dry Bed Studies

Figure 3.2 shows the behaviour of the S-statistic at three dry bed masses and three superficial gas velocities. For each superficial velocity, a reference state was chosen from one of the triplicate runs performed at the bed loading of 1.44 kg. The figure shows

statistically significant variations in bed state between the reference state at 1.44 kg and the other bed masses. Less variation is noted at the highest superficial gas velocity (3.41 m/s) compared to the lower gas velocity (1.46 m/s). This result indicates that the variations in hydrodynamics associated with changes in bed mass become less intense at higher superficial gas velocities as noted by Chaplin et al. [18].

Figure 3.3 demonstrates the changes in the S-statistic with changes in PSD in a 2 kg dry bed. One reference time series is chosen from PSD 1 at each superficial gas velocity. Two evaluation sets at the same velocity and PSD (PSD 1) demonstrate the comparison to a bed under identical fluidization conditions (PSD and superficial velocity) to the reference state (black circles). Three evaluation data sets from the second PSD (PSD 2) have also been compared to the reference state at each superficial gas velocity (open circles). There is a significant change in the S-statistic accompanying the shift in particle size distribution between PSD 1 and PSD 2 but more uniformity between the beds is evident at higher superficial gas velocities. Uniformity at high superficial velocities may be consistent with a segregation effect. At superficial gas velocities below 2.6 m/s, larger particles were found at the base of the vessel after shutdown. At higher superficial gas velocities, these larger particles become involved in the fluidization and the bed is more uniformly mixed. The rather large change in PSDs studied here would be unlikely to arise from batch-to-batch variations in wet granulation. Hence, we conclude that the chaos analysis of the fluidized bed dryer operated at high gas velocities will not be strongly influenced by slight changes in PSD between the batches of granule prepared in our experiments.

3.5.3 Drying Studies

Figure 3.4 shows the progression of bed moisture and temperature for a typical drying experiment. Outlet air temperature is also included. The bed and outlet temperatures remain constant throughout the experiment, increasing only towards the end of the experiment. This increase signifies the loss of surface moisture from the particles. After this loss of surface moisture, the drying rate decreases. However, this data shows that the falling-rate period does not occur over a significant portion of the drying curve. The lack of a significant falling-rate period demonstrates the efficiency of the drying process under highly turbulent fluidization conditions and highlights the need to determine the drying endpoint accurately. Moisture content curves for all experimental runs exhibit the similar profile to that in Figure 3.4. Drying time was increased with lower inlet air temperature and higher bed mass.

For each factorial drying experiment, a pressure time-series was recorded for the duration of the drying experiment. From the original 45-90 minutes of data (depending on the experimental conditions), successive time segments of two minutes were transformed into a single S-statistic value. Two minute data sets were selected as was done in the work of van Ommen [1, 2] for the application of the S-statistic to fluidized beds. Reference time series for the statistic were chosen for two moisture contents: 26-wt% and 8-wt%, corresponding to two separate points in time near the beginning and toward the end of drying. If a change in state results from a change in moisture, these points (hydrodynamic states) should demonstrate this effect when they are compared to all other points in the data set using the S-statistic. Figure 3.5 shows the typical behaviour of the S-statistic when referenced to these two moisture contents. The S-

statistic referenced to 26-wt% exhibits hydrodynamic consistency ($S<3$) at the start of drying and then diverges from that state as moisture is driven from the granules. The value of the statistic increases continuously before becoming constant at a later time. When the S-statistic is referenced to 8-wt% moisture, its value is initially far away from 3 but gradually reaches a value less than 3 near the end of drying. This point in time coincides closely with the time where the S-statistic becomes constant when referenced to 26-wt% moisture, and the time at which the bed and outlet temperature begins to rise (see Figure 3.4). It would appear therefore, that the S-statistic is sensitive to the changes in bed hydrodynamics arising from the loss of surface moisture.

Visual observations through the acrylic insert provided further insight into the hydrodynamic changes occurring during drying. A central core of bubbles was observed in the very wet bed. This behaviour coincides with the initial periods of more gradual change in hydrodynamic state seen in Figure 3.5. After this early behaviour, the entire bed exhibited more homogeneous fluidization for the remainder of the drying process, indicated by the presence of bubbling action near the viewing window. Experiments planned by our group to image the bed using a tomographic technique may reveal the details of this behaviour and its relationship to bed moisture content more clearly.

In assessing the performance of the S-statistic in response to the variables of inlet air temperature and bed mass, it is necessary to normalize the responses with respect to time. The fact that drying times will be significantly shorter at higher inlet air temperatures and lower bed masses is the motivation behind this normalization. Since the intention of this study is to examine the performance of the S-statistic with changes in moisture, and moisture decreases in a similar manner in each experiment, this

normalization is a reasonable approximation to the ideal on-line measurement of moisture. Since sensor positioning did not have an impact on the rate of drying, the S-statistic results for this variable did not require the above normalization. Therefore, the results from this factorial variable may be presented in terms of absolute time. The effect of sensor position on the performance of the S-statistic in the drying process is demonstrated in Figure 3.6. Sensor position can be seen to have no effect on the performance of the test over the measurement heights examined.

In Figure 3.7 we can see that, when referenced to 8-wt%, the behaviour of the S-statistic is identical for the high and low inlet air temperatures when compared at normalized times. However, since lower inlet temperatures resulted in longer drying times, the appearance of the second period of more gradual change in hydrodynamic state corresponds to a later absolute time when drying at a lower inlet air temperature. This behaviour indicates that the S-statistic is responding to the changes in bed hydrodynamics arising from changes in moisture within the bed.

The variation in the behaviour of the first period of more gradual change in hydrodynamic state shows no consistent trend over the factorial variables examined. Furthermore, the factorial baseline runs also exhibit more variation in the first period of more gradual hydrodynamic change than in the second. Therefore, the first period of more gradual hydrodynamic change, while appearing in each experiment does not persist for a predictable interval. Because of this inconsistency, the behaviour of the initial period of more gradual change was ignored in the factorial analysis. Nevertheless, the curves referenced to the initial state are included in the all the drying data figures for illustrative purposes. In addition, the presence of this initial period of more gradual

change in state, while not exhibiting consistent behaviour over the factorial runs, represents a distinct operating regime as noted in the visual observations above. It was noted that the bubbling behaviour did not appear near the wall at any specific experimental time. In contrast, the behaviour of the second period of more gradual hydrodynamic change is closely related to experimental time and therefore moisture.

Figure 3.8 shows the influence of bed mass on the S-statistic. The influence of bed mass on the second period of more gradual change in state is clear. With a lower bed mass, the second period of more gradual change in state appears at a shorter relative time compared to a higher bed mass. It follows that the second period of more gradual hydrodynamic change occurs for a longer duration of the drying process for a bed of lower mass. The S-statistic results presented in Figure 3.2 demonstrated that a significant change in fluidization state was caused by a 35 to 40-wt% change in dry bed mass. Since a similar change in bed mass occurs with moisture loss during drying, one would expect the change in the S-statistic to be of the same order of magnitude as that seen in Figure 3.2 if the S-statistic was simply responding to a bed mass. However, the change in the S-statistic is between 30 and 40, indicating a greater difference between the initial and final state of the bed. This is further evidence that the change in moisture, not bed mass, dominates the changes in bed hydrodynamics seen in the drying process.

The results from the S-statistic analysis of the pressure fluctuations presented above show strong influence of moisture on the system state. This effect is larger than the changes noted with variations in superficial gas velocity, PSD and bed mass. Sensitivity of the test statistic to moisture changes provides a means of quantifying the

changes occurring during the drying process without the use of the direct measurement of moisture.

Figures 3.9 through 3.11 examine the dominant frequency and standard deviation responses for the factorial drying data. As in the S-statistic analysis, the impact of the parameters of sensor position, inlet temperature and bed mass were assessed. Inlet temperature and bed mass data were normalized in the same manner as was described for the S-statistic with a dimensionless time of one indicating experimental completion. In each experiment, standard deviation increased throughout the drying process. Wright and Raper [10] show that a reduction in the standard deviation accompanied the increase in particle liquid loading. Although the liquid loadings and superficial gas velocities examined in their study were much lower than those encountered in our study, the consistent trend is still suggestive that the decrease in the liquid bridging between particles throughout the drying process is the cause of the large hydrodynamic change identified.

Figure 3.9 demonstrates the typical variation in dominant frequency and standard deviation at the different sensor positions investigated. The dominant frequency remains consistent at approximately 2.8 Hz after a brief startup period at approximately 5 Hz. The elevated superficial gas velocity utilized initially in the drying experiment may be the cause of this initial trend. However, no connection between this startup operation and the initial period of more gradual change in hydrodynamic state was identified by the S-statistic. The constant dominant frequency with changing moisture is consistent with the findings of McLaughlin and Rhodes [3]. Their study noted a similar dominant frequency in pressure fluctuations collected in beds at moisture loadings of less than 6-wt%.

Although our total liquid loadings are much higher, the pharmaceutical granule used in our study has approximately 30% void space. Therefore, the surface moisture is most likely similar.

Unlike the S-statistic, the standard deviation is affected by sensor position. Standard deviation is highest at the top sensor position. This does not conform to the work of van der Schaaf et al. [3] that identified larger amplitude variations lower in the bed. This discrepancy may be a result of the conical geometry of the vessel, which allows for the expansion of the dilute phase as it migrates through the bed thereby intensifying the surface eruptions. Imaging of both a dry and drying bed utilizing a tomographic technique in a conical vessel would clearly demonstrate this effect.

Figure 3.10 demonstrates the effect of changes in inlet temperature on standard deviation and dominant frequency. As with the S-statistic, this variable has no influence on these parameters. Only the drying time, not the progression of the system hydrodynamics, is influenced by inlet temperature

In Figure 3.11, we see the effect of bed mass on the standard deviation and dominant frequency. While the standard deviation exhibits no significant change at the different bed loadings, the dominant frequency measured in the final dry bed shows a distinct shift to a lower bubbling frequency at higher bed loadings. It is noted that dominant frequency is consistent between both bed masses at higher moisture contents. This indicates that the moisture dominates the bed dynamics at higher moisture contents. At lower moisture, the effect of bed mass has a more significant effect on bed

hydrodynamics. This sensitivity to bed mass is consistent with the results shown in both Figure 3.2 and Figure 3.8.

3.6 Conclusions

A factorial set of drying experiments was carried out in a fluidized bed dryer in which the influence of inlet air temperature, initial wet bed mass and pressure sensor position on bed pressure fluctuations was examined. Time series of absolute pressure fluctuations were analyzed with the S-statistic test of van Ommen [1] as well as frequency analysis and standard deviation. Additional experiments were undertaken in a dry bed to assess the influence of changes in bed mass and particle size distribution on the S-statistic.

Two regions of gradual hydrodynamic change in state were identified when the pressure fluctuations from the drying bed were analyzed with the S-statistic. These regions were separated by a region of more rapid change. These regions of gradual hydrodynamic change could not be identified with standard deviation or dominant frequency. The first period of gradual hydrodynamic change occurs near the start of the drying experiment and lasts for variable lengths of time depending on bed height and temperature. The second period of gradual hydrodynamic change identifies the consistent behaviour of a dry bed toward the end of each experiment. Performance of the second period of gradual change in hydrodynamic state is only influenced by bed mass with a longer period of consistent behaviour apparent with lower bed loadings. Comparison of the onset of second period of gradual change in hydrodynamic state with the drying curves and profiles of bed temperature as a function of time indicates that the

S-statistic is sensitive to hydrodynamic changes in the bed arising from the loss of moisture from the granules.

From the performance of the S-statistic in a dry bed of changing mass, it is clear that changes in bed hydrodynamics are a strong function of the reduction in moisture during the drying process. Standard deviation increased throughout the drying process. This is consistent with the reduction in the cohesion caused by the presence of surface moisture. A lower bubbling frequency was apparent near the end of the drying experiment for an elevated bed mass.

The fact that the S-statistic could discern hydrodynamic changes not apparent utilizing the techniques of frequency and amplitude analysis shows the advantage of the application of the S-statistic to the fluidized bed drying process. What is of particular benefit is the response of the technique to the moisture content of the bed. While the disturbances such as PSD and superficial gas velocity also influence the S-statistic, the bed moisture content is the parameter to which it responds most intensely.

The response of the S-statistic to moisture changes resulting from hydrodynamic state changes not only provides for new means of tracking moisture content within the bed but also allows for the identification of a specific hydrodynamic state at any point in the drying process. This tracking of the hydrodynamic state can be utilized as an input for control loop used to maintain a desired fluidized state by manipulating the superficial gas velocity. Utilizing the correct superficial gas velocity throughout the drying process will optimize drying time and product quality.

3.7 Acknowledgements

The authors would like to thank Merck Frosst Canada & Co. (Montreal) and the Natural Sciences and Engineering Research Council of Canada (NSERC) for their financial support. We also gratefully acknowledge Helen Tanfara of Merck Frosst Canada & Co. for her technical assistance in running the fluid bed dryer and Dr. Ruud van Ommen, Delft University of Technology for consultation regarding the implementation of the S-statistic.

3.8 Nomenclature

d	Bandwidth for the smoothing in state space (nondimensional)
g	Function defined by Equation 11 (nondimensional)
H	Function defined by Equation 10 (nondimensional)
$h(Z_i,Z_j)$	Function defined by Equation 5 (nondimensional)
h'	Average value of h over $L \times L$ pairs of Z_i, Z_j (nondimensional)
L	Segment length (seconds or nondimensional)
m	Embedding dimension (nondimensional)
N	Number of segments in set Z (nondimensional)
N_1	Number of segments is set X (nondimensional)
N_2	Number of segments in set Y (nondimensional)
N_P	Number of pressure readings in the time series (nondimensional)
p_i	Pressure measurement (Pa)
Q	Squared distance between two attractors (nondimensional)
$\hat{Q}$	Estimator for the squared distance between two attractors (nondimensional)
R	State space variable defining one point in m-dimensional space
S	Normalized estimator of the squared distance between two attractors in state space (nondimensional)
V_C	Conditional variance (nondimensional)
X_i	Vector of normalized pressure values in reference time series (nondimensional)
x_i	Normalized pressure reading in reference time series (nondimensional)
Y_i	Vector of normalized pressure values in evaluation time series (nondimensional)
y_i	Normalized pressure reading in evaluation time series (nondimensional)
Z_i	Sequential combination of vectors X_i and Y_i (nondimensional)

Greek

$\rho_x(X_i)$	Probability distribution of set X_i (nondimensional)
$\rho_x'(X_i)$	Smoothed probability distribution of set X_i (nondimensional)
ψ_{pq}	Function defined by Equation 9 (nondimensional)
μ	Mean for a data set of pressure fluctuations (Pa)
σ_P	Standard deviation of data set of pressure fluctuations (Pa)

Subscripts

eval	Evaluation data set
ref	Reference data set

3.9 References

1 van Ommen, J.R., *Monitoring fluidized bed hydrodynamics*, PhD. Thesis, Delft University of Technology, (2001).

2 van Ommen, J.R., Coppens, M.C., van Den Bleek, C.M., Schouten, J.C., *Early warning of agglomeration in fluidized beds by attractor comparison*, AIChe J., 46(11), 2183-2197, (2000).

3 van der Schaaf, J., Schouten, J.C., van den Bleek, C.M., *Origin, propagation and attenuation of pressure waves in gas-solid fluidized beds*, Powder Tech., 95(3), 220-233, (1998).

4 Chong, Y.O., O'Dea, D.P., White, E.T., Lee, P.L., Leung, L.S., *Control of the quality of fluidization in a tall bed using the variance of pressure fluctuations*, Powder Tech., 53(3), 237-246, (1987).

5 Saxena, S.C., Rao, N.S., Tanjore, V.N., *Diagnostic procedures of establishing the quality of fluidization of gas-solid systems*, Exp. Ther. and Fluid Sci., 6(1), 56-73, (1993).

6 Trnka, O., Vesely, V., Hartman, M., *Identification of the state of a fluidized bed by pressure fluctuations*, AIChe J., 46(3), 509-514, (2000).

7 Karamavruç, A.I., Clark, N.N., Halow, J.S., *Application of mutual information theory to fluid bed temperature and differential pressure analysis*, Powder Tech., 84(3), 247-257, (1995).

8 Johnsson, F., Zijerveld, R.C., Schouten, J.C., van den Bleek, C.M., Leckner, B., *Characterization of fluidization regimes by time-series analysis of pressure fluctuations* Int. J. Multiphase Flow, 26(4), 663-715, (2000).

9 McLaughlin, L.J., Rhodes, M. J., *Prediction of fluidized behaviour in the presence of liquid bridges*, Powder Tech., 114(1-3), 213-223, (2001).

10 Wright, P.C., Raper, J.A., *Examination of dispersed liquid-phase three-phase fluidized beds Part 1. Non-porous uniform particle systems*, Powder Tech., 97(3), 208-226, (1998)

11 Briens, C., McDougall, S., Chan E., *On-line detection of bed fluidity in a fluidized bed coker*, Powder Tech., 138(2-3), 160-168, (2003).

12 Daw, C.S., Finney, M.V., van Goor, K.N., Bruns, D.D. Kostlelich, E.J., Grebogi, C., Ott, E., Yorke, J.A., , *Self-organization and chaos in a fluidized bed*, Phys. Rev. Let., 75(12), 2308-2311, (1995).

13 Bai, D., Bi, H.T., Grace, J.R., *Chaotic behaviour of fluidized beds based on pressure and voidage fluctuations*, AIChE J., 43(5), 1357-1361, (1997).

14 Bai, D., Issangya, A.S., Grace, J.R., *Characteristics of gas-fluidized beds in different flow regimes*, Ind. Eng. Chem. Res., 38(3), 803-811, (1999).

15 Hay, J.M., Nelson, B.H., Briens, C.L., Bergougnou, M.A., *Calculation of the characteristics of a chaotic attractor in a gas-solid fluidized bed*, Chem. Eng. Sci. 50(3), 373-380, (1995)

16 Takens, F., *Detecting strange attractors in turbulence*, Lecture notes in Mathematics, 878, Springer-Verlag, 336-381, (1981).

17 Diks, C., van Zwet, W.R., Takens, F., DeGoede, J., *Detecting differences between delay vector distributions*, Phys. Rev. E., 53(3), 2169-2176, (1996).

18 Chaplin, G., Pugsley, T., Winters, C., *Application of chaos analysis to fluidized bed drying of pharmaceutical granule*, in ***Fluidization XI: Present and Future for Fluidization Engineering***, U. Arena, R.Chirone, M. Miccio and P. Salatino, eds., Engineering Foundation, New York, 419-426, (2004). [Chapter 2]

19 Schouten, J.C., Takens, F., van den Bleek, C.M., *Estimation of the dimension of a noisy attractor*, Phys. Rev. E. 50(3), 1851-1861, (1994).

Table 3.1 Wet Placebo Granule Formulation

Component	Percentage by mass (dry basis)
Lactose Monohydrate (filler)	50%
Microcrystalline Cellulose (filler)	44%
Croscarmellose Sodium (disintegrant)	2%
Hydroxypropyl Methylcellulose (binder)	4%
USP Water*	42%

*Water used conformed to the USP (United States Pharmacopeia) standard for purity

Table 3.2 Particle size distributions compared in the PSD study

			PSD 1	PSD 2
Mesh No. (-)	**Sieve Opening (μm)**	**Mean Particle diameter (μm)**	**Mass Percent on sieve (%)**	**Mass Percent on sieve (%)**
10	2000	>2000	5.41	5.14
18	1000	1500	3.49	2.52
35	500	750	7.34	1.26
60	250	375	46.29	9.73
120	125	187.5	33.71	55.14
200	75	100	3.23	23.96
325	45	60	0.52	2.16
pan	0	<45	0.00	0.09

Table 3.3 Parameters for the S-statistic

Time window	0.1 seconds
Embedding (m)	40
Bandwidth (d)	0.5
Segment Length (L)	3 seconds

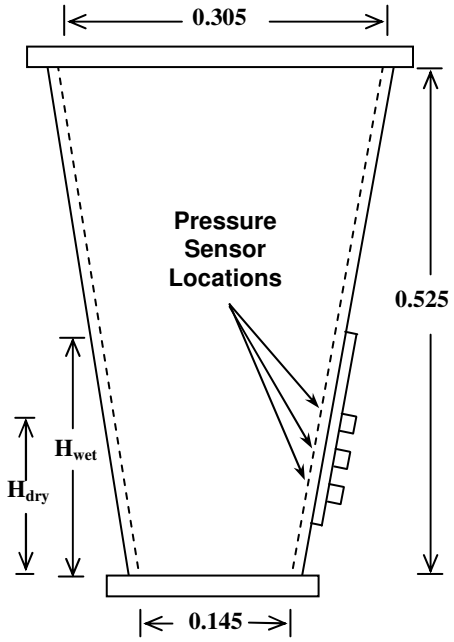

Figure 3.1 Schematic of the GPCG1 product bowl. Dimensions are given in meters. H_{wet}, H_{dry} represent approximate settled bed heights for wet and dry beds for a typical experiment and indicate complete coverage of the sensor at all sensor positions. The sensor positions used were at 9, 10.9 and 12.8 cm above the distributor.

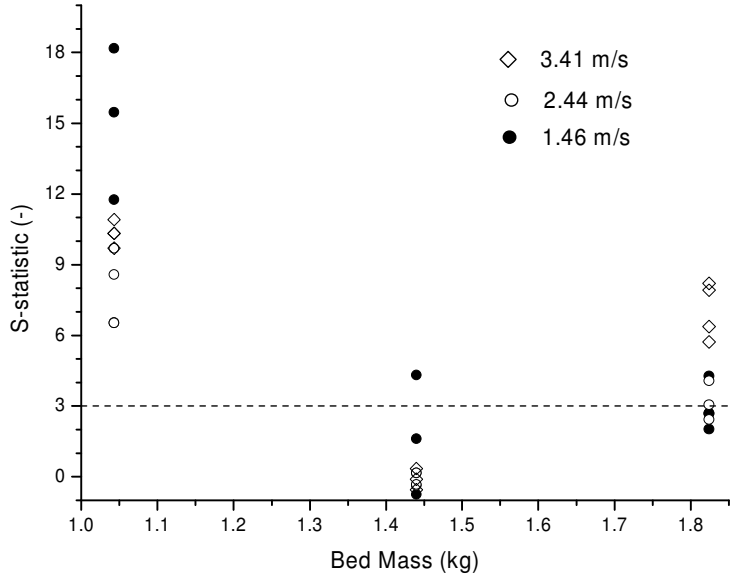

Figure 3.2 Response of the S-statistic to changes in bed mass (dry bed). Reference state chosen at 2.44 m/s and 1.44 kg.

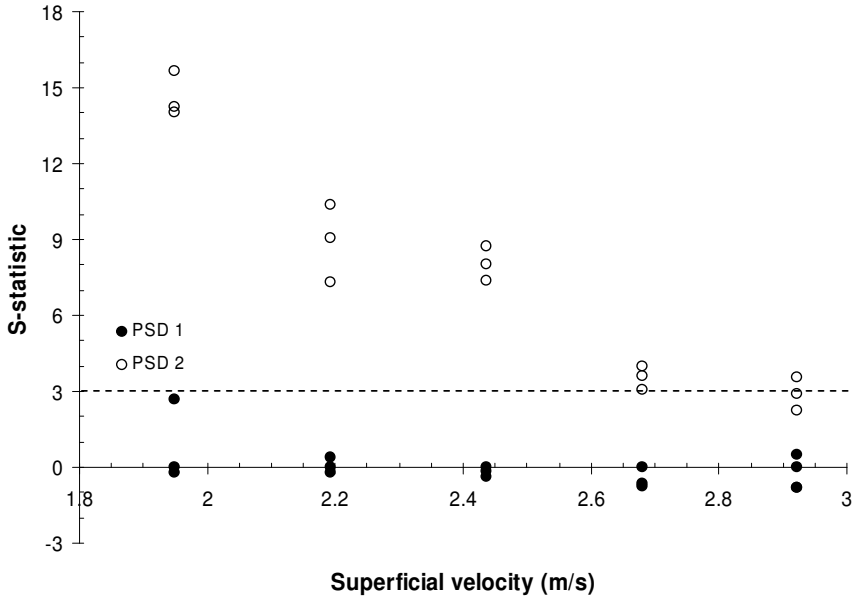

Figure 3.3 Sensitivity of the S-statistic to changes in particle size distribution at the bottom sensor position. Reference state chosen from PSD 1 at each superficial gas velocity. Bed mass is 2 kg (dry)

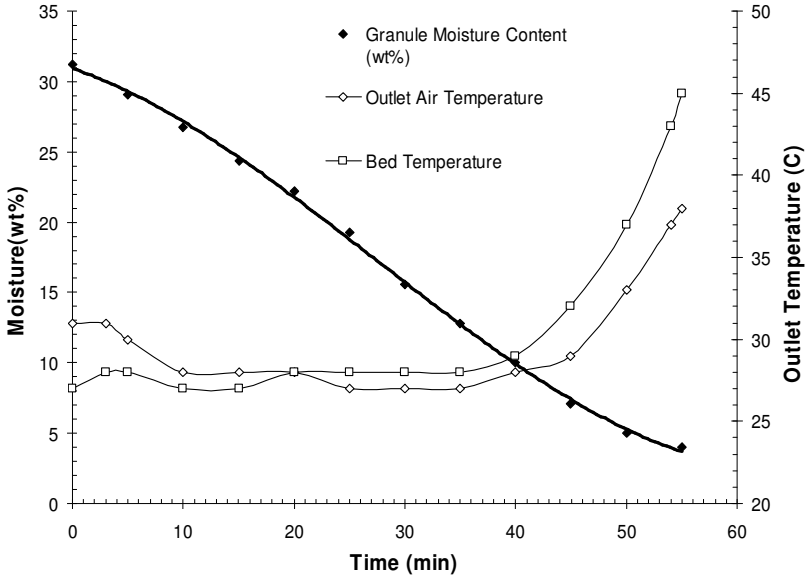

Figure 3.4 Progression of outlet air and product temperature as well as product moisture content for factorial baseline (3 kg initial mass, inlet temperature of 65°C and middle sensor position).

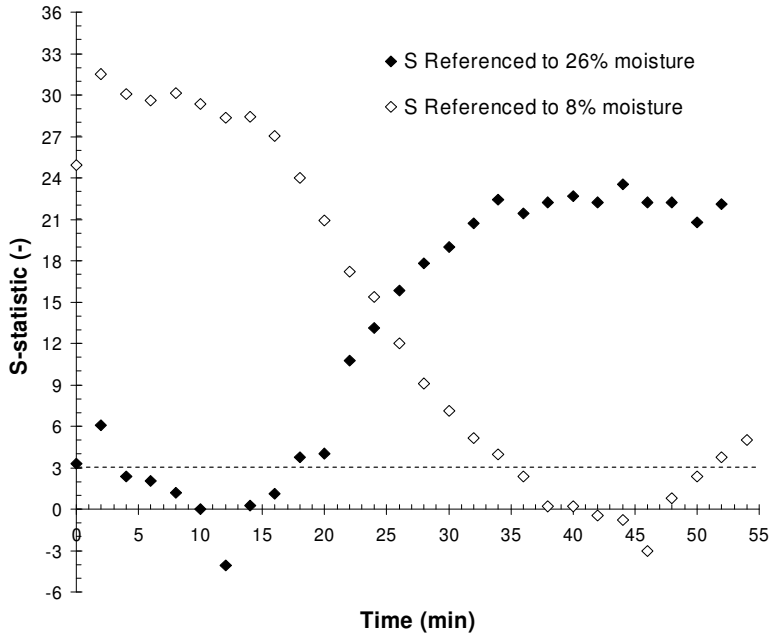

Figure 3.5 S-statistic plot for the same drying experiment shown in Figure 3.4. An S value of 3 represents a statistically significant change. Reference states were chosen at 8 and 26 wt% moisture.

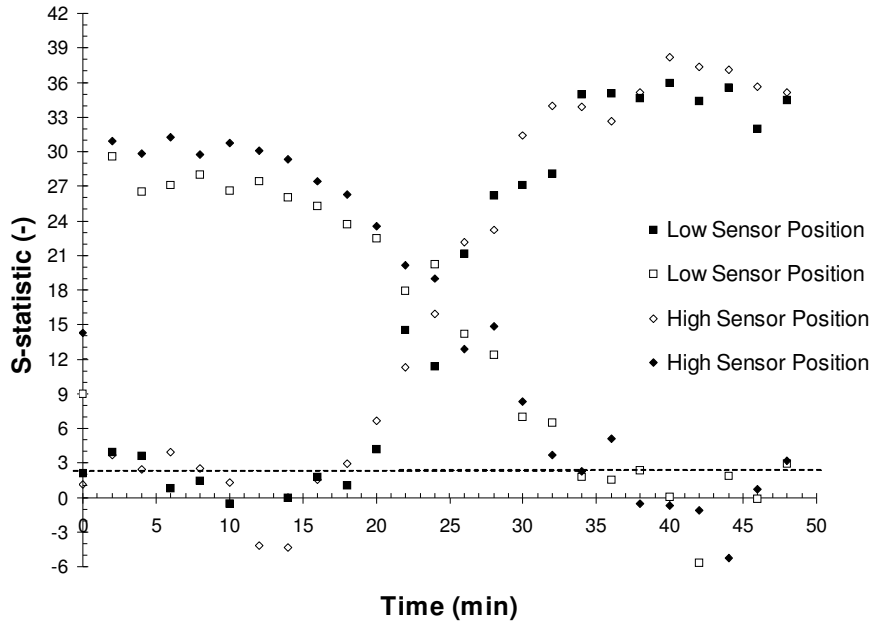

Figure 3.6 S-statistic results for changes in sensor position for a sample factorial drying experiment. Low and high sensor positions are the top and bottom sensor positions (9.0 cm and 12.8 cm above the distributor).

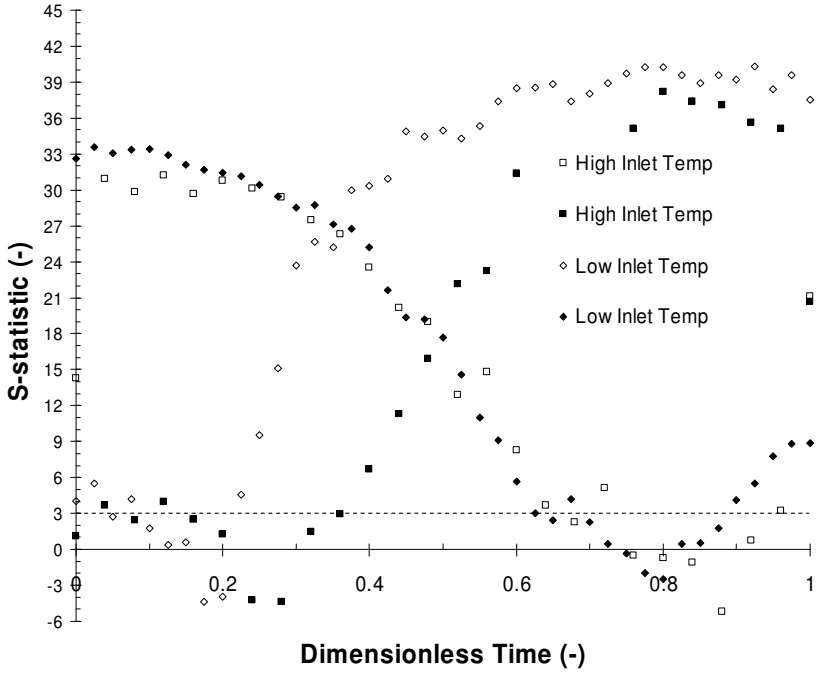

Figure 3.7 S-statistic results for changes in inlet temperature for a sample factorial drying experiment. Low and high temperatures are 55°C and 75°C.

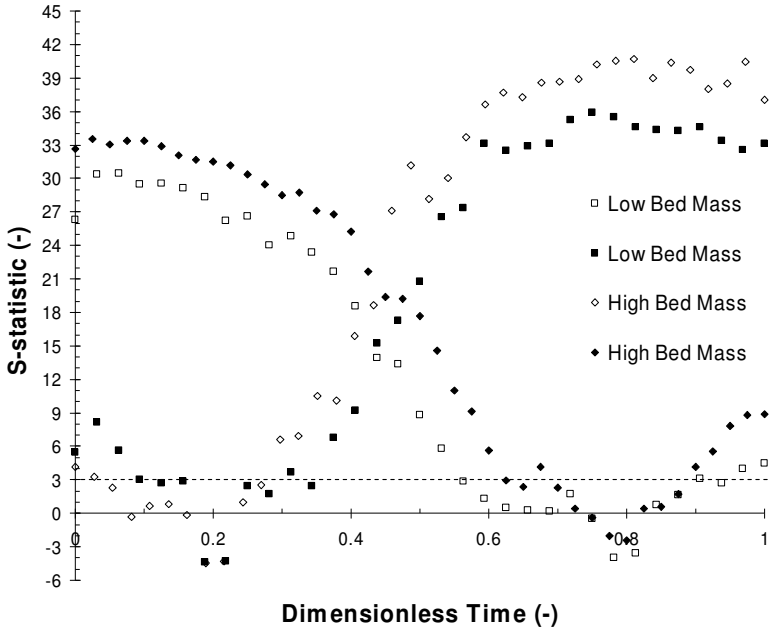

Figure 3.8 Factorial S-statistic results for changes in bed mass for a sample factorial drying experiment. High and low bed masses of 3.25 kg and 2.75 kg are compared.

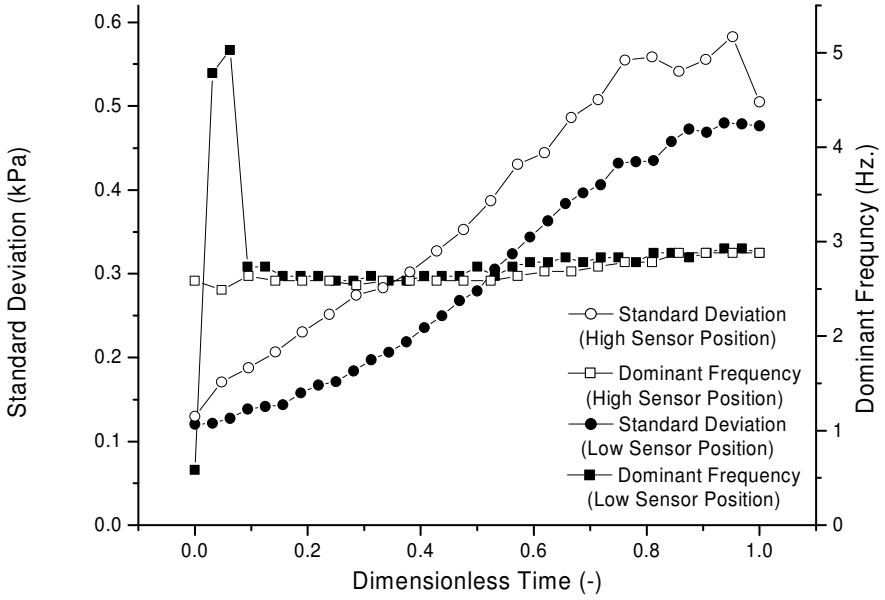

Figure 3.9 Standard deviation and dominant frequency results for changes in sensor position for a sample factorial drying experiment. Low and high sensor positions (9.0 cm and 12.8 cm above the distributor) are compared.

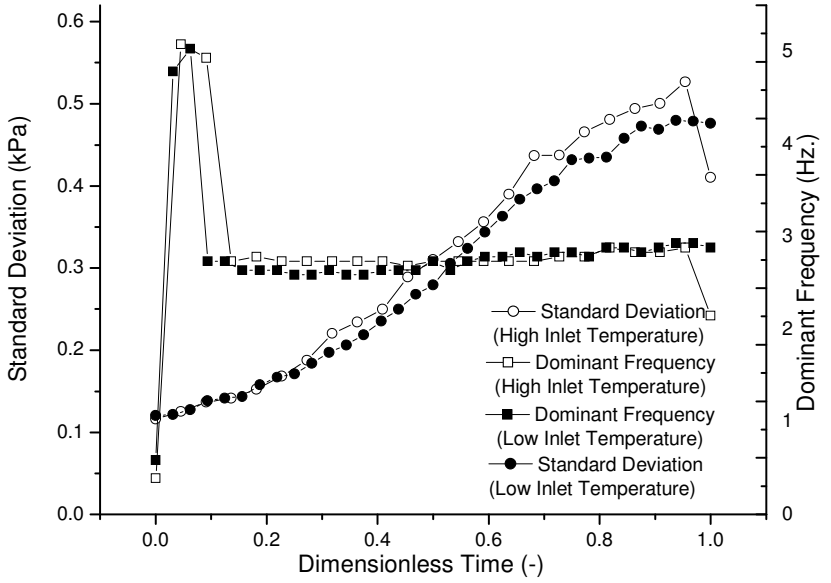

Figure 3.10 Standard deviation and dominant frequency results for changes in inlet temperature for a sample factorial drying experiment. Low and high temperatures are 55°C and 75°C.

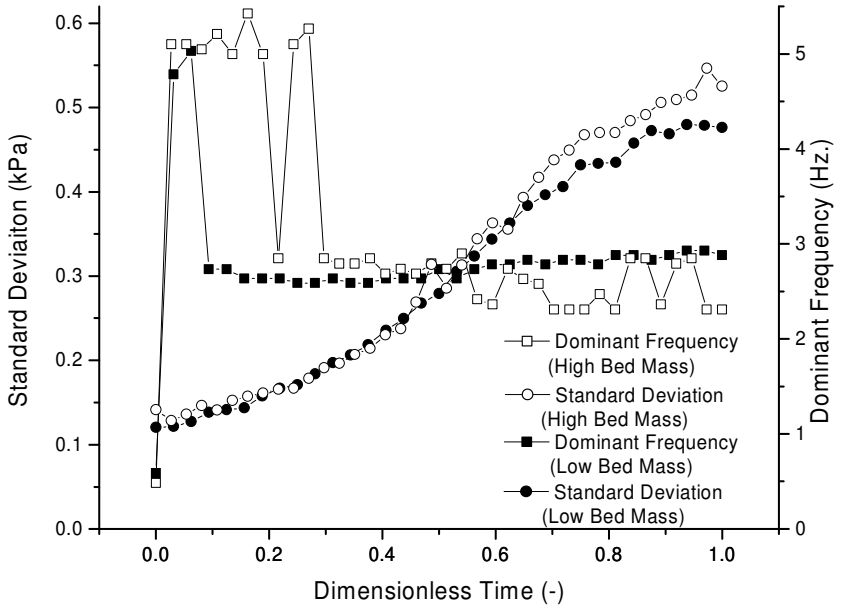

Figure 3.11 Standard deviation and dominant frequency results for changes in bed mass for a sample factorial drying experiment. High and low wet bed masses of 3.25 kg and 2.75 kg are compared.

Chapter 4 - The S-statistic as an Early Warning of Entrainment in a Fluidized Bed Dryer Containing Pharmaceutical Granule

This chapter has been slightly modified from the publication which appears in the journal ***Powder Technology***. The reference is given as the following:

Citation

Chaplin, G., Pugsley, T., Winters, C., *The S-statistic as an early warning of entrainment in a fluidized bed dryer containing pharmaceutical granule,* Powder Tech. 149(2-3), 148-156, (2005).

Contribution of PhD Candidate

With the exception of the product bowl, the design of the experimental apparatus was done by Gareth Chaplin. Todd Pugsley provided consultation regarding the design procedure. Construction of the apparatus was done by G. Chaplin with the exception of the fabrication of the acrylic elements and the windbox which were prepared in the engineering shops at the University of Saskatchewan. G. Chaplin was also responsible for installing the instrumentation (pressure transducer, thermocouples and load cell). The programming of the data acquisition interface designed in Labview was also done by G. Chaplin. Experiments were planned and performed by G. Chaplin. T. Pugsley and C. Winters provided consultation regarding the experimental program. All of the writing of the submitted manuscript was done by G. Chaplin with T. Pugsley and Conrad Winters

(Director, Formulation Development (PR&D) providing editorial guidance regarding the style content of the paper.

Contribution of this Paper to the Overall Study

From chapters 2 and 3, the applicability of the S-statistic analysis to pressure fluctuations in a drying fluidized bed has been clearly demonstrated. These papers indicate that the S-statistic responds strongly to changes in hydrodynamic state resulting from the loss of moisture from the granules during the drying process. In contrast, the effect of both particle size distribution and velocity were found to have a smaller impact on hydrodynamic behaviour. Furthermore, the variables of inlet temperature and sensor positioning were found not to influence the performance of the test. For experiments in this chapter, inlet temperature was maintained at a constant value. However, air humidity was neither monitored nor controlled. Since bed mass was found to influence the changes in hydrodynamic behaviour identified by the S-statistic, this parameter was the only variable manipulated.

This paper examines the application of the S-statistic for the early identification of the undesirable state associated with entrainment. The apparatus used has been fitted with a load cell in order to measure the quantity of fines entrained. This measurement was not made in the experiments performed for chapters 2 and 3. The entrainment of fines is a concern for the drying of pharmaceutical granule since the material entrained is a portion of the product. Therefore, entrainment can translate into a reduction in batch yield. The goal of this investigation is to exploit the response of the S-statistic to changes in hydrodynamic state as an early warning for entrainment.

Additional Experimental Details

The experimental apparatus used in this experiment was constructed around an existing conical acrylic section (product bowl) and windbox of an existing laboratory-scale fluidized bed dryer. This dryer was supplied by Merck Frosst and was only capable of superficial gas velocities between 0.05 m/s and approximately 1 m/s in a bed of dry pharmaceutical granule. The limitation was due to the small capacity of the built-in 0.75 kW fan. Superficial gas velocities of 2-3 m/s were required in the current study in order to provide good mixing throughout drying and handle quantities of granule similar to those investigated in chapters 2 and 3. This was the motivation for the modification of the existing apparatus.

Specific additions to the setup included the use of a more powerful 2 kW blower to deliver the required air flow. An orifice meter was designed to measure air flow. Air was heated in a 2 kW circulation air heater in order to achieve inlet temperatures consistent with those examined in chapters 2 and 3. The apparatus was also instrumented with thermocouples for the measurement of bed and outlet temperatures as was done in chapters 2 and 3. A transport disengagement height (TDH) was also designed to allow for the expansion of the bed and return of the majority of the fine particles to the bed. This design is also in line with the design of the apparatus presented in chapter 2 and 3. A difference in the design of this apparatus and that presented previously is the use of a cyclone for the cleaning of the outlet air stream. The particles collected from this device were not returned to the bed as was done in the apparatus in chapters 2 and 3 but collected on a load cell for the quantification of entrainment.

Granulations were performed using a 250 W Kitchen-Aid Classic mixer. This apparatus differs from the high-shear granulator presented in chapter 2 in that the rotation speed of the impeller in this appliance is much lower than that in the Fielder industrial unit. Therefore, the dry ingredients are subjected to a much lower shearing force. For this reason, this device is classified as a low-shear granulator. Low-shear granulators have been used historically in the pharmaceutical industry for the production of pharmaceutical granules and for certain contemporary laboratory investigations. Tables 3.2 and 6.2 give the particle size distribution of the pharmaceutical granules produced by high-shear granulation at Merck Frosst laboratories and low-shear granulation at the University of Saskatchewan, respectively. Differences exist in the properties of the granules produced by these devices. For example, the granules produced by low-shear granulation have a wider distribution compared to those produced by high-shear granulation. However, the quality of the granules produced by the low-shear granulator was acceptable for the determination of changes in bed hydrodynamics during the drying process.

Several differences exist between this apparatus and the laboratory-scale apparatus used in as the Merck Frosst laboratories presented in chapters 2 and 3. The removal of fines from the bed using the cyclone as mentioned above differs from the return of particles to the bed using the shaking of the filter bags. Distributor design differed in that a drilled aluminium plate was used here as opposed to the wire mesh distributor used in chapters 2 and 3. The product bowl also differs in cone angle from the dryer introduced in chapters 2 and 3. Preliminary tests in this apparatus showed that a discernable response occurred in the S-statistic during the drying process. This

confirmed the applicability of this test to pressure fluctuations collected in this apparatus. These preliminary tests also indicated that sensor positioning did not affect the performance of the S-statistic in this apparatus.

The S-statistic analysis of the pressure fluctuation data was performed with the identical Matlab programs used in chapters 2 and 3. These programs are presented in Appendix A. As in chapters 2 and 3, the use of frequency and amplitude analysis was found to give little useful information concerning hydrodynamic changes encountered in the drying process and the results of these signal analysis techniques are not presented.

The effect of superficial gas velocity on the S-statistic has not been fully quantified and is a topic of future research. As in chapters 2 and 3, a constant superficial gas velocity was utilized throughout the majority of the drying process. This period of constant superficial gas velocity was the only portion of the drying experiment considered in the identification of hydrodynamic changes.

4.1 Abstract

The chaotic attractor comparison technique known as the S-statistic has been applied to pressure fluctuation data collected in a lab-scale fluidized bed dryer containing pharmaceutical granule. Along with pressure fluctuations, this unit has also been instrumented for measurements of bed temperature and fines entrainment. It has been determined that an increase in bed temperature, corresponding to the loss of granule surface moisture, occurs simultaneously with the onset of entrainment at a granule moisture content of approximately 11 wt%. The S-statistic analysis is able to give an early warning for the undesirable hydrodynamic state where entrainment occurs provided an appropriate reference state is chosen. When a reference state of 10 wt% moisture was chosen, a statistically similar hydrodynamic state was identified by the S-statistic occurring 8 to 9 minutes prior to the onset of entrainment, thus providing an early warning of this change. The monitoring of bed temperature alone provides no such early warning that entrainment is imminent. With further development, the S-statistic could become a valuable monitoring and control tool for the drying of granular material.

4.2 Introduction

The batch-wise drying of pharmaceutical granule in a fluidized bed is an important step in the production of certain solid-dosage pharmaceuticals. The dryer product bowl is often conical and excellent gas-solid contacting is maintained by operation of the unit at superficial gas velocities well in excess of the minimum fluidization velocity. In this process, granule is dried from approximately 30-wt% to 2-wt% moisture, with the endpoint of drying determined by monitoring the outlet air or product temperature for an increase near the end of drying caused by the loss of moisture

from the granule. Reaching a limiting value for either one of these temperatures signifies the endpoint. Evidently this does not give any direct indication of bed hydrodynamics.

Fluidizing gas velocity affects the bed hydrodynamics, and can be utilized for the manual control of the drying process. Currently, the selection of appropriate superficial gas velocity is at the discretion of the operator with control decisions made based on visual observation of the fluidization behaviour through a sight-glass. No automatic control mechanism is implemented. The optimum superficial gas velocity for operation of the fluidized bed dryer may not be clear to an operator based on visual observations alone. Furthermore, batch-to-batch variations in bed loading and product particle size distribution may result in differing observed bed behaviour. While manual control of fluidization hydrodynamics results in an acceptable product quality for the drugs currently manufactured, there is concern that segregation of larger granules, entrainment of finer granules, and granule attrition could impact the quality of the drug product. High-potency or peptide-based drug products may be even more severely affected by these phenomena. Since attrition, segregation and entrainment arise from gas-particle and particle-particle interactions, a better understanding and control of bed hydrodynamics will lead to a lessening of these effects. Bed hydrodynamics also impact the homogeneity of the moisture within the bed at the end of drying. Operation of the bed at an optimum fluidized state allows for more uniform treatment of the granule within the bed, leading to uniform product.

One method of quantifying the hydrodynamic state within a fluidized bed is the time-series analysis of high-frequency pressure fluctuations collected from the bed. The sources of these fluctuations include the passage of bubbles, bulk oscillations of the bed,

and fluctuations in the fluidizing air supply. These effects will be influenced by changes in particle density as well as particle-particle interactions. Therefore, variations in the moisture content of the bed will influence the fluidized bed behaviour. Since pressure fluctuations are transmitted throughout the bed [1], they represent a global measurement of the fluidized bed dynamics. This global nature of the measured signal means that all the dynamic effects inherent in the fluidized system are expressed through the sampling of a single variable.

One technique of analysis applied to a pressure time-series is frequency analysis. Example of the application of this technique to pressure fluctuations collected in fluidized beds include Saxena et al. [2] and Kage et al. [3]. These studies identify the influence of fluidization regime on the frequency and intensity of the pressure fluctuations. Furthermore, these studies indicate the presence of multiple frequencies in the pressure fluctuation data. These frequencies can be influenced by superficial gas velocity [2, 4] or remain constant with increasing superficial gas velocity [3, 4].

The identification of changes in chaotic parameters from a time-series in a fluidized system is possible through reconstructed attractors. One technique for this is the use of correlation dimension [5]. The work of Bai et al. [6] identifies two distinct correlation dimensions in differential pressure measurements collected in bubbling, slugging and turbulent beds. Bai et al. [6] attributes the smaller dimension to particle motion or local turbulence while the larger one is attributed to larger-scale phenomena such as bubbling behaviour. Karamavruç and Clark [7] also identify two correlation dimensions in a slugging bed. The presence of a lower dimension suggests that the reconstructed attractor contains information about changes occurring in the bed on the

particle scale. Therefore, this technique identifies changes in the time-series not seen in frequency analysis techniques.

To quantify changes in fluidization behaviour, the attractor comparison technique of van Ommen [8] and van Ommen et al. [9], known as the S-statistic can be applied to measurements of pressure fluctuations. This technique tests whether or not a statistically significant change has taken place between a given evaluation hydrodynamic state and a reference state corresponding to known or desired hydrodynamics. Van Ommen et al. [9] has demonstrated the sensitivity of the S-statistic to changes in particle size distribution when applied to pressure fluctuations collected in a fluidized bed. Furthermore, the attractor comparison technique has been shown to be insensitive to the small variations in bed mass and superficial gas velocity that can occur during fluidized bed operation. Consequently, the S-statistic can be utilized to identify changes in hydrodynamic behaviour leading to an undesirable fluidized state [9]. An example of the cause of an undesirable fluidized state is the agglomeration of particles [8].

In our previous studies [10, 11], we demonstrated that the S-statistic was sensitive to hydrodynamic changes occurring in a fluidized bed dryer. These changes were related to the reduction in the interparticle liquid bridging forces as granule surface moisture was lost. In that work, time series of pressure fluctuations were logged with a computer while temperature data displayed on a control panel was manually recorded at discrete intervals. In the current study, the S-statistic analysis of pressure fluctuations is implemented in a lab-scale fluidized bed dryer that is more fully instrumented, allowing the S-statistic to be compared directly to on-line measurements of entrainment, bed

temperature and outlet air temperature. Previous applications of the S-statistic to fluidized systems [8, 9] have focused on scenarios where the bed is initially well fluidized and then becomes defluidized at a later time due to agglomerate formation. The choice of reference state is obvious in this situation. The choice of reference state is not so obvious in our drying application since the initial wet bed is at first more difficult to fluidize, but then becomes easier to fluidize as moisture is driven from the granule. Ultimately, fluidization of the very dry granule can be too vigorous, leading to attrition and/or entrainment near the end of batch drying. Therefore, the aim of the present study is to test the application of the S-statistic using reference states chosen at various times in the drying process corresponding to distinct moisture contents or hydrodynamic states. The comparison of the behaviour of the S-statistic with the on-line measurements of entrainment and temperature will illustrate how it may be used to provide an early warning of the onset of entrainment that temperature measurement alone can not.

4.3 Theory

The S-statistic represents a comparison of attractors reconstructed from two distinct time-series. These time-series are referred to as the reference and evaluation time-series. The reference and evaluation data sets can be thought of as a sample of attractors describing the system behaviour at both the reference and evaluation system states. The algorithm makes a statistical comparison between these samples of reconstructed attractors and the result of this comparison is the S-statistic. A value of the S-statistic smaller than 3 denotes consistent behaviour between the reference and evaluation states, i.e. that no statistically significant change has taken place. A value greater than 3 indicates that a statistically significant difference exists between the

attractor reconstructed from reference time-series and those reconstructed from the evaluation time-series. Statistically, if it is found that the value of S is greater than three, the null hypothesis that the attractors compared arise from the same underlying dynamics can be rejected at the 95% confidence level [12]. For the sake of brevity, the mathematics of the S-statistic is not provided here. More information has been given in chapters 2 and 3 and complete details of the mathematical development of the S-statistic are given in Diks et al. [12]. The application of the algorithm to fluidized systems is given in van Ommen [8] and van Ommen et al. [9].

4.4 Apparatus

4.4.1 Fluid-bed Dryer

The fluidized bed drying apparatus is shown in Figure 4.1 with detailed dimensions of the acrylic cone given in Figure 4.2. The acrylic cone allows for the processing of batches of wet material as large as 4 kg. The conical product bowl is fitted with a sample thief allowing for removal of a sample of approximately 1 g from the bed during operation. The distributor plate was designed according to the rules-of-thumb outlined by Kunii and Levenspiel [13] and was constructed of a 1.5 mm thick aluminium plate drilled with 2 mm diameter holes in a square pitch, giving an open area of 5.6 %. A 1.37 m tall cylindrical acrylic freeboard section is flange-connected to the top of the product bowl. Design of this section was based on calculations of the transport disengagement height (TDH) using equations presented by Kunii and Levenspiel [13]. Particles in the air stream exiting the top of the freeboard section were separated in an acrylic cyclone designed to achieve the capture of 99% of particles larger than 75 μm. Particles captured by the cyclone were collected in a vessel suspended from a load cell.

Fluidizing air was supplied by a rotary blower (the SCL V5, Effepizela, Italy) and heated by a Watlow CBEN24G6-21 electrical heater. Control of the air temperature was handled by a Watlow series 935A PID logic controller with feedback provided by a grounded type-J thermocouple inserted into in the windbox. Metering of the air supply was provided by an orifice plate designed according to the ASME standards for orifice design [14]. Pressure drop across the orifice was measured directly with a water-filled manometer and the corresponding air velocity was calculated based on the calibration provided in the standards [14]. Air velocity was manually controlled using a bypass valve located immediately downstream of the blower.

4.4.2 Instrumentation

Details of the instrumentation for the fluidized bed apparatus are given in Figure 4.1. A high-frequency piezoelectric sensor (PCB-106B from Piezotronics) was used in the measurement of pressure fluctuation data. The sensor diaphragm was flush-mounted to the inside wall of the acrylic cone at a height of 7 cm above the distributor. An Omegadyne LCL-816G load cell was used for the collection of entrainment data. One end of the load cell beam was mounted directly onto the frame supporting the fluidized bed unit. From the other end of the beam, a fines collection vessel was suspended. This entrainment monitoring system was calibrated using a number of known weights. Entrainment and pressure fluctuation data was collected simultaneously on a single computer using a Keithley KPCI-3101 12 bit data acquisition card controlled by a data acquisition interface designed in Labview 6.0 from National Instruments.

Process temperatures were monitored in the bed and the outlet air stream using two grounded type-J thermocouples encased in cylindrical aluminium sheaths. These sheaths had diameters of 1.6 mm and 3.2 mm, respectively. A separate computer to the one used for the collection of data from the load cell and pressure transducer was used to collect data from these thermocouples. Data was collected utilizing a Keithley KPCI-3107 card with a user interface designed in Labview 6.0. Load, pressure and temperature data collection was initiated simultaneously on both computers in order to establish a consistent time-base for the collected data.

4.5 Experimental

4.5.1 Granulation

Ingredients for the granulation process are summarized in Table 4.1. Dry ingredients were combined in a 250 W low-shear granulator (Kitchen-Aid Classic mixer) and mixed for 2 minutes at the lowest speed (setting 1). Low-speed mixing was continued while water was added to the mixture over a five minute period at a constant rate of 63 mL/min through a medium-flow, variable-speed peristaltic pump provided by VWR Scientific. Wet granulation was followed by 2 minutes of post-granulation mixing at a slightly higher speed (setting 2 on the mixer). The granulation product was then sieved through a 3.36 mm screen in order to remove large particles. The maximum amount of wet granule that could be produced by the granulator was 1 kg. For each experiment, wet granulations were performed in three to four batches (depending on the desired wet bed loading) using the amounts given in Table 4.1. This granulation technique differs from the high-shear process utilized in our previous works [10, 11] and, as such does not produce the same granule size distribution. This is not an issue in

the present work since we simply need wet granule to demonstrate the application of the S-statistic as an early warning of entrainment. Furthermore, Chaplin et al. [10] showed that the response of the S-statistic was most sensitive to changes in moisture while variations in particle size distribution had little effect provided the gas velocity was sufficiently high.

4.5.2 Drying Experiments

Experimental conditions in the present study were based on our findings in earlier related work. Inlet air temperature has been found to have no effect on the drying process other than to increase the drying times at lower inlet temperatures [10]. Consequently, we have chosen to maintain the temperature in the windbox at a value of 65°C which is a typical setting used industrially in the drying of pharmaceutical granule. Also in our previous study, the location of the piezoelectric transducer was found not to have a significant influence on the performance of the S-statistic [10]. However, this was not the case in the present work. The reasons for the influence of sensor position in the present work may be due to the larger bed loadings and the slightly shallower cone. This requires further study. The sensor positioning of 7 cm above the distributor, which was found to give the optimum response in the S-statistic, has been used throughout the current work. Our previous work has indicated that bed mass has an influence on the performance of the S-statistic [10]. Therefore, bed masses of 3, 3.5 and 4 kg were prepared for three test runs in accordance with the procedure outlined above.

Superficial gas velocity was selected on the basis of the findings of Chaplin et al. [11] who showed that, in a dry bed of pharmaceutical granule, superficial gas velocity

has little effect on the changes in the S-statistic at velocities well in excess of minimum fluidization. This insensitivity of the S-statistic to superficial gas velocity was also reported by van Ommen [8] and therefore makes the S-statistic suitable as a monitoring technique in a process such as batch drying where changes in superficial gas velocity could be used to optimize drying times. In the present work, a constant superficial gas velocity of 1.4 m/s was selected for the bulk of the experimental duration with a period of elevated superficial gas velocity of 2.1 m/s lasting for approximately the first 10 minutes of the drying experiment. The higher superficial gas velocity used initially facilitates good mixing of the wet bed.

Throughout the drying experiment, data was simultaneously collected from the thermocouples, load cell and piezoelectric sensor. Data was collected continuously at 1 Hz from the thermocouples and 400 Hz from the load cell and piezoelectric sensor. Samples of approximately 3 g of granule were taken from the bed at discrete time intervals via a sample thief. These samples were sealed in air-tight vials and analyzed within 2 hours of the completion of the drying experiment utilizing a Mettler-Toledo HB43 drying balance. Based on preliminary drying tests performed in this unit, it was known that moisture decreases at a constant rate early in the drying process. Therefore, longer sampling intervals were used early in the drying process due to the fact that the sample thief was subject to seizing when frequent sampling was made in a bed having moisture greater than approximately 12-wt%. Shorter intervals were utilized later in the drying process to capture the detail of the falling-rate period. Moisture readings with the drying balance were taken in duplicate in order to ensure consistency within each sample.

4.5.3 Data Analysis

Data collected from the two thermocouples and the load cell data was resampled at frequencies of 0.05 Hz and 0.1 Hz, respectively. Resampling was required to eliminate the high-frequency noise. Pressure data was filtered using a type 1 Chebychev band-pass filter design in Matlab between 0.5 Hz and 170 Hz. Filtering of the pressure time-series was performed in order to fulfill the Nyquist criterion as well as to eliminate low frequency transitory effects associated with the piezoelectric sensor.

The S-statistic algorithm of van Ommen [8] has been implemented in Matlab. The details of the Matlab program used in this study are provided in Chaplin et al. [10]. This algorithm takes 9 seconds to analyze 2 minutes of data sampled at 400 Hz on a 1.53 GHz CPU applied to our data. Therefore, this technique is capable of being implemented as an on-line process monitoring or control method. Pressure fluctuation data sets have been subdivided into a series of equivalent subsets of 2 minutes in duration. One of these subsets has been chosen as a reference time series and this is compared with all of the other time-series subsets denoted as evaluation time-series. This analysis results in a single S-statistic value for each 2 minute evaluation interval. Each value of the S-statistic represents a comparison between the dynamics at the reference state and the evaluation state.

4.6 Results and Discussion

4.6.1 Process Variables

The response of bed temperature and moisture at the 3 bed loadings examined during the drying process is shown in Figure 4.3. Outlet temperature had an identical but

less intense response compared with bed temperature. Attainment of a product temperature of 45°C, the criteria set for certain drug formulations in the pharmaceutical industry, was determined as the endpoint of the experiment. However, on the 3 and 3.5 kg runs, a malfunction in the thermocouple resulted in a loss of data after temperatures of 38°C and 36°C respectively. It was not possible to repeat these experiments due to limitations on powder ingredients for preparing wet granule and the high probability that the malfunction would recur. In order to determine the approximate drying endpoint for these runs, an extrapolation based on the rate of temperature immediately preceding failure was performed. The linear extrapolation was based on the response of bed temperature during the drying of the 4 kg bed. For this run, the rate of increase in temperature after 35°C is approximately linear. All bed temperatures remain constant at 25°C for the first part of the experiment with a later increase. This increase is a result of the fact that the maximum transfer of heat to the drying particles through evaporation is no longer possible at low moisture contents due to the lack of free moisture. Thus, the time at which there is an increase in bed temperature corresponds to the loss of surface moisture from the particles. For the bed masses of 3, 3.5 and 4 kg this occurs at approximately 38, 45 and 52 minutes respectively. These times correspond to a bed moisture content of approximately 11-wt%.

It can be seen from the moisture curves in Figure 4.3 that an increase in bed mass leads to an increase in drying time resulting from the increase in total mass to be dried. Each drying curve in Figure 4.3 exhibits a constant rate period lasting until a moisture content of approximately 4-wt%, followed by a brief falling-rate period. This moisture is significantly lower than the moisture content of 11-wt% noted for the loss of surface

moisture. Therefore, the loss of surface moisture does not appear to be connected to commencement of the falling-rate portion of the drying curve.

The mass collected on the load cell at the three bed masses examined is presented in Figure 4.4. Each curve has a similar sigmoidal shape indicating an increase in entrainment rate to a maximum followed by a subsequent decrease. The entrainment data shows the increase in the total mass of material collected by the load cell at increasing bed masses. The point at which entrainment begins corresponds with the initial increase in bed temperature noted in Figure 4.3 at a bed moisture of 11-wt% with no entrainment observed at earlier times. The volume mean diameter of the entrained particles, as determined with a Malvern Mastersizer S Long Bench particle size analyzer, was 83 μm with the maximum rate of entrainment occurring at a moisture content of approximately 5-wt%. The fact that no fines are entrained before the loss of surface moisture from the particles identified by the temperature profiles in Figure 4.3 suggests that the presence of surface moisture prevents the entrainment of finer particles.

4.6.2 The S-statistic

4.6.2.1 Calibration of the S-statistic Algorithm

Implementation of the S-statistic algorithm requires optimization of several adjustable parameters. This optimization can be referred to as a calibration. Calibration of the algorithm was performed as described by Chaplin et al. [10, 11] for this study. The optimum parameters for the S-statistic algorithm are presented in Table 4.2. Two pressure time-series collected in a single drying experiment at a moisture content of 25-wt% (reference state) and 10-wt% moisture (evaluation state) were utilized to identify

these quantities. Two of the optimum parameters were identical to those found previously, the exceptions being embedding and the bandwidth, which were found to be 20 and 0.7, respectively. This is in contrast to the values of 40 and 0.5 found in Chaplin et al. [10, 11]. An embedding of 20 at time window of 50 ms has been used by van Ommen [8, 9] for the application of the S-statistic to a fluidized bed. Diks et al. [12] have suggested that bandwidth can take on a wide range of possible values. Therefore, the optimum parameters identified, though different from our previous application of the S-statistic [10, 11], do correspond with published works. Again, the differences may be due to the differences in bed geometry and loading mentioned earlier and requires further study.

The use of differing values of embedding dimension merits brief discussion. The selection of this parameter at a constant time-window has the effect of modifying the effective sampling frequency [8] with a lower embedding dimension corresponding to a lower sampling frequency. As in our previous work [11], values of sampling frequency as low as 10 (resampling at 100 Hz), while reducing the overall magnitude of the response of the S-statistic, did not influence the identification of the statistically consistent state (i.e. the point where $S<3$). This result shows that the S-statistic could be implemented in applications where low frequency pressure fluctuation measurements are available.

4.6.2.2 S-statistic Applied to Drying

Investigation of plots of the raw pressure fluctuation data (not shown here) indicated no clearly identifiable changes in the shape of these signals throughout the

drying process other than a slight increase in intensity. Frequency and standard deviation analysis also showed no clear trends with changes in moisture. These facts emphasize the value of the S-statistic in applications where traditional methods of frequency and amplitude response do not provide information useful for process monitoring. The changes seen in the S-statistic discussed below are therefore a result of subtle changes in the signal related to the dynamic behaviour of the bed.

With the aim of the present study being the establishment of a suitable reference state for the S-statistic technique when applied to drying, several reference states were tested. These reference states corresponded to various moisture contents between 26-wt% and 2-wt%. Figure 4.5 and Figure 4.6 show the behaviour of the S-statistic at reference states corresponding to moisture contents of 5-wt% and 10-wt%, respectively. Consistent with our previous work [10, 11], the S-statistic response shows a statistically significant hydrodynamic change occurring throughout the drying process at all 3 bed loadings. In these figures, we see a gradual reduction of the value of the S-statistic as moisture is lost from the particles on the approach to a state similar to the reference state. Once a value of 3 is attained, the bed can be considered to be operating in a hydrodynamic state that is statistically similar to the reference state. The S-statistic remains at this constant state ($S<3$) for several minutes until, at a time after the reference state, the S-statistic increases to a value above 3, indicating a divergence to a state dissimilar from the reference.

Figures 4.5 and 4.6 illustrate that the behaviour of the S-statistic depends on the choice of reference state. When a reference state of 10-wt% is chosen (Figure 4.6), we see significant temporal separation in the point of convergence to a state statistically

similar to the reference state. Convergence occurs at 30, 36 and 44 minutes for the 3, 3.5 and 4 kg bed loadings, respectively. This is 8 to 9 minutes before the onset of entrainment seen in Figure 4.4 and corresponds to bed moisture of approximately 15-wt% in Figure 4.3. Therefore, when a reference state at 10-wt% is chosen, there is sensitivity in the behaviour of the S-statistic to bed mass and moisture at times preceding the reference state and the S-statistic provides an early warning of entrainment. This sensitivity is not seen with a reference state at 5-wt% (Figure 4.5). In this case, the convergence of the S-statistic to a state similar to the reference state occurs at 45 minutes for all bed loadings and is therefore not associated with identical bed moisture. At 3 kg, the convergence gives a late warning of entrainment while no early warning is given at the 3.5 kg loading. At the 4 kg loading, a 7 minute early warning is given. Consequently, the use of a reference state at 5-wt% does not provide consistent early warning of entrainment. This is likely due to the fact that, at this reference state, entrainment has begun to influence the bed hydrodynamics significantly and, given that higher bed loadings lead to more entrainment (see Figure 4.4), the impact of the hydrodynamic change caused by entrainment may not be identical at all bed loadings. Thus the behaviour of the S-statistic when referenced to 5-wt% moisture tells us that the use of a reference state too close to the end of drying is not suitable. This makes sense when one considers that the basis of the S-statistic is a comparison between a given state of operation and some reference state. Therefore the choice of a reference state in which undesirable fluidization phenomena are occurring (i.e. entrainment in the present case) is not appropriate.

The behaviour of the S-statistic at the additional reference states of 11-wt% and 12-wt% was also studied. The results, which are not shown here, exhibit a sensitivity to bed mass identical to that seen in Figure 4.6. However, the early warning provided by the S-statistic at these reference states is approximately 12 to 14 minutes. Corrective action, such as the reduction of superficial gas velocity, taken at this time during the drying process would lead to unduly long drying times.

The early warning provided by the convergence of the S-statistic to the reference state in Figure 4.6 would allow for appropriate control action, such as the reduction of superficial gas velocity to be taken in order to reduce entrainment. The convergence of the S-statistic to the reference state occurs at consistent moisture despite the changes in bed mass. This would allow for the implementation of this technique in a unit where batch-to-batch variations in bed loading are encountered. Figure 4.3 demonstrates that the temperature data increases only after entrainment is initiated. Consequently, the monitoring of temperature provides no early warning that entrainment from the bed is about to begin. Thus, while temperature may be used to monitor for product moisture content as drying proceeds, it can give no indication that the bed is operating in a non-optimal fluidized state.

The region of rapid divergence of the S-statistic from the reference state occurring toward the end of drying in Figures 4.5 and 4.6 also merits discussion. The most rapid divergence is found in the 3 kg bed while the 3.5 and 4 kg loadings exhibit less intense divergence. Rapid divergence from the reference state indicates that significant dynamic changes are taking place within the bed state as it loses moisture below approximately 2-wt% moisture. It is not entirely clear what the cause of this

departure is and why the lowest bed mass is affected most intensely. Two possible causes are the significant entrainment of fine particles which has occurred at this moisture content or an increase in static charge within the bed at very low bed moisture. Electrostatic effects were noted at low moisture content indicated by the appearance of particles adhering to the inner wall of the freeboard near the completion of the drying experiment.

The behaviour of the S-statistic in this study is different from the behaviour seen in our earlier work [10, 11]. Previously, two stable states near the beginning and end of the drying process separated by a region of rapid change in hydrodynamic behaviour was observed. In contrast, the current work shows a gradual and less intense change over the entire drying process with a rapid divergence in the final stages of drying. The presence of discernable stable states near the beginning and end of drying was not detected in the current work. The source of the disparity between the two treatments is a most likely result of differences in the dynamic behaviour between the fluid-bed drying units employed in these studies. Differences in dynamic behaviour arise from the differing bed operating condition, unit geometry, sensor positioning, granule preparation and bed loading. Further investigation of these effects is necessary in order to accurately quantify these variations.

4.7 Conclusions

The S-statistic analysis of high-frequency pressure fluctuation data collected in a bed of drying pharmaceutical granule identifies that significant hydrodynamic changes occur during the drying process. Temperature and entrainment data indicate that an

increase in bed temperature and the initiation of entrainment occur simultaneously at a moisture content of approximately 11-wt% at all three bed loadings tested. No entrainment was observed before the onset of the bed temperature rise, indicating that entrainment is initiated by a loss of surface moisture. The S-statistic can provide an early warning of entrainment when an appropriate reference state is selected. Employing a reference state at 10-wt%, which corresponds to a granule moisture content where minimal entrainment has occurred, the convergence of the S-statistic to a statistically similar state occurs 8-9 minutes before the start of entrainment. Since entrainment is potentially harmful to product quality, the early warning provided by the S-statistic allows for the implementation of preventative action in order to mitigate product degradation caused by this effect. This corrective action could involve reduction of superficial velocity or changing inlet temperature or humidity.

The implementation of the S-statistic is not limited to the detection of entrainment effects and could also be utilized to identify changes in hydrodynamic behaviour caused by other indicators of product degradation related to an undesirable fluidized state. Possible indicators of product degradation include product yield or activity, particle shrinkage and attrition. In the application of the S-statistic to these indicators, identification of an appropriate reference state is required to give adequate prediction of the undesirable fluidized state.

4.8 Acknowledgements

The authors would like to thank Merck Frosst Canada & Co. (Montreal) and the Natural Sciences and Engineering Research Council of Canada (NSERC) for their financial support.

4.9 References

1. Van der Schaaf, J, Schouten, J.C., van den Bleek, C.M., *Origin, Propagation and Attenuation of Pressure Waves in Gas-Solid Fluidized Beds*, Powder. Tech., 95, 220-233, 1998
2. Saxena, S.C., Rao, N.S., Tanjore, V.N, *Diagnostic Procedures of Establishing the Quality of Fluidization of Gas-Solid Systems*, Exp. Ther. and Fluid Sci., 6, 56-73, 1993
3. Kage, H, Iwasaki, N., Yamaguchi, H., Matsuno, Y., *Frequency Analysis of Pressure Fluctuation in Fluidized Bed Plenum*, Jour. Chem. Eng. Japan, 24(1), 76-81, 1991
4. Van der Schaaf, J., *Dynamics of Gas-Solids Fluidized Beds*, PhD. Thesis, Delft University of Technology, 2002.
5. Grassburger, P., Procaccia, I., *Characterization of Strange Attractors*, Phys. Rev. Lett., 50(3), 346-349, 1983
6. Bai D., Bi H. T., Grace J. R., *Chaotic Behaviour of Fluidized Beds Based on Pressure and Voidage Fluctuations*, AIChe. J., 43(5), 1357-1361, 1997
7. Karamavruç, A.L., Clark, N.N., *Local Differential Pressure Analysis in a Slugging Bed Using Deterministic Chaos Theory*, Chem. Eng. Sci., 52(3), 357-370, 1997
8. van Ommen, R., *Monitoring Fluidized Bed Hydrodynamics*, PhD. Thesis, Delft University of Technology, 2001.
9. van Ommen, J.R., Coppens, M.C., van Den Bleek, C.M., *Early Warning of Agglomeration in Fluidized Beds by Attractor Comparison*, AIChe J., 46(11), 2183-2197, 2000.
10. Chaplin, G., Pugsley, T., Winters, C., *Application of Chaos Analysis to Pressure Fluctuation Data from a Fluidized Bed Dryer Containing Pharmaceutical Granule*, Powder Tech. 142(2-3), 110-120, 2004 [Chapter 3]
11. Chaplin, G., Pugsley, T., Winters, C., *Application of chaos analysis to fluidized bed drying of pharmaceutical granule*, in ***Fluidization XI: Present and Future for Fluidization Engineering***, U. Arena, R.Chirone, M. Miccio and P. Salatino, eds., Engineering Foundation, New York, 419-426, 2004 [Chapter 2]
12. Diks, C., van Zwet, W.R., Takens, F., DeGoede, J., *Detecting Differences Between Delay Vector Distributions*, Phys. Rev. E., 53(3), 2169-2176, 1996.
13. Kunii, D., Levenspiel, O., *Fluidization Engineering (2^{nd} Edition)*, Butterworth-Heinemann, Toronto, 1991
14. Miller, R.W., Lee, W.F.Z., Gomez, C.J., *Measurement of Fluid Flow in Pipes Using Orifice, Nozzle and Venturi*, ASME-MFC-3M-1989, New York, 1990

Table 4.1 Wet Granule Formulation

Component	Percentage by mass (dry basis)	Amount (g) for a 1 kg (wet) batch
Lactose Monohydrate (filler)	50%	375
Microcrystalline Cellulose (filler)	44%	330
Croscarmellose Sodium (disintegrant)	2%	15
Hydroxypropyl Methylcellulose (binder)	4%	30
Water (reverse-osmosis)	43%	315

Table 4.2 S-statistic calibration results

Time window	0.1 seconds
Embedding (m)	20
Bandwidth (d)	0.7
Segment Length (L)	3 seconds

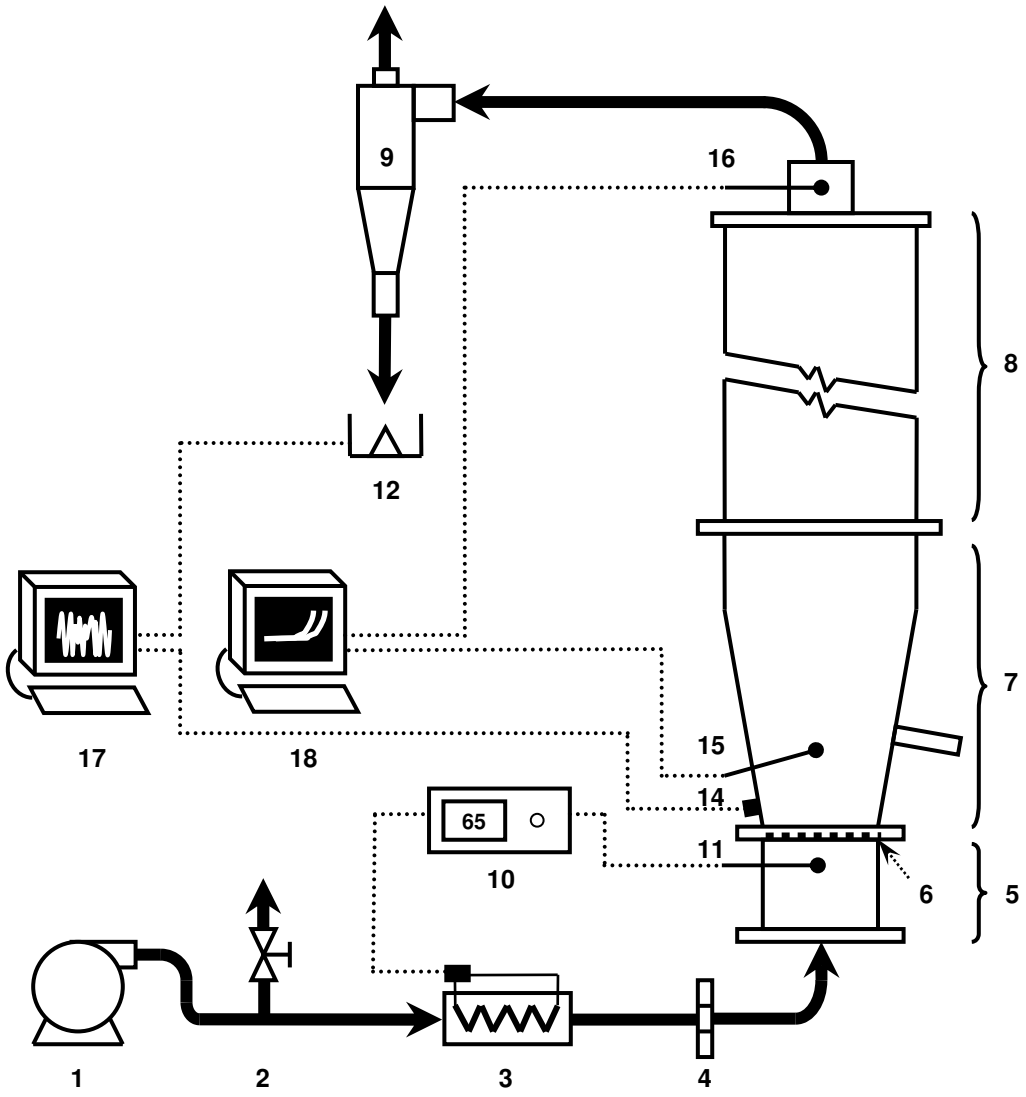

Figure 4.1 Fluidized bed dryer apparatus components and instrumentation. Blower (1), air bypass (2), air heater (3), orifice (4), windbox(5), distributor (6), product bowl (7), freeboard (8), cyclone (9), air heater controller (10), air-supply thermocouple (11), load cell and collection vessel (12), sample thief (13), piezoelectric pressure transducer (14), bed temperature thermocouple (15), outlet air temperature thermocouple (16), data acquisition computer for the load cell and pressure transducer data (17), data acquisition computer for the thermocouple data (18).

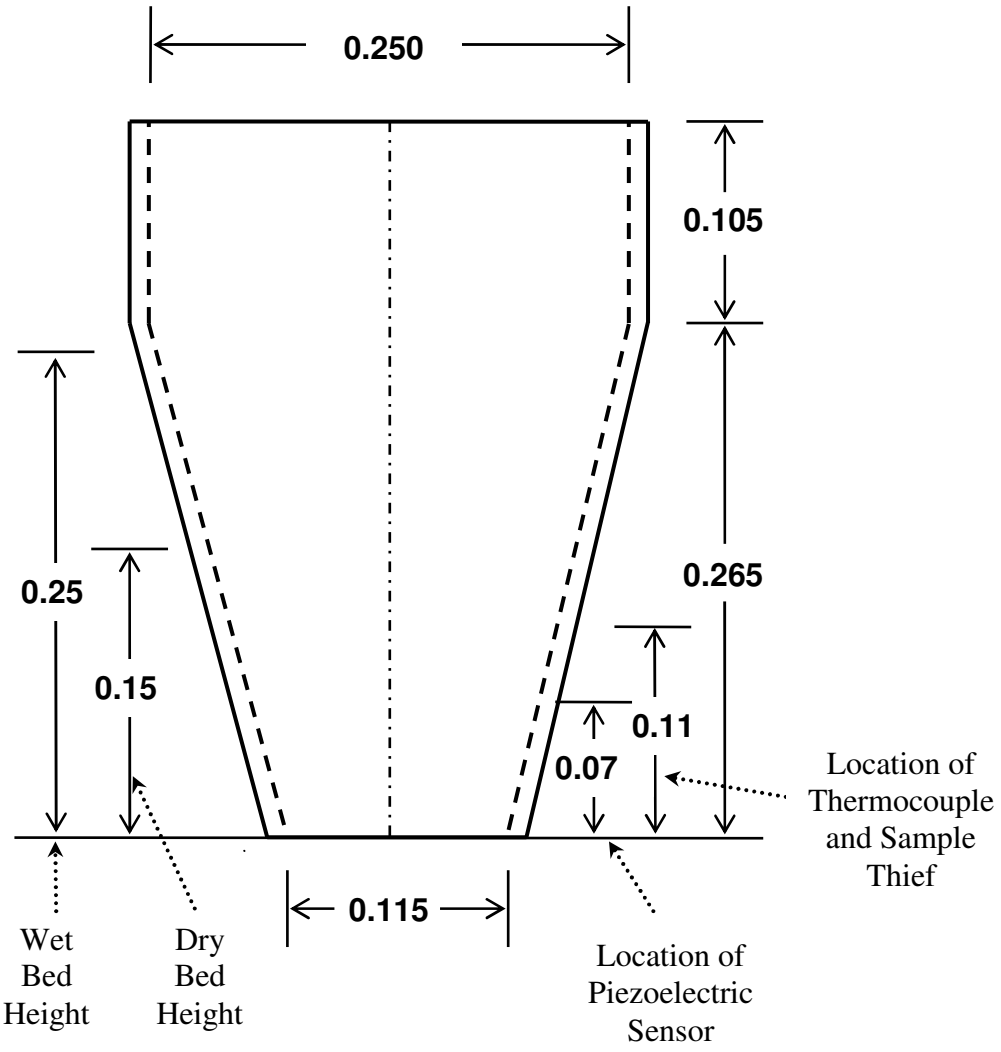

Figure 4.2 Detail of the acrylic cone dimensions in m. Bed heights indicated are the settled bed heights for a 3.5 kg batch size.

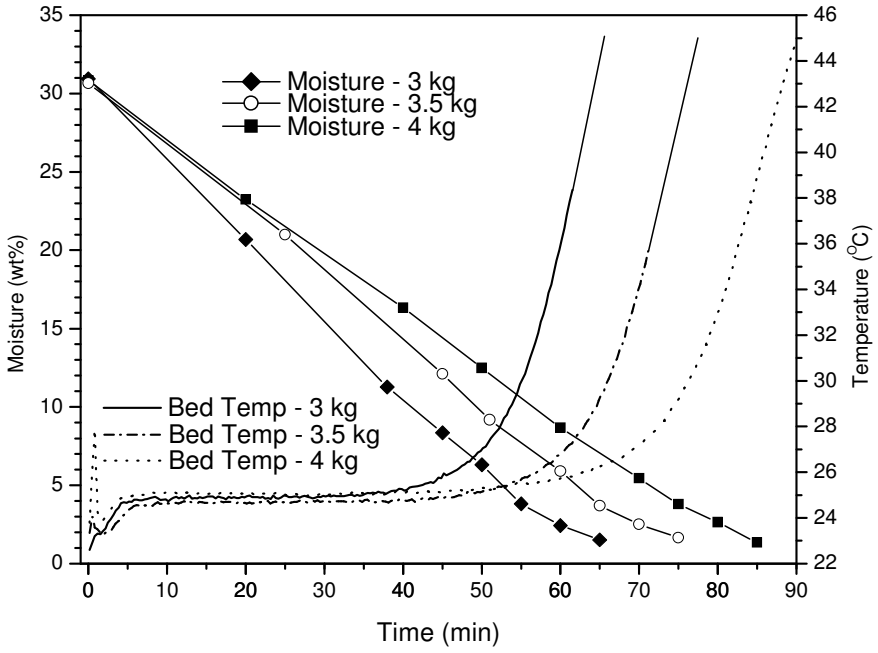

Figure 4.3 Drying curves and bed temperature for the three bed masses examined

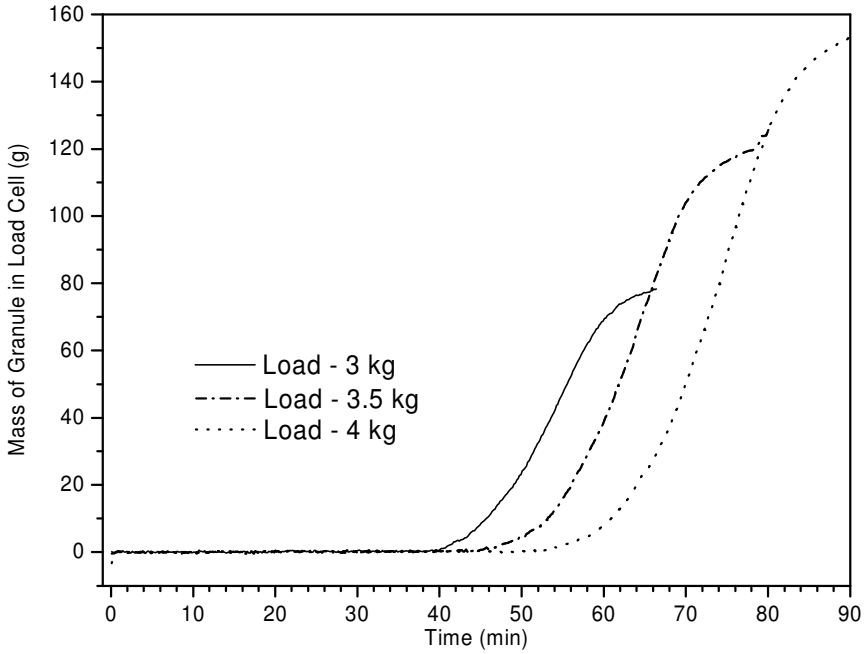

Figure 4.4 Load cell entrainment data for the three bed masses examined.

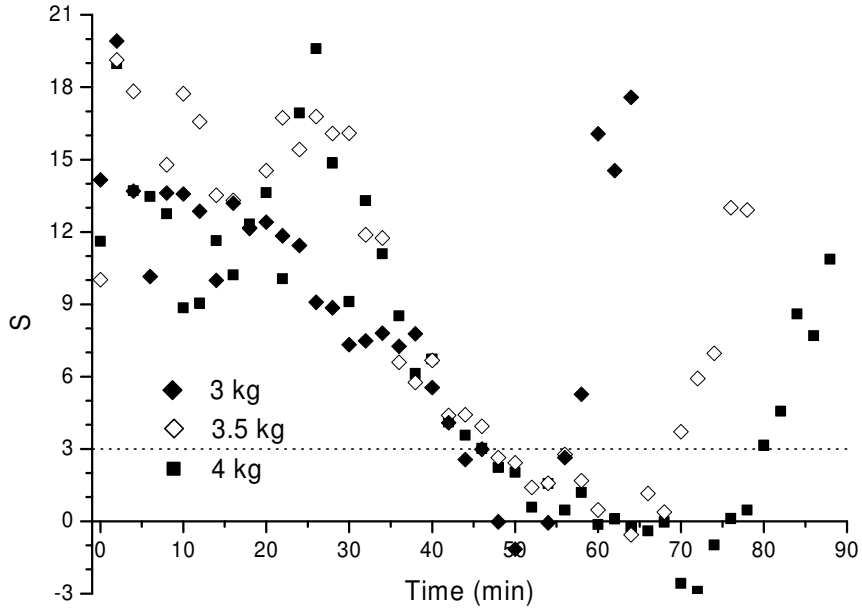

Figure 4.5 S-statistic response when the reference state is chosen at 5-wt%.

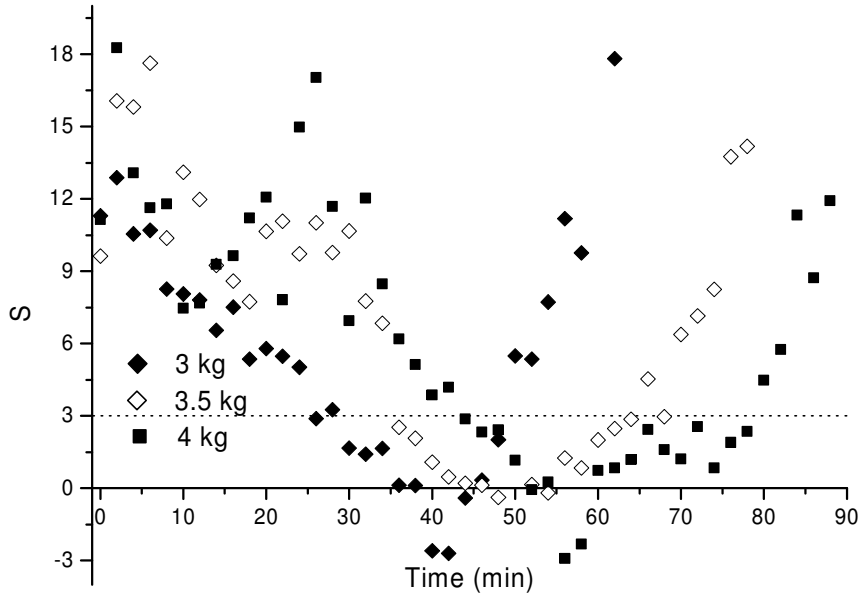

Figure 4.6 S-statistic response when the reference state is chosen at 10-wt%.

Chapter 5 - Monitoring the Fluidized Bed Granulation Process Based on S-statistic Analysis of a Pressure Time-Series

This paper has been accepted for publication as a technical note in the ***American Association of Pharmaceutical Scientists Journal*** (formerly AAPS PharmSciTech) where it appears in a version similar to what is presented in this chapter.

Citation

Chaplin, G., Pugsley, T., Winters, C., *Monitoring the fluidized bed granulation process based on S-statistic analysis of a pressure time-series,* AAPS Journal, (2005).

Contribution of PhD Candidate

This portion of the work is based on a single experiment in the apparatus introduced in chapters 2 and 3. The experiment was performed by Hubert Dumont (Merck Frosst Canada & Co.) and Gareth Chaplin. The software for all data collection and analysis was developed by G. Chaplin. All writing of the submitted manuscript was done by G. Chaplin with Todd Pugsley and Conrad Winters (Director, Formulation Development (PR&D) Merck & Co.) providing supplemental guidance regarding content and style of the paper.

Contribution of this Paper to the Overall Study

This experiment was initially conceived as a test for the data acquisition and analysis software. However, the analysis of the data using the S-statistic indicated a response to changes in the granulation process. In chapters 2 and 3, it was shown that the S-statistic responds strongly to changes in moisture during the drying process. In a fluid-bed granulation, the moisture of the particles increases in the granulation or particle growth phase as the binder is added to the dry ingredients and then is reduced in the drying phase. If hydrodynamic changes can be identified in the granulation process resulting from this change in moisture, the application of the S-statistic to pressure fluctuations collected during granulation has merit as a moisture monitoring technique.

Additional Experimental Details

Fluid-bed granulation is similar to the high and low shear granulation methods presented in the preceding chapters. In this process, the mixing of the dry ingredients is performed by the mixing action of the fluidized bed rather than an impeller. The addition of a binder solution to the mixture during this process initiates granule growth. Following the growth of the granules, the binder addition is stopped and the granules are dried in the same unit by fluidization. This process is used in a number of industries including the pharmaceutical industry to produce granulated products.

The apparatus used in this investigation is identical to that introduced in chapters 2 and 3 (Glatt GPCG1). However, it was fitted with a spray nozzle for top-spray fluid-bed granulation. The apparatus is diagrammed in Figure 5.01. A beaker containing a pre-determined quantity of binder solution was placed on a balance before the beginning of

the experiment. During granulation, this solution was pumped into the bed through the spray nozzle by a constant speed peristaltic pump. The mass given by the scale allowed for the determination of the binder flow rate and the total amount of binder added to the bed. When the required amount of binder had been introduced into the bed, the pump was turned off to stop binder addition and the granules were dried in the unit.

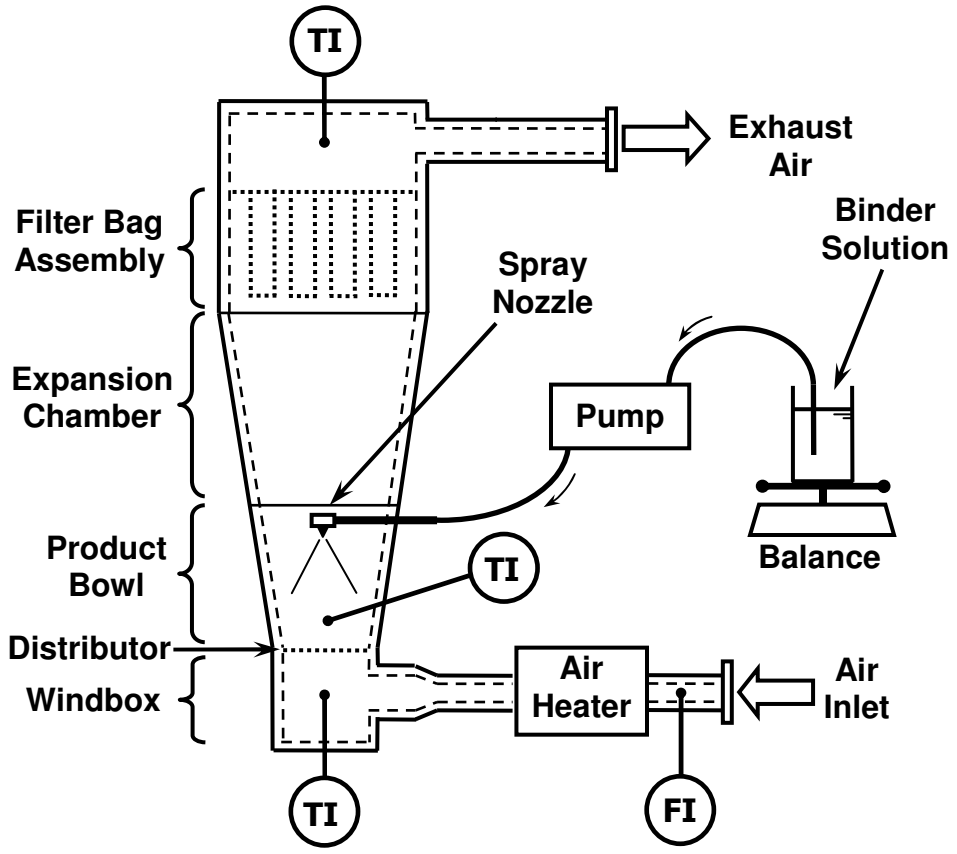

Figure 5.01 Schematic of the GPCG1 unit configured for fluid-bed granulation (not to scale). The abbreviations TI and FI respectively indicate temperature and flow indicators.

The measurement of pressure fluctuations was done in an identical manner as presented in chapters 2 and 3. Data analysis was accomplished using the Matlab programs presented in Appendix A.

5.1 Summary

Pressure fluctuations collected during the fluidized bed granulation of pharmaceutical granule have been analyzed using the attractor comparison technique denoted as the S-statistic. Divergence of the bed state from the reference during granulation is followed by a return to a condition statistically similar to the original state of the dry fluidized ingredients upon drying. This suggests insensitivity of the S-statistic technique to the changes in particle size distribution occurring during the granulation process. Consequently, the monitoring of pressure fluctuations alone may provide an easily-implemented technique for the tracking of granule moisture.

Keywords: Fluidized bed, Granulation, S-statistic, Hydrodynamics, Chaos, Pressure fluctuations

5.2 Introduction

The batch fluidized bed granulation process is an important step in the preparation of certain solid-dosage drug products. In this process, the addition of binder directly into a bed of fluidized material causes the agglomeration of particles to form granules. The vigorous granule mixing provided by the fluidized bed allows both even distribution of binder and uniform drying of the granule product. Control of granule moisture is accomplished by the monitoring of outlet air and product temperatures. The attainment of a limiting value of either of these quantities signifies the completion of the drying phase. Since, the bed temperature only begins to increase once surface moisture is lost from the particles, this type of temperature monitoring only provides information about bed moisture content late in the drying process. Furthermore, temperature measurement provides no information about the fluidization behaviour of the bed.

The direct on-line measurement of bed moisture during fluid-bed granulation has been performed by Kawai [1], Watano et al. [2], Gore et al. [3] and Rantanen et al. [4] using infra-red spectroscopy. Rantanen et al. [4] have shown that different drying times are required for different formulations. This highlights the importance of the quantification of changes in moisture. The moisture profiles in Gore et al. [3] and Rantanen et al. [4] show an increase in moisture to a maximum in the granulation phase followed by an immediate decrease during the drying phase to bed moisture content similar to the initial moisture of the dry ingredients. In Kawai [1] and Watano et al. [2], a period of constant moisture is maintained at the maximum moisture to allow for the growth of granules before the drying phase. Watano et al. [2] have shown that infra-red measurements can be utilized to control the rate of binder addition throughout the constant moisture phase in order to maintain the desired bed moisture content. Kawai [1] has indicated that moisture content is a major factor affecting granule size and bulk density. Therefore, measurement and control of moisture is crucial in order to control product quality. Although moisture content is a key process parameter, its measurement gives no indication of the hydrodynamic changes taking place within the bed during granulation. Furthermore, the spectroscopic technique utilized for the on-line measurement of moisture in the above studies can be costly to implement and subject to measurement uncertainties caused by the presence of surface moisture [1]. The present work demonstrates an alternative method for the monitoring moisture content in a fluidized bed granulator through the use of pressure fluctuations.

Pressure fluctuations in a fluidized bed arise from a number of sources including bubble generation, bubble coalescence and bulk bed oscillations [5]. Several analysis

techniques have been applied to these fluctuations including standard deviation [6], frequency [7, 8] and chaos analysis [8]. The chaos analysis technique denoted as the S-statistic represents a statistical comparison between two bed states described by chaotic attractors reconstructed from separate time-series of pressure fluctuations [9]. The S-statistic has been applied to pressure fluctuations collected in the drying of pharmaceuticals by Chaplin et al. [10, 11]. In these studies, it has been shown that this statistical test responds strongly to reduction of interparticle forces associated with changes in granule moisture. In the current study, we will apply the S-statistic test to pressure fluctuations collected in a fluidized bed granulator used for the production of pharmaceuticals.

5.3 Theory

The S-statistic represents a comparison of attractors reconstructed from two distinct sets of discretely sampled data denoted as the reference and evaluation time-series. These data sets can be thought of as a sample of attractors describing the system behaviour at two distinct system states. The algorithm makes a statistical comparison between these states and outputs a numerical value denoted as the S-statistic. A value of the S-statistic smaller than 3 indicates that no statistically significant change has taken place between reference and evaluation states. Likewise, a value of S greater than 3 indicates that a statistically significant difference exists between the attractors reconstructed from reference time-series and those reconstructed from the evaluation time-series. Details of the mathematical development of the S-statistic are given in Diks et al. [12]. The application of the algorithm to fluidized systems is given in van Ommen [9] and van Ommen et al. [13].

5.4 Materials and Methods

The dry granulation ingredients were Mannitol (Pearlitol SD200) from Roquette (Keokuk, IA) and Red ferric oxide (0.15%) from Elementis Pigments Inc., (Easton, PA). This material has a volume mean diameter of 130 μm. The aqueous binder solution consisted of 8% Hydroxypropylcellulose (HPC, Klucel LF, 5% viscosity grade, 107 cp, MW approximately 95000) from Hercules Inc., (Wilmington, DE)., Aspartame (0.50%) supplied by The NutraSweet Company (Augusta, GA) and Cherry flavour (1.50%) supplied by Givaudan (Cincinnati, OH).

5.4.1 Fluid-bed Granulation

A schematic of the product bowl for the batch fluidized bed processor used in this study is shown in Figure 5.1. This unit, the GPCG1 (Glatt-Powder-Coater-Granulator) from Glatt Air Technologies Inc., Ramsey NJ allows for the manipulation of inlet air temperature and air velocity and is fitted with a top-spray granulation nozzle. The humidity of the fluidizing air was not controlled by the processor but was measured to be approximately 50% relative humidity at an ambient temperature of 20°C. Fitted with a 12% open area wire mesh distributor, the conical product bowl fits into the air-supply/conditioning module. For the granulation experiment, dry ingredients were placed in the product bowl. Subsequently, heated air was introduced into the bottom of the conical section in order to fluidize this material. Inlet air temperature was maintained at 30°C for all three phases of the granulation process. Superficial velocity was maintained at 2.9 m/s based on the average velocity across the inlet to the product bowl throughout the experiment. After an initial mixing phase, binder addition was performed over 27 minutes. 250 g of binder solution was added to an initial dry bed mass of 469.3

g. The binder solution was introduced at a rate of 9.2 g/min. After the completion of binder addition, drying of the granule was performed over the following 12 minutes. The final dry mass of granules produced was 492.5 g and had an approximate average volume diameter of 250 μm.

5.4.2 Instrumentation

Product and outlet air temperature measurements were made using type-J thermocouples placed directly within the bed and in the outlet air stream. These thermocouples had a diameter of 1.6 mm and 1 mm, respectively. The temperatures were read directly from a digital instrumentation panel at intervals of 5 minutes.

A high-frequency piezoelectric sensor (PCB-106B from Piezotronics) was used in the measurement of pressure fluctuation data. The sensor diaphragm was flush-mounted to the inside wall of the fluidized bed at 90 mm above the distributor. This was accomplished by replacing the product bowl viewing window with an acrylic insert threaded to accept the mounting of the pressure transducer 9 cm above the distributor as shown in Figure 5.1. A Keithley KPC-3101 12 bit data acquisition card was used for the acquisition of pressure data. Card control and data logging was made possible by the use of a graphical user interface developed in Labview. The raw data set was collected at a sampling rate of 400 Hz throughout the granulation and drying phases. Data was filtered offline using a type 1 Chebychev band-pass filter design in Matlab between 0.5 Hz and 170 Hz. Filtering was performed in order to fulfill the Nyquist criterion as well as to eliminate low frequency transitory effects associated with the piezoelectric sensor.

5.4.3 Data Analysis

Pressure fluctuation data was analyzed in Matlab utilizing the S-statistic algorithm described in our earlier work [10, 11]. This technique was calibrated for the optimum test parameters as described previously [10, 11] and the optimum parameters were found to be identical to those found for the drying of pharmaceutical granule in this fluidized bed unit. The pressure time-series collected during the granulation process was broken into evaluation data sets lasting 1 minute. These data sets were compared to a reference data set of 2 minutes in duration. Each evaluation data set was transformed into a single S-statistic value. Previously, an evaluation time-series of 2 minutes was used for each S-statistic value [10, 11]. The shorter evaluation time-series of 1 minute was selected in order to track the rapid changes observed in this process. It has been determined that the use of time segments of 1 minute did not affect the performance of the test.

5.5 Results and Discussion

Figure 5.2 shows the behaviour of the outlet air and bed temperatures. From this plot, we can see that the temperatures of both the outlet air and bed begin to increase at 30 minutes. This increase occurs immediately following the completion of binder addition at 27 minutes. An increase in these temperatures at the end of drying is indicative of the loss of surface moisture from the particles. Completion of the drying process was identified at the attainment of a bed temperature of 30°C.

The behaviour of the S-statistic, when reference states were selected at 7 and 35 minutes from the start of the granulation phase is given in Figure 5.3. When a reference state beginning at 35 minutes is chosen, the S-statistic identifies two periods of

statistically similar hydrodynamic behaviour (i.e. an S value less than 3). The first consistent region occurs between 3 and 10 minutes while the second lasts from 34 minutes to the completion of the drying phase. The S-statistic diverges from a state consistent with the reference state at 11 minutes, indicating a change in the hydrodynamic behaviour of the bed at this time. Immediately following completion of binder addition at 27 minutes, the bed state begins to return to a state statistically similar to the initial state. A similar behaviour of the S-statistic is seen when the reference state is chosen at 7 minutes. The resemblance of these hydrodynamic conditions can be verified using the second reference state. A second reference state was chosen within the initial period of consistent hydrodynamic behaviour seen early in the granulation. Similarity in the shape of both S-statistic responses confirms the existence of the two consistent hydrodynamic states occurring in the early stages of granulation and the final stages of drying.

The shape of the S-statistic response given in Figure 5.3 is similar to the moisture profiles seen in both Gore et al. [3] and Rantanen et al. [4]. In these studies performed utilizing pharmaceuticals, an increase in moisture content observed during binder addition is followed by a decrease in moisture in the drying phase. The identical behaviour is seen in the performance of the S-statistic with maximum divergence from the reference state occurring at 25 minutes. This is near the completion of binder addition or a time when the bed has the highest moisture content. We conclude that the S-statistic is responding to hydrodynamic changes arising from the introduction of moisture into the bed.

The fact that the second consistent hydrodynamic state is similar to that seen early in granulation when a small volume of binder has been added indicates insensitivity of the S-statistic to the growth of granules in this granulation process. Insensitivity in the S-statistic to changes in particle size distribution was noted by Chaplin et al. [10] where reduced sensitivity to changes in particle size distribution in the S-statistic at superficial gas velocities greater than 2.8 m/s was observed in the same GPGC1 unit operated as a dryer. In Figure 5.3, it can also be noted that the S-statistic is initially above three followed by an immediate drop to a consistent state within 2 minutes of the start of the experiment. This initial separation from the reference state may be characteristic of a differing hydrodynamic state in a very dry bed. A similar separation is also seen at 39 minutes where the particles have the lowest moisture near the end of drying.

The initial separation of the S-statistic from the reference state over the first 2 minutes of the granulation experiment is of interest. Inspection of the pressure time-series collected during this portion of the experiment indicates that it has a lower intensity to that seen in the subsequent region of consistent behaviour between 2 and 14 minutes. It is not clear what the cause of this change in hydrodynamic behaviour and requires further investigation.

5.6 Conclusions

The S-statistic analysis of pressure fluctuations collected in the fluidized bed granulation process has identified two regions of consistent behaviour existing in the initial stages of granulation and the final stages of drying. These regions of consistent behaviour are separated by a divergence toward a dissimilar state. This divergence and

return is similar to the rise and fall of bed moisture in the granulation process [3, 4]. The fact that the two regions of consistent hydrodynamic behaviour are statistically similar indicates that the increase in moisture, not the growth of granules, has the most significant impact on the hydrodynamic changes identified by the S-statistic. The use of this technique to determine changes in moisture within the granulator will lead to better on-line monitoring and control of this process without the need for the direct measurement of moisture. Further experimentation is needed in order to quantify this connection fully but the potential use of this technique for process monitoring in the granulation process is clear.

5.7 Acknowledgements

The authors would like to thank Merck Frosst Canada & Co. (Montreal) and the Natural Sciences and Engineering Research Council of Canada (NSERC) for their financial support. We would also like to acknowledge the technical assistance in the running of the fluid bed granulator provided by Dr. Hubert Dumont of Merck Frosst Canada & Co. and consultation offered by Dr. Ruud van Ommen, Delft University of Technology regarding the implementation of the S-statistic.

5.8 References

[1] Kawai S. Granulation and drying of powdery or liquid materials by fluidized-bed technology. Drying Tech. 1993; 11(4): 719-731.

[2] Watano S, Takashima H, Miyanami K. Control of moisture content in fluidized bed granulation by neural network. J. Chem. Eng. Japan. 1997; 30(5): 223-229.

[3] Gore, AY, McFarland, DW, Batuyios, NH. Fluid-bed granulation: factors affecting the process in a laboratory development and production scale-up. Pharm. Tech. 1985; 9: 114-122.

[4] Rantanen, J, Jørgensen A, Räsänen E, Luukkonen P, Airaksinen S, Raiman J, Hänninen K, Antikainen O, Yliruusi J. Process analysis of fluidized bed granulation. AAPS PharmSciTech. 2001; 2(4): article 21.

[5] van der Schaaf J, Schouten JC, van den Bleek CM. Origin, propagation and attenuation of pressure waves in gas-solid fluidized beds. Powder Tech. 1998; 95(3): 220-233.

[6] Chong YO, O'Dea DP, White ET, Lee PL, Leung LS. Control of the quality of fluidization in a tall bed using the variance of pressure fluctuations. Powder Tech. 1987; 53(3): 237-246.

[7] Kage H, Iwasaki N, Yamaguchi H, Matsuno Y. Frequency analysis of pressure fluctuation in fluidized bed plenum. Jour. Chem. Eng. Japan. 1991; 24(1): 76-81.

[8] Bai D, Bi HT, Grace JR. Chaotic behaviour of fluidized beds based on pressure and voidage fluctuations. AIChE J. 1997; 43(5): 1357-1361.

[9] van Ommen JR. Monitoring Fluidized Bed Hydrodynamics. PhD. Thesis: Delft University of Technology; 2001.

[10] Chaplin G, Pugsley T, Winters C. Application of chaos analysis to pressure fluctuation data from a fluidized bed dryer containing pharmaceutical granule. Powder Tech. 2004; 142(2-3), 110-120. [Chapter 3]

[11] Chaplin G, Pugsley T, Winters C. Application of chaos analysis to fluidized bed drying of pharmaceutical granule, In Arena U, Chirone R, Miccio M, Salatino P, eds. Fluidization XI, New York: Engineering Foundation, 2004; 419-426. [Chapter 2]

[12] Diks C, van Zwet WR, Takens F, DeGoede J. Detecting differences between delay vector distributions. Phys. Rev. E. 1996; 53(3): 2169-2176.

[13] van Ommen JR, Coppens MC, van Den Bleek CM. Early warning of agglomeration in fluidized beds by attractor comparison. AIChe J. 2000; 46(11): 2183-2197.

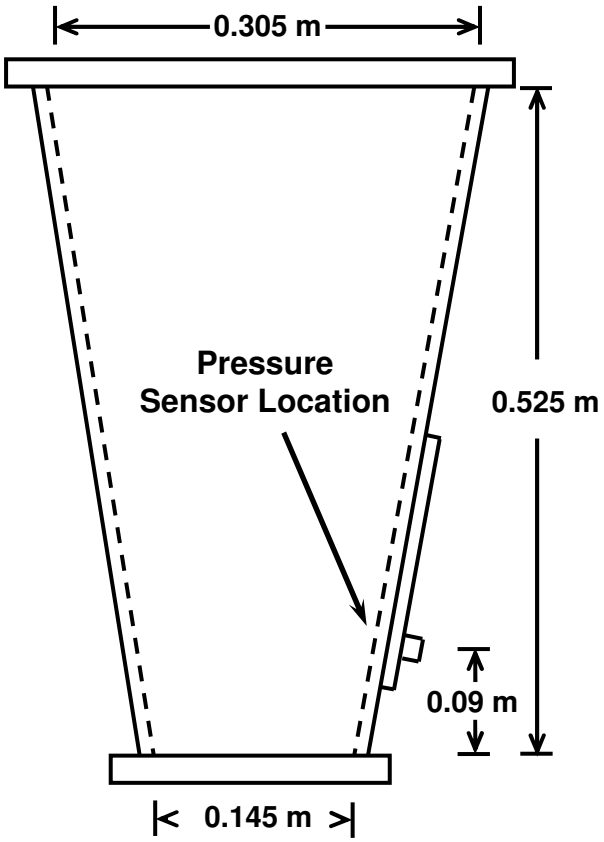

Figure 5.1 Schematic of the fluid-bed granulator product bowl. Dimensions given in meters.

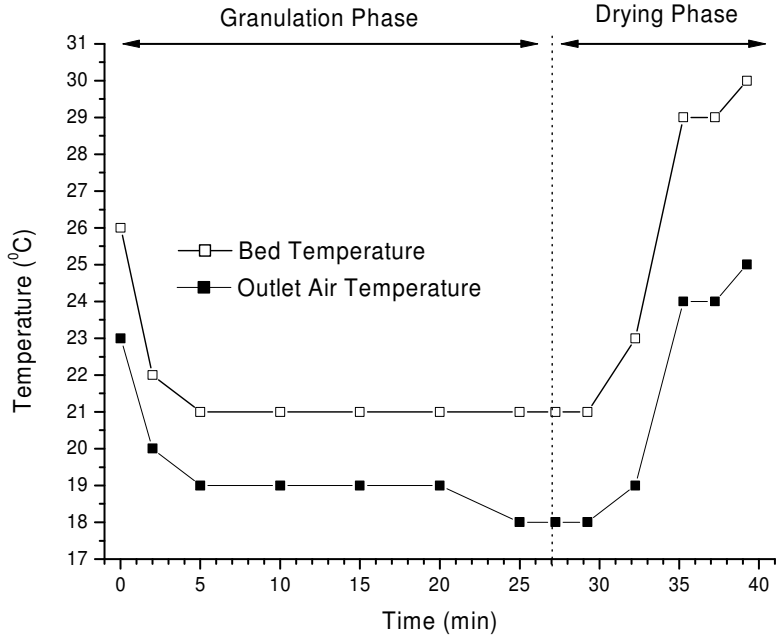

Figure 5.2 Outlet air and Product temperature profiles along with the S-statistic when referenced to 35 minutes. An S-statistic value greater than three indicates that a statistically significant change has taken place.

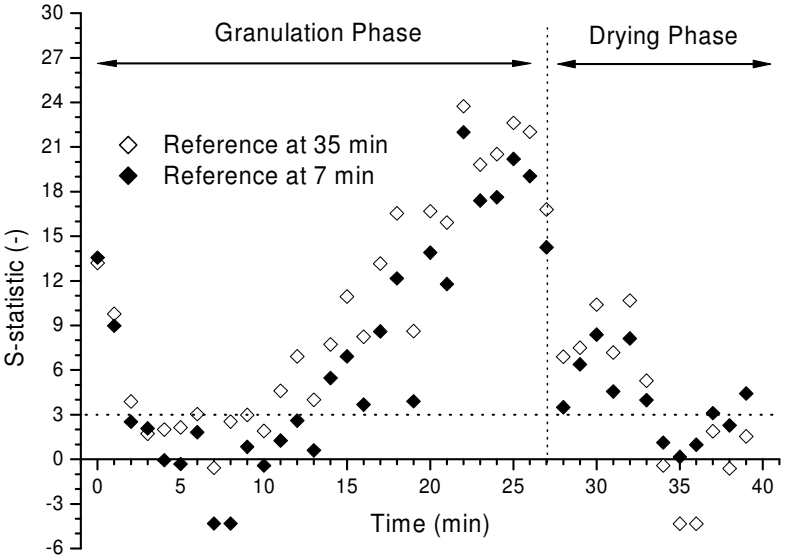

Figure 5.3 S-statistic references to times of 7 and 35 minutes. An S-statistic value greater than three represents a statistically significant change.

Chapter 6 - The Dynamic Calibration of an Electrical Capacitance Tomography Sensor Applied to the Fluidized Bed Drying of Pharmaceutical Granule

This manuscript has been submitted for publication in the journal ***Measurement Science and Technology***. It is currently in revision after receiving the referees' comments.

Citation

Chaplin, G., Pugsley, T., van der Lee, L., Kantzas A., Winters, C., *The dynamic calibration of an electrical capacitance tomography sensor applied to the fluidized bed drying of pharmaceutical granule,* Meas. Sci. Tech., in revision (2005).

Contribution of PhD Candidate

The experimental apparatus used for the x-ray tomography experiments was identical to that presented in chapter 4. For the ECT experiments, the conical acrylic product bowl was replaced with a conical ECT sensor manufactured by Process Tomography Limited (PTL) U.K. Experiments were planned by G. Chaplin. ECT experiments were performed by G. Chaplin while x-ray tomography experiments were performed by Loni van der Lee of the University of Calgary's Tomographic Imaging and Porous Media Laboratory (TIPM). T. Pugsley and Apostolos Kantzas (Director, TIPM) provided consultation regarding the experimental program. The correction procedure for eliminating the influence of moisture from ECT data was developed by G.

Chaplin. Matlab code for the calibration and off-line correction of ECT data was written by G. Chaplin. All writing of the submitted manuscripts was done by G. Chaplin. Todd Pugsley, Conrad Winters (Director, Formulation Development (PR&D) Merck & Co.), L. van der Lee and A. Kantzas provided editorial guidance regarding the style and content of the paper.

Contribution of this Paper to the Overall Study

ECT (electrical capacitance tomography) provides information about the temporal behaviour of a fluidized system because of the high sampling frequency possible with this technique. This attribute makes it an attractive non-invasive process monitoring technique for the determination of localized changes occurring in a fluidized system. The localized information provided by ECT contrasts the global information provided by the pressure fluctuation analysis presented in the preceding chapters.

ECT has not been applied to a fluidized bed dryer due to the reduction in particle electrical permittivity associated with moisture loss. In this chapter, the implementation of a novel correction technique allows for the application of ECT to a drying bed. This correction was verified using a secondary non-invasive measurement technique, x-ray tomography. The x-ray tomography was done with a computer assisted tomography (CAT) scanner at the Tomographic Imaging and Porous Media Laboratory in Calgary. This device, originally designed for medical imaging, gives slices or tomograms at low temporal but higher spatial resolution compared with what is possible with ECT. This makes this technique ideal for the verification of the corrected time-averaged data from the ECT sensor and was the motivation for the collaboration with the TIPM laboratory.

Additional Experimental Details

The x-ray tomography unit used in this study is given in Figure 6.01.

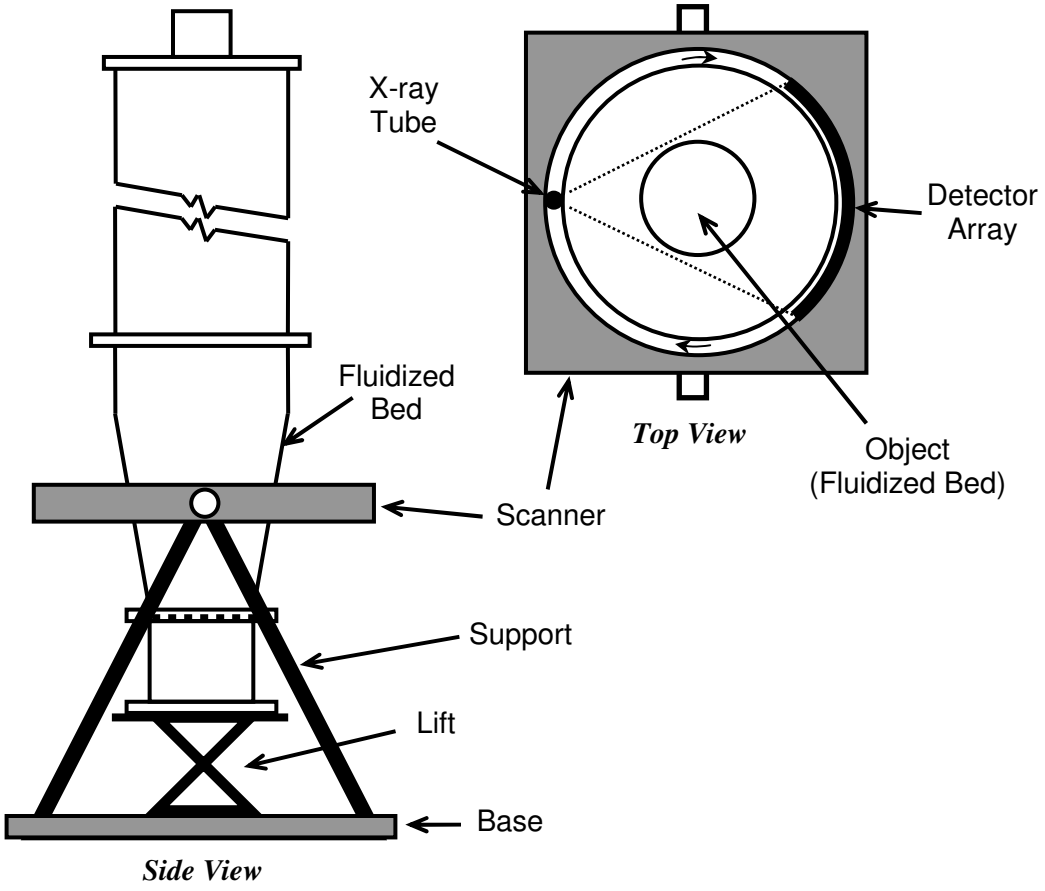

Figure 6.01 Schematic of the x-ray tomography unit used in this study (not to scale).

This unit is a third generation CAT scanner. In this type of scanner, a single x-ray source is coupled to an array of detectors which receives the radiation transmitted as a fan beam. For accurate scans, the projection fan angle must be large enough to encompass the entire object. The tube-detector assembly rotates to collect a complete set of projection measurements for each tomogram. For this reason, third generation scanners are also known as a rotate-rotate scanner. The scanner is rigidly supported in the

horizontal position with the height of the measurement plane above the distributor controlled with the use of a lift supporting the experimental apparatus.

Two drying experiments were performed in both the ECT unit and the CAT scanner under identical experimental conditions. The apparatus used in the x-ray experiments was identical to that presented in chapter 4 while, for the ECT experiment, the acrylic product bowl was replaced with a second acrylic product bowl fitted with the ECT sensor. Granulations were performed using a Kitchen-Aid mixer as was introduced in chapter 4. The creation of calibration curves and the correction of ECT data were done using the Matlab programs presented in Appendix B.

6.1 Abstract

Electrical capacitance tomographic data collected in a lab-scale fluidized bed used for the drying of pharmaceutical granule has been corrected for the influence of moisture on the permittivity of the drying material. The correction is based on a linear least-squares fit to measurements of capacitance in a packed bed of granule at various moisture contents. X-ray tomography has been used to independently verify this correction procedure. The influence of permittivity models and number of iterations used for the reconstruction of tomograms has also been examined. It has been determined that the Böttcher permittivity model performs best at bed moistures above approximately 5-wt% while the parallel model is superior at bed moisture below this value. The reconstruction technique based on iterative linear back-projection utilized for the reconstruction of ECT data required approximately 50 iterations to successfully reproduce the density behaviour seen in the x-ray tomographs. Instability in the reconstruction technique at higher numbers of iterations indicates that a linear least-squares fit does not completely capture the response of the sensor to moisture changes. For future applications, changes in bed voidage associated with the drying of pharmaceuticals must be addressed and included in this calibration procedure in order to implement this calibration technique throughout the drying process. Nevertheless, the viability of this technique for on-line calibration of an ECT sensor applied to the drying process has been demonstrated.

6.2 Nomenclature

Symbols

a	Constant in Equation 5 ($wt\%^{-1}$)
b	Constant in Equation 5 (nondimensional)
C_H	Capacitance measurement in a packed bed or dense phase (F)
C_L	Capacitance measurement in an empty bed or dilute phase (F)
C_M	Measured capacitance (F)
C_N	Normalized capacitance (nondimensional)
M	Moisture content (wt%)
p	Normalized pixel permittivity (nondimensional)
PR	Packed bed permittivity ratio (nondimensional) $= C_H/C_L$
x	Fraction of dense-phase material (nondimensional)

Greek

ρ_{pb}	packed bed density (kg/m^3)
ρ_{air}	air density (kg/m^3)

6.3 Introduction

Tomographic imaging of fluidized beds allows for the determination of local information about the distribution of the dense and dilute phases within the imaging cross-section. In fluid-bed drying applications, this direct knowledge is invaluable for the operation of the unit in a specific hydrodynamic regime in order to optimize the drying process or to determine important changes in bed hydrodynamics related to the loss of particle moisture. This type of information is not provided by pressure fluctuation measurements [1] which are a global measurement of bed behaviour. Other local measurement techniques, such as capacitance [2], heat transfer [3] or fibre optic probes [4] have the potential to interfere with the bed dynamics. Furthermore, in this fluid-bed drying application, there is significant potential for the fouling of such probes. In contrast, tomographic techniques are non-intrusive.

Electrical Capacitance Tomography (ECT) has recently been utilized by a number of researchers to assess the hydrodynamic behaviour of fluidized beds [5, 6, 7]. The ECT sensor consists of a series of electrodes placed around the periphery of the vessel to be imaged. In the measurement sequence, each electrode is sequentially supplied with an electrical potential while the others remain grounded [8]. Thus, an electrical field is applied across the measurement cross-section. From the interaction of this electric field with the material within the sensor, the distribution of phases within the measurement plane can be determined.

ECT is described as a 'soft-field' tomographic technique indicating that measurements of capacitance resulting from the projections of electrical field lines are influenced by the distribution of high and low permittivity phases. This is in contrast to a 'hard-field' technique such as x-ray tomography where only the change in distribution of material along the projection paths affects the measurements. Therefore, the tomographs derived from 'soft-field' tomographic techniques are more qualitative or semi-quantitative and have low spatial resolution while a 'hard-field' technique results in more quantitative measurements with higher spatial resolution. However, conventional x-ray tomography generally has a lower temporal resolution compared to ECT [9]. Therefore, ECT is useful in the evaluation of rapid changes in hydrodynamic behaviour such as the passage of individual bubbles.

An early example of the imaging of fluidized beds using x-rays can be found in Rowe et al. [10]. The works of Kantzas and Kalogerakis [11] and Wright et al. [12] have shown the benefits of x-ray computer assisted tomography (CAT) for the determination of the phase distribution in gas-solid fluidized systems. Recently, Newton et al. [13] has

shown that the fluidization regime transition from bubbling to turbulent fluidization behaviour can be determined through the use of direct x-ray data. The operation of a fluidized bed within a desired fluidization regime is an important means of optimizing its performance. In fluidized bed drying, tomographic imaging can reveal flow behaviour specific to a hydrodynamic regime which can improve mixing, thus increasing drying rate and bed homogeneity. Furthermore, deleterious effects such as the entrainment of fines can be mitigated by operating within a specific fluidization regime. Both x-ray tomography and ECT are non-invasive techniques for determining fluidization behaviour directly.

In the current study, we apply ECT to a fluidized bed containing drying pharmaceutical granule. Capacitance data provided by the ECT sensor is to be corrected utilizing a dynamic calibration technique which accounts for the significant change in bed (dense phase) permittivity occurring throughout the drying process. X-ray tomography will be utilized as a secondary measurement technique to confirm the validity of this calibration procedure. In addition, the validity of our ECT image reconstruction technique will be tested with respect to both the permittivity models applied to the raw measurements of capacitance and the number of iterations utilized.

6.4 Experimental

6.4.1 Overview of Drying Experiments

The fluidized bed drying apparatus is shown in Figure 6.1 when configured for the collection of ECT data. The acrylic cone fitted with the ECT sensor has the internal dimensions shown in Figure 6.2(a) while the internal dimensions of the acrylic cone

utilized for the x-ray imaging and auxiliary drying experiments are given in Figure 6.2(b). The acrylic cones in Figure 6.2, which are very similar in geometry, allow for the processing of batches of wet material as large as 4 kg. These conical sections, which are commonly referred to as the product bowl in the pharmaceutical industry, are attached to a 10 cm tall cylindrical windbox having a diameter of 11.5 cm. The acrylic cone shown in Figure 6.2(b) is fitted with a sample thief constructed of a Teflon cylinder having a sample cavity which could be inserted into the fluidized bed. This sample thief allowed for the removal of a sample of approximately 1 g from the bed during operation. However, the ECT cone in Figure 6.2(a) has no such capability due to the location of the electrodes. Thus, for ECT experiments, moisture samples could only be taken from the surface of a defluidized bed.

Fluidizing air was supplied by a rotary blower (the SCL V4, Effepizela, Italy). Heating of this air was provided by a Watlow CBEN24G6-21 electrical heater. Control of the air temperature was handled by a Watlow series 935A PID logic controller with feedback provided by a grounded type-J thermocouple inserted into the windbox. Metering of the air supply was provided by the measurement of pressure drop across an orifice plate. Air velocity was manually controlled using a bypass valve located immediately downstream of the blower. In order to provide even distribution of air within the fluidized bed, a distributor plate was constructed of a 1.5 mm thick aluminium plate drilled with 2 mm diameter holes in a square pitch giving an open area of 5.6 %. A 1.37 m tall cylindrical acrylic freeboard section is flange-connected to the top of the product bowl. Particles in the gas stream exiting the top of the freeboard

section were separated from the air stream utilizing an acrylic cyclone designed to achieve the capture of 99% of particles larger than 75 μm.

For the preparation of wet pharmaceutical granules, dry ingredients were combined in a low-shear granulator (250 W Kitchen-Aid Classic mixer) and mixed for 2 minutes at the lowest speed (setting 1). Low-speed mixing was continued while water was added to the mixture over a five minute period at a constant rate of 63 mL/min through a medium-flow, variable-speed peristaltic pump provided by VWR Scientific. Wet granulation was followed by 2 minutes of post-granulation mixing at a slightly higher speed (setting 2 on the mixer). The granulation product was then sieved through a 3.36 mm screen in order to remove large particles. The maximum amount of wet granule that could be produced by the granulator was 1 kg. The quantities of dry granule ingredients and water required for a 1 kg batch are given in Table 1. These particles have a porosity of approximately 30% and have a particle size distribution given in Table 2 as determined with a Malvern Mastersizer S Long Bench particle size analyzer. Three granulations were performed in order to produce 3 kg of wet granule required for each experimental run. To ensure consistent moisture and a representative measurement for the baseline moisture, these batches were well mixed before removal of the first moisture sample and subsequent drying. Three types of experiments were performed. These included; a drying experiment in the ECT acrylic cone presented in Figure 6.2(a), an x-ray imaging experiment with the acrylic cone in Figure 6.2(b) and an auxiliary experiment utilizing the acrylic cone in Figure 6.2(b). The auxiliary experiment was performed in order to determine the drying curve to apply to the x-ray data since it was not possible to make moisture measurements during the x-ray experiment. Samples of 3

g were taken at discrete intervals throughout the auxiliary drying experiment and moisture samples were analysed within 2 hrs of its completion using a Mettler-Toledo HB43 drying balance.

For all three experiments, fluidizing air was heated to an inlet temperature of 65°C measured in the windbox. The superficial gas velocity, defined as the average velocity across the inlet to the conical section, was maintained at 1.35 m/s. An elevated superficial gas velocity of 2.1 m/s was required initially in order to maintain good mixing within the unit in a very wet bed. These operating conditions are in line with those used in the pharmaceutical industry for the drying of pharmaceuticals.

6.4.2 Tomographic Experimental Details

The ECT unit utilized in this imaging study consists of an 8 electrode sensor with 2 measurement planes manufactured by Process Tomography Limited (PTL) U.K. Data acquisition is handled by a data acquisition module (DAM-200) and personal computer supplied by Process Tomography Limited. Further description of the sensor is given in Pugsley et al. [4]. In the current study, only the lower measurement plane was used. This was done because of loss of the top measurement plane sensor coverage at reduced moisture caused by particle shrinkage during the drying process. A schematic of the electrode configuration of the ECT sensor used in this study is given in Figure 6.3. Each electrode has a length of 4 cm and the measurement region encompasses a height between 8.57 and 12.38 cm above the distributor for the lower measurement plane used in this study. Therefore, each pixel in the ECT tomograph represents an axial average over this conical measurement volume.

Throughout the ECT experiment, both dynamic and packed bed readings of capacitance were taken using the ECT sensor. Dynamic measurement data sets were collected for 2 minutes at 100 Hz. These dynamic measurements were interspersed with capacitance measurements of a packed bed. These packed bed readings were taken by shutting off the fluidizing air and allowing the bed to attain a packed state. 10 seconds of ECT data (corresponding to 1000 frames) was recorded in the packed bed state. A full description of the analysis of the ECT data is given in Section 6.4.3. Before continuing the drying experiment after a packed bed reading, a 3 g sample of granule was removed from the bed and placed in a sealed sample vial for moisture analysis. Moisture samples were performed within 2 hrs of the completion of the drying experiment utilizing the Mettler-Toledo HB43 drying balance.

The x-ray CAT scanner used in this study consists of a third generation medical scanner (Advantage GE9800) with its gantry positioned horizontally allowing for the scanning of the vertically positioned acrylic cone in Figure 6.2(b). Images of the bed were taken throughout the drying process at a number of axial locations. Each pixel in the x-ray tomograph represents an average reading over an axial thickness of 1.5 mm. The scanning locations utilized for comparison with the ECT data were at 9.5 and 12.5 cm above the distributor and are shown in Figure 6.2 (b). These heights correspond to the ECT measurement volume defined in Figure 6.2(a). Further description of the CAT scanner used in this study is given in Kantzas et al. [11] and Wright et al. [12].

Measurements from the x-ray CAT scanner were analysed in house. The scanner generates 512x 512 pixel tomographs consisting of CT (computed tomography) numbers. The data from the area describing the bed cross-section or region of interest

was then separated from each image. CT numbers in the region of interest were converted to a density map through a linear calibration based on CT measurements of a number of materials placed within the CAT scanner having densities between that of air and wet pharmaceutical granulate. The result of this analysis is a density map over the region of interest. The centerline pixels in the x and y directions from this image were then separated from this density map. From these selected pixels, a single average radial profile was generated. This procedure is similar to that used for the generation of radial profiles from ECT density data given in Section 6.4.3.2. Each density map corresponds to an average of ten scans each of 4 seconds duration.

6.4.3 ECT Data Analysis

6.4.3.1 Correction of ECT data for moisture

Measurements of capacitance form the basis of the image generated by the ECT sensor. For an 8 electrode sensor, there are 28 unique combinations of electrodes resulting in 28 unique readings of capacitance for each image. In order to implement the reconstruction technique to generate tomographs, the normalization of the raw capacitance measurements is necessary. This normalization is based on capacitance readings made in a packed bed of solids or the dense phase filling the sensor (C_H) and with air or the dilute phase filling the sensor (C_L). These high and low measurements of capacitance are performed at the start of the experiment and are applied to all 28 measurements. Normalized capacitance is defined through Equation 1.

$$C_N = \frac{C_M - C_L}{C_H - C_L} \qquad [1]$$

This normalization of the 28 measurements is valid as long as the permittivity of the two phases remains constant. In the current application, we are drying pharmaceutical granulate from approximately 33-wt% to approximately 2-wt%. Since permittivity is proportional to capacitance and water has a relative permittivity of approximately 81 compared with a relative permittivity of approximately 2.6 for the dry pharmaceutical granule, the above calibration does not remain valid throughout drying process. Although the value of C_L will remain fixed as the permittivity of air, the permittivity of the full sensor C_H is influenced by changes in moisture. Therefore, a dynamic calibration based on the change in capacitance readings in a sensor filled with the dense phase as a function of moisture must be determined.

In order to generate this dynamic calibration, the packed bed ECT readings described in Section 6.4.2 can be utilized to relate C_H to moisture. A linear least squares fit can then be applied to this data for each of the 28 unique electrode combinations. From these calibration curves, the value of C_H could be determined and integrated into Equation 1 in order to generate normalized capacitance readings at any point in the drying process. The calibration procedure could have been simplified to reduce the number of calibration curves to the four possible electrode combinations in an 8-electrode sensor (i.e. opposite electrodes, adjacent electrodes etc.). However, it was found that this approach led to image artifacts in the reconstructed tomographs.

Correction of the dynamic ECT data collected throughout the drying process was made off-line to measurements of capacitance (C_M). Bed moisture was determined from the drying curve and utilized to determine C_H from each of the 28 linear calibration

curves. These values of C_H along with measurements (C_M) were used in Equation 1 to generate the normalized capacitance readings suitable for image reconstruction.

6.4.3.2 Image Reconstruction

An overview of ECT image reconstruction techniques is given in Isaksen [14]. The reconstruction techniques used in the current study are basic linear back-projection (LBP) and the iterative linear back-projection algorithm provided by Process Tomography Limited. Further discussion of these techniques is given in McKeen and Pugsley [8]. A thresholding between values of 0 and 1 for the individual pixels and truncation of the error vector (-0.05< ΔC <0.05) was performed for each iteration. A gain factor of 1.25 was selected based on the convergence criterion suggested by Yang et al. [15] for a similar iterative reconstruction algorithm.

The application of permittivity models to ECT measurements is discussed in McKeen and Pugsley [8] where the parallel, series and Maxwell models were examined. In the current work, we will apply these models to the dynamic ECT data along with the Böttcher model [2, 16, 17] given in Equation 2.

$$\frac{C_M - C_L}{3C_M} = \frac{x(C_H - C_L)}{C_H + 2C_M} \qquad [2]$$

This equation can be rewritten in terms of normalized capacitance and permittivity ratio:

$$x = \frac{PR \cdot C_N}{3C_N(PR-1)+1} + \frac{2}{3}C_N \qquad [3]$$

Mixture models, such as the Böttcher model, are based on the assumed contribution of each component substance to the overall capacitance measurement. Equation 2 has been derived from the assumption that the dielectric constant of the mixture is equivalent to the contribution of the solid material (high permittivity phase) suspended in a continuous medium having a dielectric constant equal to that of the mixture. This contrasts the model of Maxwell, which assumes that the high permittivity material is dispersed within a medium having a permittivity equal to that of the low permittivity component. The Böttcher model is valid for mixtures of powders having higher permittivity ratios (C_H/C_L) or solids concentrations [17] and lies between the extremes of the parallel and series models. The Böttcher model reduces to the Maxwell model at low values of permittivity or low solids concentrations [16].

Since significant changes in permittivity ratio accompany the drying process and this ratio is a factor in Equation 3, calculation of the permittivity ratio throughout the drying process is required. Permittivity ratio can be determined from the capacitance data collected in the packed bed from the opposite electrodes (i.e. electrode pairs 1-5, 2-6, 3-7 and 4-8). Capacitance readings from opposite electrodes provide the best estimate due to the fact that their electrical field lines are influenced mostly by material within the acrylic cone. This is in contrast to, for example, adjacent electrodes. Electrical field lines between adjacent electrodes may be influenced by the permittivity of the acrylic wall of the ECT cone. By dividing the opposite electrode packed bed capacitance readings (C_H) by the corresponding readings obtained in an empty bed (C_L), a reasonable estimate of the packed bed permittivity ratio as a function of moisture can be determined.

The reconstructed ECT data results in 32x32 matrices having pixels in the form of normalized permittivity between the extremes of full sensor (1) and empty sensor or air (0). To compare this information directly with x-ray data, which is in the form of absolute density, the transformation given in Equation 4 is employed.

$$\rho = p\left(\rho_{pb} - \rho_{air}\right) + \rho_{air} \qquad [4]$$

From the data, transformed through Equation 4 from the ECT image, a radial profile was then generated by averaging the centerline pixels in the x and y directions. These cross-sections were then combined to form a single average radial profile from the centreline to the wall of the cone. A schematic of the region of interest and the pixels used to generate the average radial profile from the ECT data is given in Figure 6.3. In order to compare the ECT data to the x-ray radial profiles, an average over 40 seconds or 4000 frames of ECT data collected at 100 Hz was compared with each x-ray radial profile.

6.5 Results and Discussion

Drying curves for the ECT experiment and the auxiliary experiment are given in Figure 6.4. As can be seen in this plot, there is a slight variation in the performance between the ECT cone and the acrylic cone. This is possibly due to the slight difference in geometries seen in Figure 6.2. Furthermore, samples from the ECT experiment were taken from a defluidized bed while samples from the acrylic cone were taken while the bed was in the fluidized state. This difference in sampling technique could have resulted in a slight variation in the determined moisture content. Bed moisture was assumed to follow the identical profile to that observed in the auxiliary experiment for the x-ray

experiment since identical cone geometry, inlet temperature and superficial gas velocity was utilized in all experiments. In the ECT experiment, the drying curve was used to determine the bed moisture at any point in time. Dynamic ECT data, collected at a specified point in the drying process, could then be related to a specific moisture content. This moisture content was then used to determine permittivity ratio (Figure 6.5) and dense phase capacitance readings (C_H) through the dynamic calibration curves.

Figure 6.5 demonstrates the calibration curve for permittivity ratio based on a linear least squares fit. As described in Section 6.4.3.2, this data is derived from packed bed capacitance measurements of the four possible opposite electrode combinations. The equation for the fit function is given by Equation 5.

$$PR = a \cdot M + b$$
$$f(a,b) = \sum_{i=1}^{n} \left[PR_i - \left(a \cdot M_i + b \right) \right]^2 \qquad [5]$$

Here the objective function, *f(a,b)*, is minimized over *i=1…n* data points and is used to determine the vales of constants *a* and *b*. For the 28 calibration curves relating absolute packed bed readings of capacitance with moisture, Equation 5 is applied to capacitance measurements (C_H). These curves were found to follow an identical shape to the curve in Figure 6.5. A slight separation in the data from the linear fit can be noted at moisture contents of 8-wt% and 22-wt%. Below 5-wt%, there is also slight divergence from the linear fit. Some success has been achieved in fitting both the parallel and Böttcher permittivity models to this data (not shown). These models assumed a constant voidage and resulted in a calibration curve similar to the linear fit function in Figure 6.5 with the divergence near the identical moistures noted above. The divergence in the data

suggests that changes are occurring in bed voidage caused by particle shrinkage or surface changes during drying which are not approximated by the linear fit functions or the permittivity models. Despite these inconsistencies, for this initial investigation of the correction technique, linear fit functions have been used for all 28 dynamic calibration curves relating dense-phase capacitance readings to moisture.

Figures 6.6 and 6.7 show ECT radial profiles reconstructed utilizing the four capacitance models. These profiles are compared to the x-ray radial profile collected at identical moisture. The raw ECT data has been corrected with the linear fit function relating capacitance to moisture discussed above. Each ECT radial profile is a time-averaged profile of 40 seconds of ECT data corresponding to the time taken to generate each x-ray profile. X-ray radial density profiles for both figures were collected at 9.5 cm above the distributor in the acrylic cone. Figure 6.6 compares ECT and x-ray profiles in a bed having a moisture content of 21-wt% while Figure 6.7 compares data collected in a bed which has a moisture content of 1.6-wt%. The permittivity ratio of the packed bed material in Figure 6.6 and Figure 6.7 are 14 and 3.3 respectively as determined from the relationship in Figure 6.5. The superficial gas velocity is 1.35 m/s for all data presented.

The ECT data presented in Figures 6.6 and 6.7 were reconstructed utilizing 100 iterations as recommended in the work of McKeen and Pugsley [8] for the application of ECT to bubbling fluidized beds. It was found that the time-averaged ECT radial profiles were not affected significantly by the number of iterations in excess of 50 iterations. This result is in line with the speculation in Pugsley et al. [4] where it is stated that a lower number of iterations would be required to accurately reconstruct ECT data at

velocities 2 to 3 times higher than their highest velocity investigated of 0.6 m/s. The superficial gas velocity of 1.35 m/s utilized in the current study is within this range.

The Böttcher model predicts the radial density distribution of the two phases most accurately in Figure 6.6. The improved agreement of the ECT radial profiles with the x-ray data provided by the Böttcher model at higher moisture is similar to the results of Louge and Opie [16]. This study demonstrated that the Böttcher model provides a better estimate of the permittivity ratio compared to Maxwell, series and parallel models for the measurement of relative permittivity as high as 8 in moist porous particles suspended in petroleum jelly. The similarity of the ECT radial profile in Figure 6.6 reconstructed after the application of the Böttcher model demonstrates that the variation in hydrodynamic behaviour between the conical geometries is negligible at this moisture.

At bed moisture below approximately 5-wt%, the parallel model was found to provide a better prediction of the solids distribution. This is illustrated in Figure 6.7. In comparison to Figure 6.6, where the parallel model under-predicts the x-ray data, the profiles in Figure 6.7 all over-predict the x-ray data and are more flattened in shape. Variations in hydrodynamic behaviour occurring as a result of changes in geometry are not a likely cause of differences in the radial profiles since the shape of the radial profiles generated from x-ray tomography and the ECT sensor (parallel model) have the similar point of inflection near 0.05 m and similar overall curvature. The disparity between profiles can be better explained by the limitations of the ECT sensor at low dense phase permittivity. At the lower moisture content or particle permittivity in Figure 6.7, the ECT sensor can not as clearly distinguish between the dense and dilute phases.

The fact that the parallel model appears to predict the radial profile of the bed best at reduced moisture or low permittivity (Figure 6.7) is consistent with the findings of McKeen and Pugsley [8]. This study indicated that this model is superior in a bed of FCC catalyst having a permittivity ratio of 2.4. The findings of Wiesendorf and Werther [2] also indicate that a parallel model gives the most accurate estimate of solids concentration for capacitance probe measurements of gas-solids suspensions of quartz particles having a low permittivity ratio of between 2.4 and 2.9. The fact that the suitability of the permittivity model is dependent on the permittivity ratio of the bed has implications for the interpretation of ECT data since the correct permittivity model required for an accurate representation of the hydrodynamics may not be the same depending on the bed moisture content. From Figures 6.6 and 6.7, the accuracy of the parallel or the Böttcher permittivity models depends on the bed moisture content.

In both Figure 6.6 and Figure 6.7, close agreement is seen between the Böttcher model and the Maxwell model towards the centre of the bed where the flow exhibits a low solids concentration. This is especially true in Figure 6.7, where the bed density and, therefore, dense phase permittivity ratio is low. This is in agreement with the findings of Louge and Opie [16] who point out that, at low permittivity ratios or low concentration of the dense phase, the Böttcher model reduces to the Maxwell model.

The influence of number of iterations on the ECT radial profile is examined in Figure 6.8. The ECT and x-ray data compared in this figure were collected in a bed having a moisture content of 8-wt% and a permittivity ratio of 6.7. The Böttcher permittivity model was applied to the measured capacitance data for all curves. X-ray data was collected at a height of 12.5 cm above the distributor. As stated above, the

majority of reconstructed ECT radial profiles did not exhibit any change in their time-averaged behaviour with increased iterations. However, for a number of data sets, the reconstruction algorithm did not converge to a single density distribution. This is demonstrated in Figure 6.8. The periodic appearance of a high density region in the centre of the imaging plane is evident upon examination of tomographs from the 4000 frames used to generate the radial profile in Figure 6.8. In Figure 6.9 the density distribution of the 39^{th} frame from this data set is shown. It is doubtful that the central region approaches the density of the packed solids as suggested by this contour plot when one considers the high superficial gas velocities examined in this study. It can be seen in Figure 6.5 that, at 8-wt% moisture, the linear fit function relating moisture to permittivity under-predicts the packed bed readings. This discrepancy suggests a possible problem with the calibration procedure. Since all calibration curves relating capacitance to moisture follow this same profile, normalization of each of the 28 capacitance measurements will suffer from this error.

The effect of inconsistency between the linear fit function and the data is examined in Figure 6.10. Figure 6.10 presents the identical data sets shown in Figure 6.8. However, here, the correction in Equation 2 was applied utilizing a linear interpolation between the data points near 8-wt% on the 28 calibration curves. As can be seen in Figure 6.10, the ECT data now agrees more closely to the x-ray profile. The region of elevated density near the centre is still apparent in the diagram. However, the density in the centre does not increase after 50 iterations, indicating convergence of the reconstruction algorithm. Figure 6.11 shows the identical frame seen in Figure 6.9 using the revised calibration procedure presented in Figure 6.10. Again, the elevated density at

the centre is still apparent but it no longer approaches that of a packed bed (500 kg/m^3) as is seen in Figure 6.9. This correction demonstrates the sensitivity of the calibration to errors and highlights the need for an accurate determination of the changes in voidage accompanying the drying process.

Another contribution to the difficulties encountered in the comparison of tomographic techniques is the assumed packed bed density of 500 kg/m^3 used in Equation 4 to determine the ECT density profile. An increase in packed bed density from 495 kg/m^3 to 505 kg/m^3 was recorded over the entire drying process based on two x-ray packed bed measurements taken before and after drying. The use of these values in Equation 4 was found to have little effect on the ECT radial profiles in Figure 6.7 and Figure 6.10. Some variation in density with measurement height was also identified in the x-ray data. Although this variation was also slight, the effect of this change was not independently verified using ECT and may have implications for the application of ECT to fluidized beds where bed height is variable. Future investigations applying the dynamic calibration procedure will require more precise quantification of the influence of packed bed density and particle density if more quantitative measurements of density or bed voidage are required from the measurements of relative permittivity provided by ECT.

6.6 Conclusions

A dynamic calibration procedure based on moisture has been implemented for the ECT imaging of a bed of drying pharmaceutical granule. This calibration is based on a least-squares linear fit of packed bed capacitance readings taken throughout the drying

process. This calibration has been validated by the use of a secondary technique, x-ray tomography. On a time-averaged basis, ECT provides similar radial profiles to those obtained through x-ray tomography. The Böttcher permittivity model has been found to more accurately predict the permittivity distribution at high moisture contents or permittivity ratios while the parallel model provides a better prediction of the bed density distribution at low moisture or permittivity.

In the reconstruction of ECT images, it was found that 50 iterations were sufficient to describe the density distribution within the column on a time averaged basis. Excessive iterations were found to generate image artifacts for certain data sets. By repeating the correction procedure utilizing linear interpolation of the data in the vicinity of the dynamic data, better agreement of the ECT data with the x-ray radial profiles has been achieved for these data sets. This improvement to the images caused by this slight modification to the calibration highlights the sensitivity of the correction to errors the calibration curve. This indicates that the dynamic calibration curve may need to be non-linear in order to achieve a higher accuracy. Changes in bed voidage or packing density need to be examined more closely in order to accomplish this.

For practical implementation of the dynamic calibration of an ECT sensor, a means of determining the bed moisture content on-line is required. A technique such as near infra-red (NIR) could be used for this purpose. Data from this sensor could be relayed to a computer handling acquisition of the ECT data. The calibration would then be implemented in real time as data is collected as normalized capacitance. Although reconstruction of ECT images must be done off-line presently, newer high-speed ECT

reconstruction techniques such as that presented by Warsito and Fan [18] will allow for real-time visualization of the fluidization dynamics in a fluidized bed dryer using ECT.

6.7 Acknowledgements

The authors would like to thank the Natural Sciences and Engineering Research Council of Canada (NSERC) and Merck Frosst Canada & Co. for financial assistance. The technical assistance of the staff at the Tomographic Imaging and Porous Media Laboratory (TIPM) is gratefully acknowledged in the running of the x-ray tomography experiments as well as for consultation regarding the interpretation of the data. The technical assistance of Michael Wormsbecker is also much appreciated for the particle size analysis.

6.8 References

[1] Chaplin G, Pugsley T, 2004 The S-statistic as an early warning of entrainment in a fluidized bed dryer containing pharmaceutical granule *Powder Technol.* **149** 148-156 [Chapter 4]

[2] Wiesendorf V, Werther J, 2000 Capacitance probes for solids volume concentration and velocity measurements in industrial fluidized bed reactors *Powder Technol.* **110** 143-157

[3] Karamavruç A I, Clark, N N, 1997 A fractal approach for the interpretation of local instantaneous signals around a horizontal heat transfer tube in a bubbling fluidized bed *Powder Tech.* **90** 235-244

[4] Pugsley T, Tanfara H, Malcus S, Cui H, Chaouki J, Winters C 2003 Verification of fluidized bed electrical capacitance tomography measurements with a fibre optic probe *Chem Eng Sci.* **58** 3923-3934

[5] Makkawi W T, Wright P C 2002 Fluidization regimes in a conventional fluidized bed characterized be means of electrical capacitance tomography *Chem. Eng. Sci.* **57** 2411-2437

[6] Tanfara H, Pugsley T, Winters C 2002 Effect of particle size distribution on local voidage in a bench-scale conical fluidized bed dryer *Drying Technol.* **20** 1273-1289

[7] Sidorenko I, Rhodes M J 2004 Influence of pressure on fluidization properties *Powder Technol.* **141** 137-154

[8] McKeen T R, Pugsley T S 2002 The influence of permittivity models on phantom images obtained from electrical capacitance tomography *Meas. Sci Technol.* **13** 1822-1830

[9] Toye D, L'Homme G, Crine M, Marchot P Perspective in data fusion between x-ray computed tomography and electrical capacitance tomography in an absorption column *Proc. 3rd international Congress on Industrial Process Tomography, Banff, September 2-5 2003* pp 68-73

[10] Rowe, P N, Partridge B A 1965 An x-ray study of bubbles in fluidised beds *Trans. Instn. Chem. Engrs*. **43** 157-175

[11] Kantzas A, Kalogerakis N 1996 Monitoring the fluidization characteristics of polyolefin resins using x-ray computer assisted tomography *Chem. Eng Sci.* **51** 1979-1990

[12] Wright I, Hamilton K, Kruychkov S, Chen J, Li F, Kantzas A 2001 On the measurement of hydrodynamic properties of an air-polyethylene fluidized bed system *Chem. Eng Sci.* **56** 4085-4097

[13] Newton D, Fiorentino M, Smith G B 2004 Comments and experimental data on the transition from bubbling to turbulent fluidization *Proc. Fluidization XI., Ischia (Naples) 9-14 May 2004 ed. U. Arena, R. Chirone, M. Miccio, P. Salatino* pp 531-538

[14] Isaksen Ø, 1996 A review of reconstruction techniques for capacitance tomography *Meas Sci Technol.* **7** 325-337

[15] Yang W Q, Spink D M, York T A, McCann H 1999 An image reconstruction algorithm based on Landweber's iteration method for electrical-capacitance tomography *Meas. Sci. Technol.* **10** 1065-1069

[16] Louge M, Opie M 1990 Measurements of the effective dielectric permittivity of suspensions *Powder Technol.* **62** 85-94

[17] Böttcher, C. J. F., Bordewijk, P., Theory of Electric Polarization, Volume 2: Dielectrics in time-dependent fields, Elsevier Scientific Publishing Company, New York, 1978

[18] Warsito W, Fan L-S 2001 Neural network based multi-criterion optimization image reconstruction technique for imaging two- and three-phase flow systems using electrical capacitance tomography *Meas. Sci Technol.* **12** 2198-2210

Table 6.1 Wet granulation ingredients

Component	Percentage by mass (dry basis)	Amount (g) for a 1 kg (wet) batch
Lactose Monohydrate (filler)	50%	375
Microcrystalline Cellulose (filler)	44%	330
Croscarmellose Sodium (disintegrant)	2%	15
Hydroxypropyl Methylcellulose (binder)	4%	30
Water (distilled)	43%	315

Table 6.2 Particle size distribution of dry pharmaceutical granule

Particle Size (µm)	Mass percentage in range
<75	3.41
75-105	6.04
105-149	11.32
149-210	12.95
210-297	10.99
297-420	8.23
420-590	6.89
590-850	8.32
850-1190	9.6
1190-1680	10.41
1680-2380	7.96
2380-3360	3.71
>3360	0.17

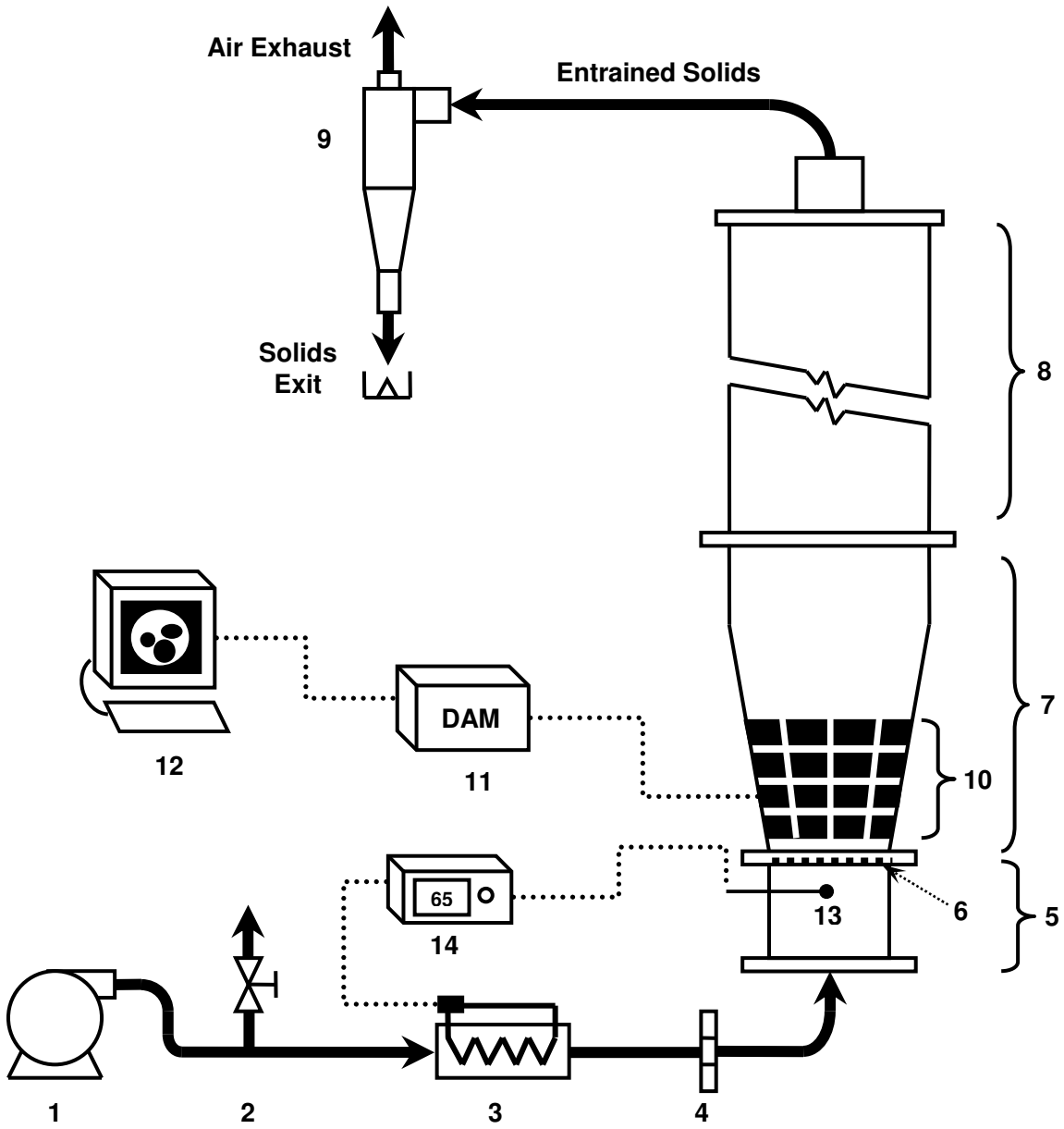

Figure 6.1 Fluidized bed dryer apparatus components and instrumentation. Blower (1), air bypass (2), air heater (3), orifice (4), windbox (5), distributor (6), product bowl (7), freeboard (8), cyclone (9), electrical capacitance tomography sensor (10), ECT data acquisition module (11), data acquisition computer (12), air-supply thermocouple (13), air heater controller (14).

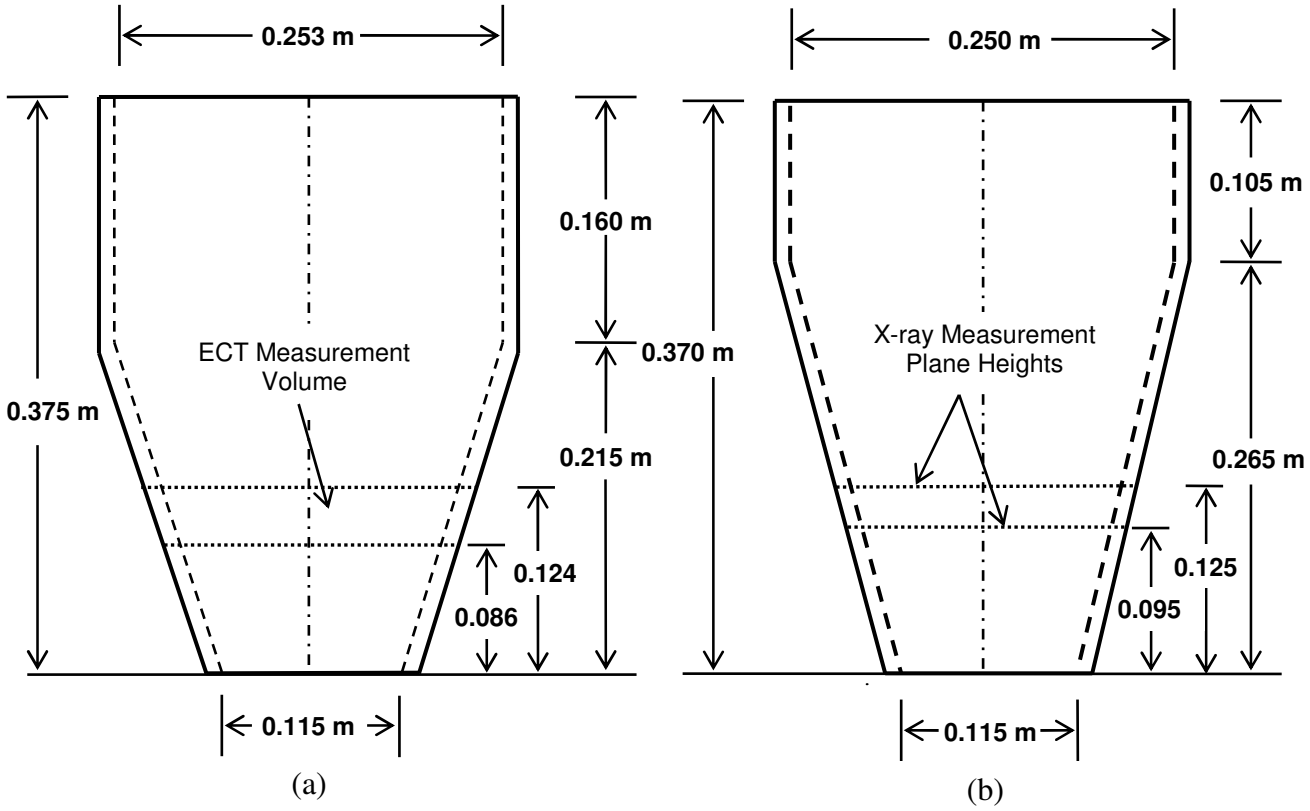

Figure 6.2 Internal dimensions and tomographic measurement heights in the acrylic cones used in this study. Conical section utilized for the ECT experiment (a). Acrylic cone utilized for the x-ray experiment (b).

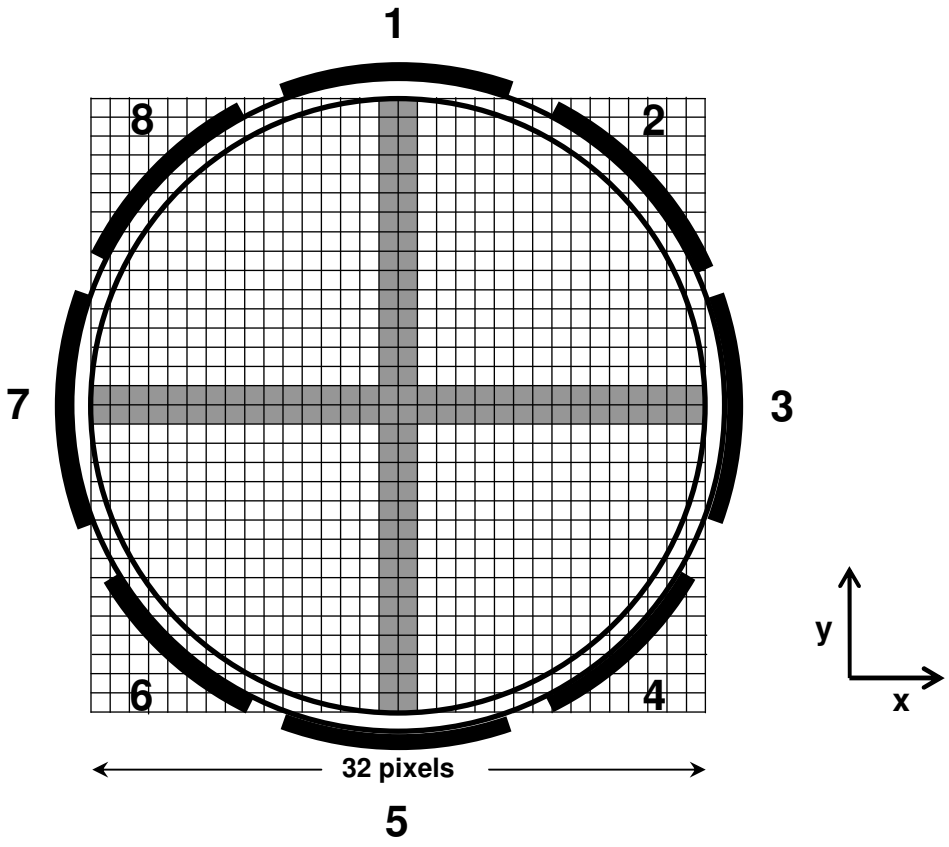

Figure 6.3 Electrode configuration for the ECT sensor used in this study. The pixel layout for the region of interest is shown. Shaded pixels are those used for the generation of radial profiles from ECT data.

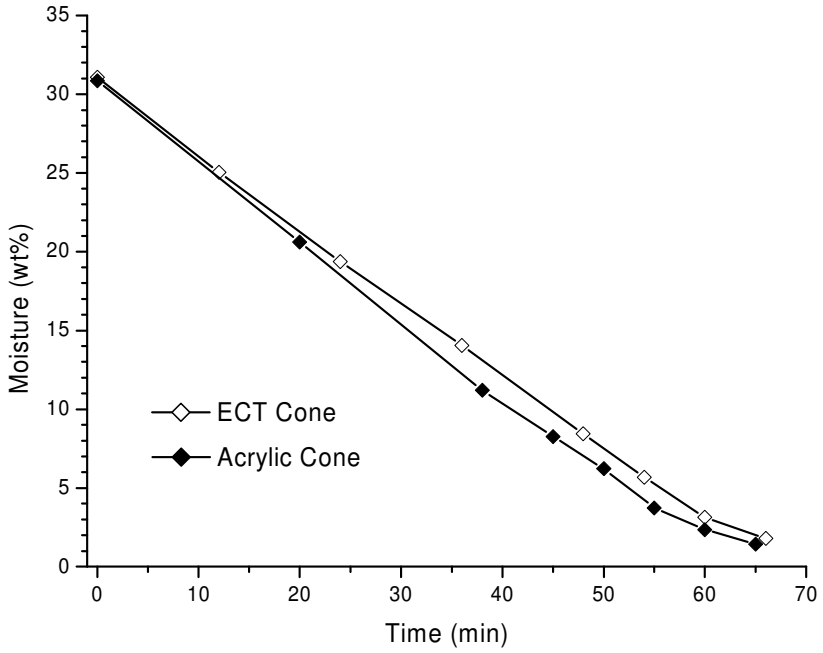

Figure 6.4 Drying curves for experiments performed in the two conical units shown in Figure 6.2.

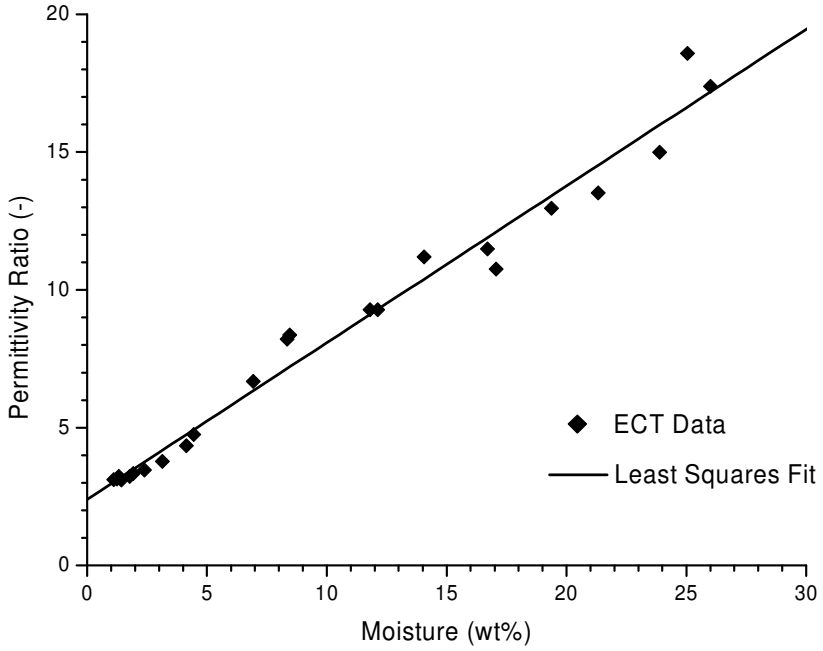

Figure 6.5 Calibration curve for the permittivity ratio calculated from packed bed ECT capacitance measurements at opposite electrodes throughout the drying process.

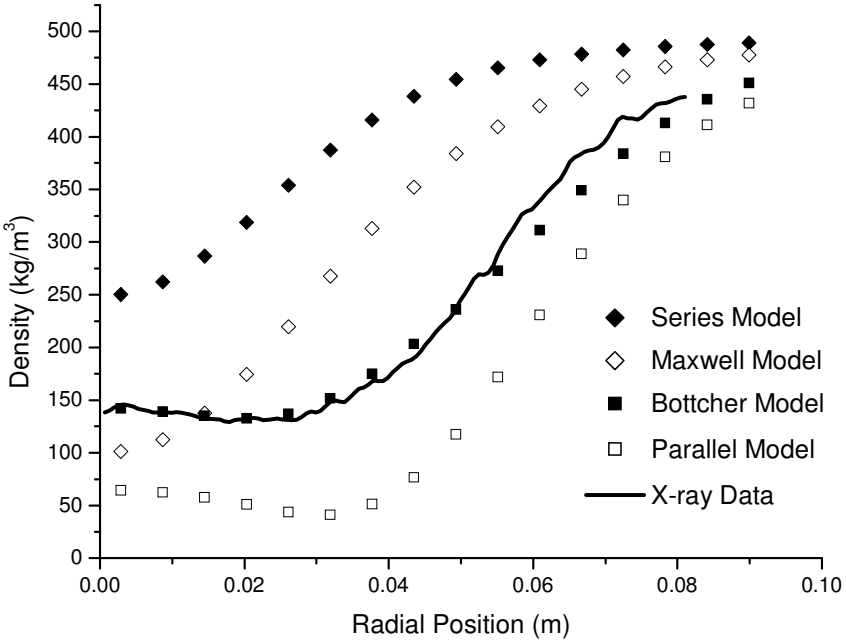

Figure 6.6 Comparison of time-averaged ECT radial density profiles reconstructed using the four permittivity models with the x-ray tomography radial profile. Bed moisture is 21-wt% for both the ECT and x-ray data.

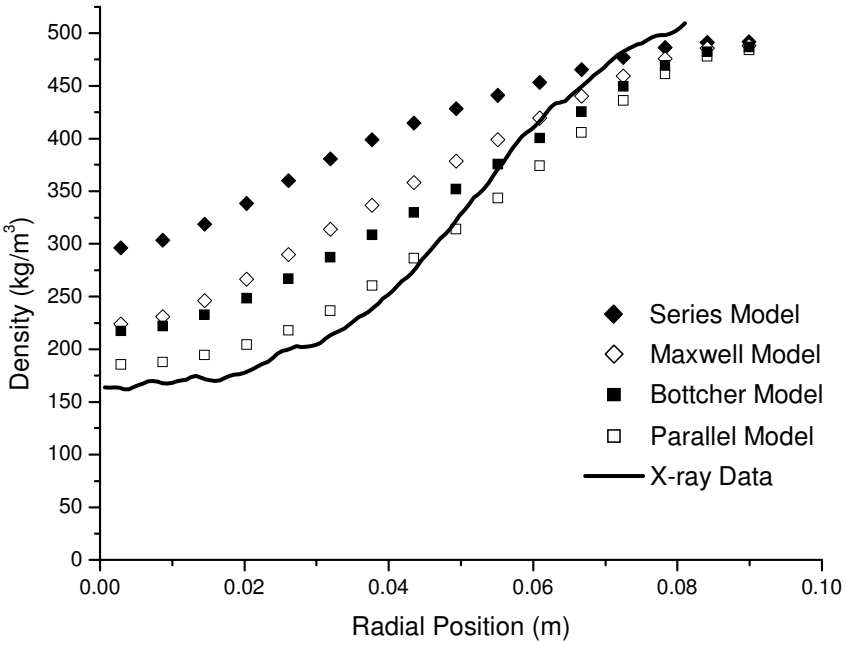

Figure 6.7 Comparison of time-averaged ECT radial density profiles reconstructed using four permittivity models with the x-ray tomography radial profile. Bed moisture is 1.6-wt% for both the ECT and x-ray data.

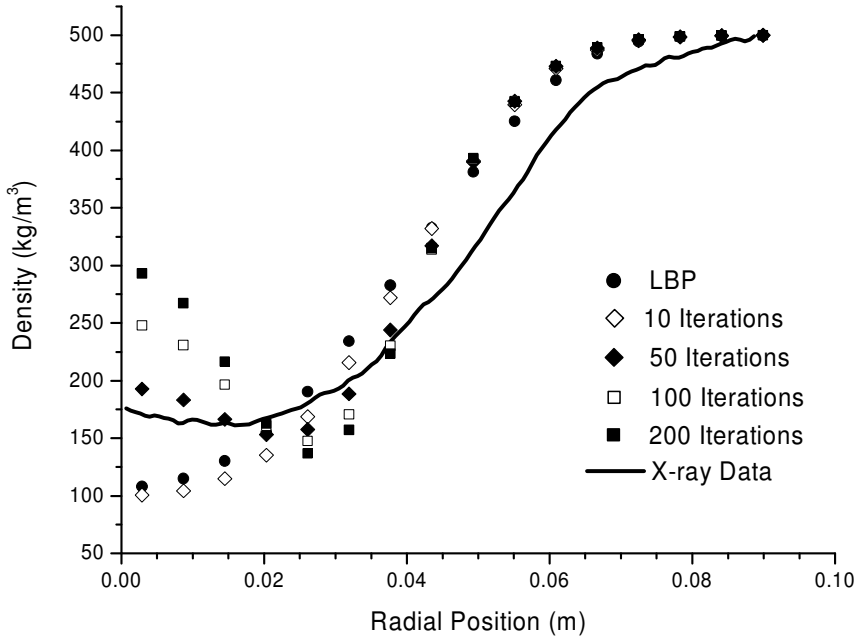

Figure 6.8 Influence of the number of iterations in the iterative LBP algorithm on the ECT radial profile reconstructed using the linear calibration presented in Figure 6.5.

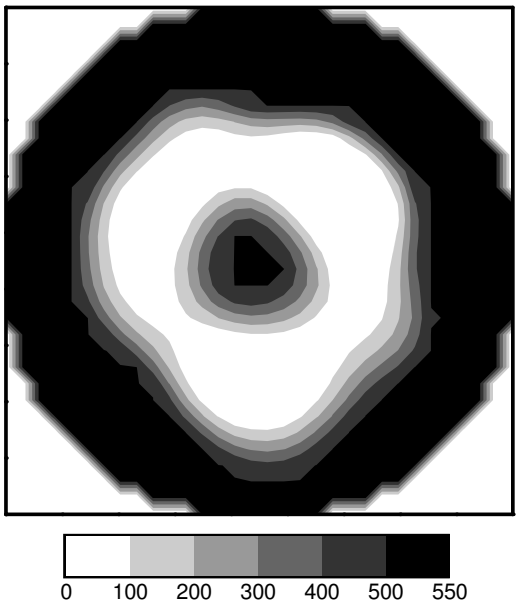

Figure 6.9 A single ECT tomogram from the data set presented in Figure 6.8. Legend represents density readings in kg/m^3.

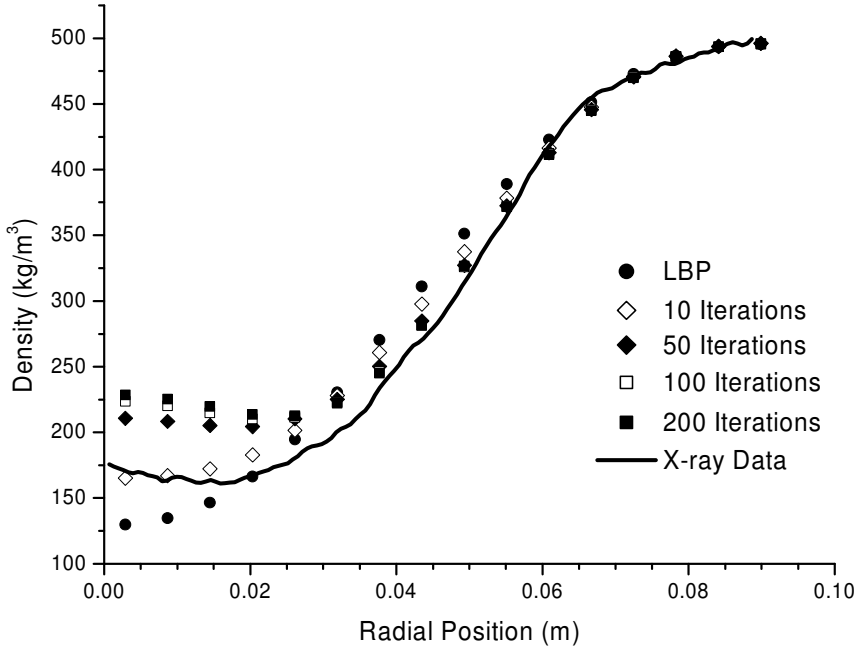

Figure 6.10 Influence of the number of iterations in the iterative LBP algorithm on the ECT radial profile reconstructed using the modified calibration.

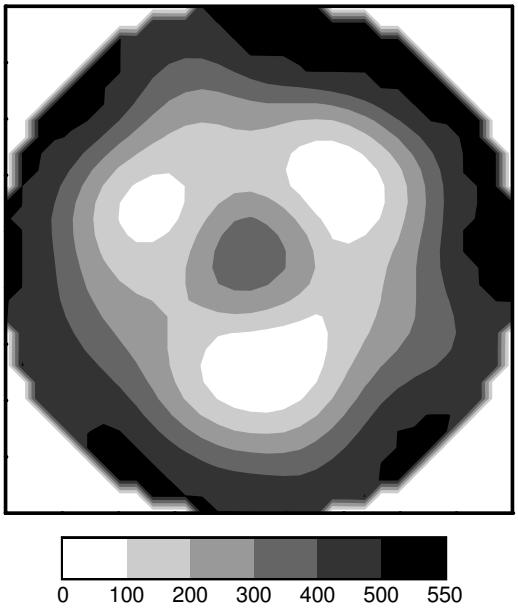

Figure 6.11 A single ECT tomogram from the data set presented in Figure 6.10. Legend represents density readings in kg/m^3.

Chapter 7 - Application of Electrical Capacitance Tomography to the Fluidized Bed Drying of Pharmaceutical Granule

This manuscript has been submitted for publication in the ***Chemical Engineering Science*** and is currently under review.

Citation

Chaplin, G., Pugsley, T., Winters, C., *Application of Electrical Capacitance Tomography to the Fluidized Bed Drying of Pharmaceutical Granule,* Chem Eng. Sci., in review (2004).

Contribution of PhD Candidate

The experimental apparatus used in this investigation is identical to that introduced in chapter 6 for the collection of ECT data. All experiments were planned and performed by G. Chaplin. The application of the S-statistic analysis to ECT data was developed by G. Chaplin. The Matlab code for the S-statistic analysis of individual pixels was written by G. Chaplin. All writing of the submitted manuscripts was done by G. Chaplin with T. Pugsley and Conrad Winters (Director, Formulation Development (PR&D) Merck & Co.) providing supplemental guidance regarding the content and style of the paper.

Contribution of this Paper to the Overall Study

The successful verification of the correction technique presented in chapter 6 allows for the use of ECT in a bed of drying pharmaceutical granule. This paper utilizes this correction technique to image such a bed. Chapters 2, 3 and 4 have demonstrated that changes in the S-statistic analysis of pressure fluctuation signals can be related to bed moisture or hydrodynamic state in a drying bed of pharmaceutical granule. However, the changes identified by this technique are global and, therefore, it can not be determined if these changes are a function of radial position. Since ECT provides high-frequency localized information about voidage fluctuations in the bed at discrete radial locations, it may be used to determine localized changes in hydrodynamic behaviour. This paper applies the S-statistic signal analysis technique to measurements of voidage made by ECT. The information about localized hydrodynamic changes gained from this analysis will be used to explain changes in voidage distribution seen in individual tomograms collected in the drying process.

Additional Experimental Details

Experiments were performed using the techniques and apparatus outlined in chapter 6. The correction technique for ECT data developed in chapter 6 is utilized in this chapter in order to correct the ECT data for moisture. This program is given in Appendix B. Appendix C Gives the Matlab code for the calculation of the S-statistic for individual pixels as well as the code for reducing the image files into signal data suitable for the application of the S-statistic.

7.1 Abstract

A novel calibration technique that accounts for the presence of moisture in wet pharmaceutical granulate has allowed for the application of electrical capacitance tomography (ECT) to a drying fluidized bed of pharmaceutical granule. A statistical attractor comparison test denoted as the S-statistic has been used to analyze both the reconstructed and non-reconstructed ECT images. This analysis has shown that, throughout the majority of the drying process, variations in the bed dynamics are most intense near the walls of the dryer while the central region is dominated by consistent dynamics. Through investigation of the voidage distribution in the individual tomograms over this period in the drying process, the changes in the S-statistic correspond to a reduction in the region involved in bubbling behaviour. Tomograms from early in the drying process indicate a central core of gas channelling through the very wet material of the bed. This is due to the high cohesive forces present at high moisture. At moisture contents below 5-wt%, near the end of drying, significant divergence in dynamic behaviour is identified in the S-statistic. This divergence can be associated with the appearance of less homogeneous bubbling behaviour in the individual tomograms.

7.2 Introduction

Drying of pharmaceutical granule in a fluidized bed is one part of the production of certain solid-dosage pharmaceuticals. These dryers are often conical in design and are operated at superficial velocities much greater than the minimum fluidization velocity. A significant reduction in granule moisture content occurs during this drying process. The reduction in moisture from an initial value of approximately 30-wt% to approximately 2-wt% is accompanied by a change in bed hydrodynamic state. The application of a

tomographic technique to image this unit operation can be used to identify local changes in bed hydrodynamics associated with fines entrainment, segregation or non-uniform mixing, all of which may contribute to product degradation.

An example of a tomographic technique is electrical capacitance tomography (ECT). ECT utilizes the difference between the dielectric constant of the gas and solid phases inside a fluidized bed in order to determine the distribution of these phases. Electrodes wrapped around the vessel periphery make rapid measurements of capacitance within the measurement volume. These measurements are then reconstructed into tomograms representing the permittivity distribution over the vessel cross-section where the sensors are mounted. Tomograms are collected at 200 Hz (Dyakowski et al. 2000), allowing the dynamic behaviour of the bed to be captured. Tomographic images give the distribution of the phases as well as allowing for the calculation of properties such as the dimensions of voids (McKeen and Pugsley 2003, Wang et al. 1995) or void velocity (Wang et al. 1995). Furthermore, the identification of regime transitions (Makkawi and Wright 2002) can be ascertained utilizing ECT data. These changes are important in determining the performance of the fluidized bed unit (Kunii and Levenspiel 1991).

The use of ECT as a monitoring or control tool for gas-solid systems has been discussed in Makkawi and Wright (2002) and Dyakowski et al. (2000, 1997). In these studies, frequency and amplitude analysis techniques have been applied to ECT data. Makkawi and Wright (2002) have shown that regime transitions are more clearly identified using these signal analysis techniques rather than determining changes from the visual interpretation of the reconstructed tomograms. In the work of Dyakowski et al.

(1997), it was shown that non-reconstructed ECT measurements of capacitance could be utilized to identify changes occurring in the pneumatic conveying of particulate solids. The use of non-reconstructed measurements of capacitance has the advantage of being less computationally time-consuming, allowing for the potential application of ECT as a process control technique.

The work of Kühn et al. (1996) has shown that signal analysis of ECT data can be used to characterize localized chaotic behaviour in a fluidized bed. In the current study, we wish to apply the S-statistic chaotic attractor comparison technique in order to determine changes in the local permittivity fluctuations in the reconstructed ECT tomograms. The S-statistic is a statistical comparison between reconstructed attractors and has been applied to pressure fluctuations collected in fluidized beds by van Ommen et al. (2000). This technique has shown sensitivity to subtle changes in global changes in a fluidized bed state bed resulting from changes in particle size distribution. The S-statistic has also been used by Chaplin et al. (2004a,b) to track significant changes in the global bed behaviour of a drying fluidized bed of pharmaceutical granule using pressure fluctuations. The current study will extend this application to localized measurements of permittivity allowing for the determination of local changes in hydrodynamic behaviour. The non-reconstructed capacitance measurements will also be analyzed using the S-statistic. The use of the non-reconstructed data will allow for the verification of the correction technique and image reconstruction. To explain the changes seen the in hydrodynamic state identified by the S-statistic, individual tomograms from discrete times in the drying process will be investigated visually. This investigation represents the first application in the published literature of ECT to a fluidized bed of changing

permittivity. Information from ECT will be invaluable for the determination of regime transitions resulting from the reduction of bed moisture in the drying process.

7.3 Experimental

7.3.1 Drying Experiments

Granulation ingredients are summarized in Table 7.1. A low-shear granulator (250 W Kitchen-Aid Classic mixer) was utilized to produce each 1 kg batch of wet granule. The dry ingredients were combined for 2 minutes at the lowest speed (setting 1). Subsequent to this initial mixing, water was added to the mixture over a five minute period at a constant rate of 63 mL/min through a medium-flow, variable-speed peristaltic pump provided by VWR Scientific. Following wet granulation, 2 minutes of post-granulation mixing at the slightly higher mixing speed (setting 2) was performed in order to ensure mixture homogeneity. The granulation product was then sieved through a 3.36 mm screen in order to remove large particles. Depending on the desired wet bed loading required for each experiment, wet granulations were performed in three or four batches using the quantities given in Table 7.1. The pharmaceutical granule was found to have the particle size distribution given in Table 7.2 upon the completion of drying. Particle size distribution was determined with the use of a Malvern Mastersizer S Long Bench particle size analyzer.

The components of the fluidized bed drying apparatus and ECT data acquisition system are presented in Figure 7.1. An SCL V4 rotary blower (Effepizela, Italy) supplied the fluidizing air. The incoming air was heated using a Watlow CBEN24G6-21 heater to an inlet temperature of 65°C. Temperature control was provided by Watlow

series 935A PID logic controller. Metering of the airflow was provided by an orifice designed and calibrated in accordance with ASME standards (Miller et al. 1990). A bypass valve located immediately downstream of the blower allowed for manipulation of the air velocity. Fluidizing air was introduced into a 10 cm tall cylindrical windbox with a diameter of 11.5 cm. The distributor was designed in accordance with the rules-of-thumb provided by Kunii and Levenspiel (1991) and consisted of a drilled aluminium plate having holes of 2 mm diameter separated by 7.5 mm on a square pitch yielding an open area of 5.6%. Above the windbox and distributor, an acrylic conical section, which is commonly referred to as the product bowl in the pharmaceutical industry, was fitted with an 8-electrode ECT sensor. The internal dimensions of the product bowl are given in Figure 7.2. Following contact with the fluidized material in this conical section, fluidizing air was transferred through the transport disengagement height (TDH) to a cyclone separator where any entrained solids were separated from the air and collected in a fines pot. Entrainment out of the TDH was observed to be negligible except near the very end of drying.

Three drying experiments were performed to investigate the influence of bed mass on the dynamic behaviour. Bed loadings of 3 kg, 3.5 kg and 4 kg of wet pharmaceutical granule were tested. For all three experiments, fluidizing air was heated to an inlet temperature of 65°C as measured in the windbox. Superficial gas velocity was defined as the average velocity across the inlet to the conical section. An elevated superficial gas velocity of between 2 and 3 m/s was required over the first 20 minutes of drying in order to maintain good mixing within the very wet bed. The superficial gas velocity of this initial mixing period was selected depending on the observed hydrodynamic behaviour.

Following this initial period, superficial gas velocity was maintained at 1.35 m/s for the remainder of the drying process. These operating conditions are in line with those used in the pharmaceutical industry for the drying of pharmaceuticals.

7.3.2 Electrical Capacitance Tomography

The ECT system used in the present study consists of two planes of measurement electrodes with eight electrodes per plane. This system is manufactured by Process Tomography Ltd (Cheshire, U.K.) and has been discussed in detail in previous publications from our group (Pugsley et al. 2003, Tanfara et al. 2002). The ECT sensor and controlling electronics are identified in Figure 7.1 while the internal dimensions of the conical electrical capacitance tomography unit given in Figure 7.2. The data acquisition module and computer shown in Figure 7.1 control the sensing and storage of capacitance data. Capacitance data is collected as 28 unique measurements corresponding to all the possible combinations of electrodes for an 8-electrode sensor at a frequency of 100 Hz. This data is written to an ASCII text file and subsequently reconstructed offline into individual tomograms at the identical frequency. Tomographic reconstruction involves the conversion of the 28 measured capacitances into permittivity data in a 32x32 pixel array defined by the sensor map. A schematic of the electrode configuration of the ECT sensor used and the sensor map pixel locations are given in Figure 7.3. Each electrode has a length of 4 cm and the lower plane measurement region encompasses a height between 8.57 and 12.38 cm above the distributor. Therefore, each pixel in the ECT tomograph represents an axial average over this conical measurement volume shown in Figure 7.2. Although the sensor has the potential for the dynamic capture of tomographic data at two axial measurements locations, only the lower

measurement plane was used in the current study due to loss of top sensor coverage at reduced granule moisture arising from particle shrinkage during the drying process.

For all three drying experiments, the ECT unit was used for both dynamic and packed bed measurements of capacitance. Dynamic ECT data sets were collected for 2 minute intervals at 100 Hz. These measurements were interspersed with ECT measurements of a packed bed, which were taken by shutting off the fluidizing air and allowing the bed to attain a packed state. 10 seconds of ECT data corresponding to 1000 frames collected at 100 Hz was then recorded in the packed bed state. After each packed bed reading a 3 g sample of granule was removed from the bed and sealed in a sample vial for analysis of moisture content utilizing using a Mettler-Toledo HB43 drying balance. Moisture analysis of all samples was completed within 2 hrs of the completion of the drying experiment. The bed was then re-fluidized for another two minutes of drying for the recording of another sequence of dynamic ECT measurements. This sequence of packed bed and dynamic ECT measurements was repeated until the completion of drying. Completion of drying was estimated from the time taken to dry granule in separate experiments performed under similar operating conditions without intermittent packed bed readings. Moisture content given by the drying balance was used to confirm attainment of the drying endpoint.

7.4 Data analysis

7.4.1 Reconstruction of ECT data

The generation of tomograms from capacitance data requires image reconstruction. The reconstruction technique used in the current study is the iterative

linear back-projection algorithm provided by Process Tomography Ltd. with truncation of the capacitance error vector ($-0.05 < \Delta C < 0.05$) performed for each iteration and a gain factor of 1.25 applied based on the convergence criterion suggested by Yang et al. (1999). The description of this technique is given in several previous works (Yang et al. 1999, Yang and Peng 2003, Isaksen 1996). However, in the present work, the algorithm has been modified through the use of a novel correction procedure which accounts for the changing moisture content of the granule throughout the drying process.

In the application of ECT, dynamic measurements of capacitance (C_M) are made while the bed is fluidized. In order to produce tomograms from these measurements, this data is normalized according to Equation 1 before being reconstructed into tomograms describing the permittivity distribution across the imaging cross-section.

$$C_N = \frac{C_M - C_L}{C_H - C_L} \tag{1}$$

Here, C_H and C_L are measurements of the high and low permittivity phases. These phases correspond to packed bed and air in a fluidized system respectively. In the drying process, the permittivity of the granule decreases significantly from the initial moisture of approximately 30-wt% to the endpoint of drying near 2-wt%. This change is a result of loss of water, which has a high relative electrical permittivity of approximately 81 compared with a value of approximately 3 for the dry powder. To account for this change, a correction procedure has been developed based on a linear fit of the measurements of packed bed capacitance as a function of moisture. This correction procedure for dynamic ECT measurements has been verified using x-ray tomography in a 3 kg bed of pharmaceutical granule by Chaplin et al. (2004c). It was demonstrated in

this study that the Böttcher permittivity model using approximately 50 iterations of the iterative linear back projection image reconstruction technique gives good agreement with time-averaged x-ray data in a fluidized bed of pharmaceutical granule having a moisture content above approximately 5-wt%. Since the bed moisture content remains above this threshold for the bulk of the drying process, these parameters were also used for the reconstruction of all ECT data in the present work.

7.4.2 The S-statistic

The S-statistic is a statistical comparison based on attractors reconstructed from two data sets denoted as the reference and evaluation time-series. The result is a comparison between the dynamics of the reference and evaluation states. A value of the S-statistic smaller than 3 indicates that no statistically significant change has taken place between hydrodynamic states. Likewise, a value of S greater than 3 indicates that a statistically significant difference exists between the attractors reconstructed from reference time-series and those reconstructed from the evaluation time-series. Details of the mathematical development of the S-statistic are given in Diks et al. (1996). The application of the algorithm to fluidized systems was first reported in van Ommen (2001) and van Ommen et al. (2000).

Our group has applied the S-statistic to pressure fluctuations collected in the drying of pharmaceutical granule using an algorithm developed in Matlab (Chaplin et al. 2004a,b). In the present work, an identical S-statistic algorithm has been implemented in Matlab for the analysis of ECT data. Since the reconstruction of ECT data results in the relative permittivity distribution across the imaging cross-section, each pixel can be

regarded as an individual signal collected at a discrete spatial location. Therefore, the S-statistic analysis has been applied to individual pixels in order to detect changes in local hydrodynamic state. In addition to a pixel-by-pixel analysis, the 28 non-reconstructed capacitance measurements taken by the ECT have also been analyzed using the S-statistic. In the work of Chaplin et al. (2004d), the use of a reference time series corresponding to a bed state of 10-wt% was determined appropriate to identify the fluidization state corresponding to the initiation of fines entrainment. However, in the current investigation, the use of this reference state was impossible due the discrete nature of the data. ECT data could not be collected continuously and was limited to 2 minute segments of data separated by 1 minute where no data was collected. This resulted in no ECT data being collected at the required reference moisture of 10-wt%. The closest possible reference state to the condition used previously was at a bed moisture content of 9-wt%. This reference state, though being slightly lower in moisture to that used previously, was taken to be an appropriate reference state.

7.4.2.1 Pixel analysis

The pixels used for the S-statistic analysis of the permittivity fluctuations collected by the ECT sensor are shown in Figure 7.3. The signals from four pixels at identical radial locations in the vessel cross-section were combined as described below to increase the sensitivity of the S-statistic to changes in hydrodynamic behaviour. This allows for determination of the changes associated with bed hydrodynamic as a function of radial position. Since we are only concerned about radial variations in dynamic behaviour in the current investigation, the combination of signals also removes any possible angular

variation in behaviour. Both the reference and evaluation time series were selected to be 2 minutes in duration.

In the work of van Ommen (2000, 2001), a technique was presented for increasing the sensitivity of the S-statistic to hydrodynamic changes through the combination of multiple pressure signals collected at several locations in a single fluidized bed. In this extension to the S-statistic analysis, multiple normalized signals are combined as follows for four signals:

$$\begin{aligned} s_1 &= \left[x_{1,1}, x_{1,2}, x_{1,3} \ldots x_{1,n}\right] \\ s_2 &= \left[x_{2,1}, x_{2,2}, x_{2,3} \ldots x_{2,n}\right] \\ s_3 &= \left[x_{3,1}, x_{3,2}, x_{3,3} \ldots x_{3,n}\right] \\ s_4 &= \left[x_{4,1}, x_{4,2}, x_{4,3} \ldots x_{4,n}\right] \\ &\downarrow \\ s_C &= \left[x_{1,1}, x_{2,1}, x_{3,1}, x_{4,1} \ldots x_{1,n}, x_{2,n}, x_{3,n}, x_{4,n}\right] \end{aligned} \tag{2}$$

Before this combination is performed, the data is resampled in order to maintain a consistent embedding. Therefore, the signals, denoted as s_1 to s_4 above have been resampled at one quarter of their original sampling frequency. In the current application, we combine four signals and a resampling of the signals at 25 Hz is used. The individual pixels used for this analysis are shown in Figure 7.3. The locations of the pixels to be combined are selected at an identical distance from the centerline in each case. One pixel from each set of four combined pixels is identified on the 135° axis.

Every iteration of the iterative back projection technique results in updated values of the normalized pixel permittivity. In order to prevent physically unrealistic values, normalized permittivities above one are set to a value of one while values less than zero

are set to zero. This process is referred to as thresholding (Yang et al. 1999, McKeen and Pugsley 2002) and is applied after each iteration. In the application of the S-statistic to the reconstructed tomograms, it was found that thresholding adversely affected the S-statistic analysis of pixels near the centre and close to the walls of imaging cross-section, giving little information about the dynamics in these areas. In the work of Kühn et al. (1996), thresholding was not used for the determination of Kolmogorov entropy from reconstructed ECT data. The disabling of the thresholding function was found to give a more continuous description of the chaotic behaviour of the system compared to reconstructed data where thresholding was applied. Furthermore, the values obtained for the chaotic parameters were comparable to those obtained using pressure fluctuation data. Therefore, in the current work, the thresholding routine in the reconstruction algorithm has been disabled for the S-statistic pixel analysis.

7.4.2.2 The analysis of non-reconstructed ECT data

The signal combination described in Section 7.4.2.1 was also applied to the 28 non-reconstructed capacitance signals recorded by the ECT sensor throughout the drying process. Four signals measured at diametrically opposite electrodes as well as four signals from adjacent electrodes were combined. S-statistic analysis was then applied to this combined signal utilizing a reference data set collected at 9-wt% granule moisture at the identical radial location.

Since the non-reconstructed capacitance signals are utilized by the reconstruction algorithm to generate the permittivity distribution data described above, changes seen in the S-statistic analysis of individual pixels should be evident in the capacitance data as

well. The use of non-reconstructed capacitance signals also removes the influence of any errors associated with the correction for moisture described in Section 7.3.2. Furthermore, since this data requires no reconstruction, the processing time is reduced significantly allowing this technique to be practically implemented for the on-line application of ECT for process monitoring.

7.5 Results and Discussion

7.5.1 Calibration of the S-statistic

Calibration of the S-statistic algorithm was performed as described by Chaplin et al. (2004a,b). Optimum parameters are given in Table 7.3. The reference and evaluation hydrodynamic data sets utilized for the identification of the optimum parameters were 26-wt% and 4-wt% respectively. These parameters are in agreement with our previous studies (Chaplin et al. 2004a,b,d) with the exception of embedding dimension. The embedding of 10 used in the current application to ECT is the maximum possible value given a time window of 0.1s and a sampling frequency of 100 Hz. It is possible that a higher sampling frequency would result in a higher optimum embedding. However, this is unlikely to affect the results. We base this statement on our previous findings (Chaplin et al. 2004a). When an embedding of 10 was applied to pressure fluctuation measurements in that work, which was significantly lower than the optimum value of 40, the identification of a consistent hydrodynamic state by the S-statistic analysis was not affected.

7.5.2 Drying behaviour

The drying curves for the three bed loadings examined in this study are presented in Figure 7.4. These profiles exhibit a constant rate period lasting until a moisture content of approximately 4-wt%, followed by a brief falling-rate period. It may be noted that the drying curve for the 3.5 kg bed loading shows a rapid decrease initially resulting in this drying curve falling below the 3 kg drying curve. This is not consistent with supplemental drying experiments performed in this unit where an increase in bed mass increased the drying time. This is most likely a result of the slightly elevated average superficial gas velocity of 2.5 m/s used for the first 20 minutes of the 3.5 kg drying experiment. Slightly lower superficial gas velocities of 2.0 m/s and 2.1 m/s were used at the 3 and 4 kg loadings, respectively. This discrepancy in superficial gas velocities was a result of the manner in which superficial gas velocity is controlled during this period. Selection of the appropriate superficial gas velocity in this early phase of drying was based on visual observations of the fluidization behaviour. At the 3.5 kg loading, a higher superficial gas velocity was utilized to promote good mixing because of the observation of stagnant regions in the bed. This discrepancy in the superficial gas velocity only influences the rate of moisture loss indicated by the drying curves over the first several minutes of drying. After the reduction of the superficial velocity to a constant value at 20 minutes, the drying behaviour becomes consistent. Any influence of the dynamic behaviour caused by this variation is inconsequential to the S-statistic analysis, since the behaviour for the first 20 minutes will not be considered in the determination of hydrodynamic changes.

7.5.3 S-statistic analysis of ECT data

Figures 7.5 through 7.7 show the behaviour of the S-statistic applied to the combined signals for the pixels located at the wall, at the centre and at an intermediate location respectively (see Figure 7.3). In all plots, a reference state corresponding to 9-wt% has been chosen. In Figure 7.5 the behaviour of the S-statistic analysis of the combined signals collected at the wall pixels is given for the three bed loadings. In this plot, we see the reduction of the value of the S-statistic as drying proceeds. The S-statistic drops below a value of 3 as the bed approaches the reference state. As the bed is dried further, the S-statistic increases as the system state diverges from the reference state. The times at which the hydrodynamic state becomes consistent with the reference state (i.e. an S-statistic value less than three) occurs at 31, 28 and 40 minutes for the 3, 3.5 and 4 kg bed loadings respectively. These times correspond to a bed moisture content of approximately 15-wt% for all experimental runs. This result is identical to that seen by Chaplin et al. (2004d) in the application of the S-statistic to pressure fluctuations in a bed of drying pharmaceutical granule having a similar geometry and operating conditions. This suggests that the hydrodynamic changes identified in the pressure fluctuations originate near the walls of the fluidized bed dryer. Furthermore, the fact that the value of the S-statistic drops below a value of 3 at a consistent moisture for all experimental runs despite the elevated superficial gas velocity used initially, indicates that this disturbance does not influence the performance of the S-statistic following the reduction of superficial gas velocity. This result is further confirmation of the findings of Chaplin et al. (2004a,b) where it is indicated that the S-statistic responds most strongly to changes in moisture.

In Figure 7.6, we see the behaviour of the S-statistic analysis of the combined signals from the four central pixels for each of the three bed loadings. By the time of the superficial gas velocity is reduced, the hydrodynamic state at this location in the bed is consistent with the reference state for all bed loadings. This consistency remains until a divergence is seen after the reference state. Therefore, no change in hydrodynamic state can be identified at the center of the bed between bed moistures of approximately 20-wt% and 5-wt%. This result contrasts the dynamic behaviour seen at the wall pixels where convergence to a state similar to the reference state occurs several minutes following the reduction of superficial gas velocity.

Figure 7.7 shows the behaviour of intermediate pixels in the fluidized bed cross-section. The behaviour of the combined signals from these pixels shows a similar consistent hydrodynamic state to that seen at the centre of the bed in Figure 7.6 following the reduction in superficial velocity at 20 minutes. This demonstrates that the consistency in dynamic state identified by the S-statistic at the centre is similar at this location. Therefore, a consistent hydrodynamic condition dominates a large portion of the fluidized bed cross-section throughout the drying process.

The behaviour seen at pixels near the vessel wall in Figure 7.5 is only seen in the three pixels closest to the wall. All pixels from the centre to this location show little or no identifiable change in hydrodynamic state throughout the drying process except for a rapid divergence following the reference state. This suggests that the changes seen in the hydrodynamics of the dryer originate near the walls of the unit. Consequently, ECT signals can be divided into those occurring centrally over a large portion of the central

region where little variation in hydrodynamic behaviour is observed and the region close to the wall where there is significant variation.

Figure 7.8 shows the S-statistic analysis of four combined raw capacitance signals for the adjacent and opposite electrodes at the 4 kg bed loading. As in Figures 7.5 through 7.7, a reference state corresponding to 9-wt% has been chosen. In this plot, the S-statistic response of the adjacent electrodes is similar to that seen in Figure 7.5 for the wall pixels while the opposite electrodes show a behaviour analogous to that seen in the central pixels in Figure 7.6. The fact that the performance of the S-statistic is similar to that seen in the reconstructed pixel-by-pixel analysis seen in Figure 7.5 to Figure 7.7 of the reconstructed images confirms that the correction technique for moisture does not adversely affect the signal behaviour and that the reconstruction technique has been correctly implemented. As mentioned above, the analysis of non-reconstructed ECT signals in Figure 7.8 provides a means of rapidly analyzing ECT data without the computationally time-consuming step of image reconstruction.

The divergence seen in the S-statistic after the reference state in Figure 7.5 through Figure 7.8 is of significance. In Figure 7.6, increased sensitivity to this effect is seen near the wall. The wall sensitivity is also seen in Figure 7.8 where this is indicated by the divergence at adjacent electrodes and consistency at opposite electrodes. At the central pixels, sensitivity to bed mass can be seen. Here, increased divergence is seen at the lowest bed loading of 3 kg. However, the central pixels at the 4 kg bed loading in Figure 7.6 show no statistically significant change following the reference state while 3.5 kg loading lies between these extremes. A similar divergence has been identified by Chaplin et al. (2004d) for the analysis of pressure fluctuations in a bed of drying

pharmaceutical granule. The cause of this effect is a point for further research. Potential causes of this divergence may be the entrainment of fines or an increase in static charge within the bed at very low bed moisture.

7.5.4 Hydrodynamic interpretation of tomograms

Since changes in tomograms collected at each of the three bed loadings were visually similar, sequential representative tomograms from only the 3.5 drying experiment are given in Figures 7.9 through 7.12. These figures present composites of the frames from data sets collected at 28, 18, 10 and 1.5-wt%. Since changes in individual tomograms could not be detected visually over five frames, every fifth frame is presented. Therefore, there is an interval of 50 ms between frames and each sequence of 20 frames spans 1 second. Each tomogram spans a relative permittivity between 0 and 1 corresponding to the relative permittivity of air and the packed bed. Time increases from left to right in the sequence. The first frame of the sequence is in the top left hand corner of the composite while the final frame is in the bottom right hand corner. A frame index is given at the top left hand corner of each image.

In Figure 7.9, tomograms are given for a bed having a moisture content of 28-wt%. At this moisture content, the superficial gas velocity is 2.5 m/s. As can be seen in Figure 7.9, the measurement plane is dominated by a stable core of fluidizing air, while a dense bed of solids remains near the wall. The cause of this early channelling behaviour is most likely a result of high liquid bridging forces between particles initially caused by the presence of moisture. The higher liquid loading leads to increased cohesion resulting in channelling of air through the centre of the bed. As the liquid

loading is reduced by the drying process, the liquid bridging forces are also reduced and the bed begins to exhibit the regular passage of voids. This breakup of the core into discrete voids begins at around 5 minutes from the start of drying. However, this transition is difficult to relate directly to bed moisture. A similar early transition in the behaviour of a bed used for the drying of pharmaceuticals has been noted by Chaplin et al. (2004a,b). In these studies, the initial stable state identified by the S-statistic analysis of pressure fluctuations was correlated with visual observation of changes occurring in centralized bed behaviour over the first 5 minutes of each drying experiment. In the current investigation, visual observation made of bubble eruptions from the bed surface early in the drying process also indicates a centralized hydrodynamic behaviour. This observation confirms the centralized behaviour indicated by the ECT in Figure 7.9.

Figure 7.10 shows tomograms taken at a moisture content of 18-wt%. This moisture corresponds to a time following the reduction of superficial gas velocity to a constant value of 1.36 m/s. This moisture corresponds to the early portion of the drying data examined for hydrodynamic changes utilizing the S-statistic. In Figure 7.5, this corresponds to a bed state significantly different from the reference state. From the sequence in Figure 7.10, the fluidizing air appears to pass through the measurement region as an annulus of low-density material. It is likely that portions of this annulus are image artifacts and not a true representation of the distribution of the fluidizing gas. This annular shape is clearly visible in the second row of the sequence in Figure 7.10. What appear to be two or three voids can be seen in the final two images in this row. These voids lie along the ring of low-density material. Halow and Nicoletti (1992) report ‘ghosting’ or false images appearing between voids when more than two objects are in

the imaging plane. This ghosting effect is the most likely the source of portions of the annulus, which connects true voids in the measurement plane. Visual observations made of the behaviour at the bed surface indicate that the eruption of bubbles occurs in an annular pattern close to the walls of the vessel. This is consistent with the above interpretation of the image artifacts and the assertion that the voids are distributed in an annular pattern.

In Figure 7.11, the moisture of the bed has been reduced to 10-wt%. In Figure 7.5, this corresponds to a bed state consistent with the reference state. At this point, the hydrodynamics are visually similar to those seen in Figure 7.10. However, the dynamic behaviour is confined to a smaller fraction in the centre of the vessel cross-section. This change is consistent with the results given in the S-statistic analysis, which indicated that the dynamic behaviour at the vessel centre is consistent between the moisture contents of 18-wt% and 10-wt% (Figure 7.6). As the area of consistent hydrodynamic behaviour reduces in area, changes seen in the dynamics of the bed are only identified by the S-statistic near the periphery of the vessel in Figure 7.5. In contrast, no change in hydrodynamic state is identified in Figure 7.6 at the central pixels. Therefore, the changes in hydrodynamic behaviour identified by the S-statistic between these conditions are a result of the reduction in the area involved in consistent dynamic behaviour.

Below the moisture of approximately 5-wt% a significant change in dynamic behaviour is seen in the tomograms. This change is demonstrated by the tomograms given in Figure 7.12. This ECT data was collected near the end of drying at a moisture content of 1.5-wt%. This moisture corresponds to the region of rapid divergence seen at

the end of drying in Figures 7.5 through 7.8 and a hydrodynamic state significantly different from the reference state. A more asymmetric behaviour is seen in Figure 7.12 compared with Figures 7.10 and 7.11. Although the annulus is still evident in several of these tomograms, it is often observed to be asymmetrical in shape indicating a more uneven distribution of the fluidizing air. In addition, single large voids appear close to the walls and or in centre of the bed in several frames. This dynamic behaviour was not observed at any other time in the drying process and is most likely responsible for the divergence noted in the S-statistic after the reference state in Figures 7.5 through Figure 7.8. Furthermore, sensitivity to bed mass was seen in the intensity of this change. At a bed loading of 3 kg, the appearance of the annulus of low-voidage material occurred infrequently in favour of single large voids appearing throughout the vessel cross-section. Less asymmetrical hydrodynamics were observed at the 4 kg bed loading. At this higher bed loading, the bubbling behaviour was more reminiscent of the behaviour observed at higher moisture with the annulus still evident in most of the frames. This observation correlates directly with the divergence seen in the S-statistic at the central pixels in Figure 7.6 with a larger bed mass delaying or suppressing the divergence in hydrodynamic behaviour from the reference state.

7.6 Conclusions

Localized changes in dynamic behaviour have been identified in the batch fluidized bed drying of pharmaceutical granule using ECT. This has been accomplished utilizing a correction for the effect of moisture on capacitance measurements. The application of the S-statistic and the visual interpretation of the tomographic data collected in the bed throughout the drying process both show that the centre of the bed

exhibits little variation in hydrodynamic behaviour between moisture contents of between 20-wt% and 5-wt%. Near the wall, significant changes occur over this period with a convergence to a statistically similar state at identical moisture to that identified by Chaplin et al. (2004a,b) for the S-statistic analysis of pressure fluctuations in a similar apparatus. The similarity seen in these results suggests that the changes in hydrodynamic behaviour identified by pressure fluctuations take place near the walls of the dryer.

The visual interpretation of the reconstructed tomograms indicates several changes in the dynamic behaviour of the dryer. A distinct fluidization regime exists over the first 5 minutes of the drying process. This regime is characterized by centralized channelling of the fluidizing gas and is a result of the high particle liquid loading at this time. Between moisture contents of 18-wt% and 10-wt%, reduction in the area of the region involved in fluidized behaviour causes the change in state identified by the S-statistic near the walls of the dryer. The similarity of the central regions of the tomograms during this period is analogous to the consistent hydrodynamic state identified by the S-statistic at the centre of the bed. At bed moisture below 10-wt%, a divergence in the S-statistic is observed. This divergence corresponds to a more asymmetrical bubbling behaviour over the vessel cross-section evident in the individual tomograms. This divergence in state at low moisture shows sensitivity to bed mass, with an increasing divergence in the S-statistic occurring at reduced bed loadings.

The similarity of the results identified from the analysis of reconstructed and non-reconstructed ECT data indicates that this analysis can be implemented on ECT data on-line without the need for direct reconstruction of the ECT data. Therefore, the S-

statistic analysis of ECT data can be utilized for the control of the drying process without the need for image reconstruction methods.

7.7 Acknowledgments

The authors would like to thank Merck Frosst Canada & Co. (Montreal) and the Natural Sciences and Engineering Research Council of Canada (NSERC) for their financial support.

7.8 Notation

C_H Capacitance measurement of the high permittivity phase or packed bed (fF)

C_L Capacitance measurement of the low permittivity phase or the empty vessel (fF)

C_M Dynamic measurement of capacitance made by the ECT sensor (fF)

C_N Dynamic normalized capacitance measurement (nondimensional)

s_i Signal collected at pixel or electrode combination i (nondimensional)

s_C The combined signal (nondimensional)

$x_{i,j}$ j^{th} measurement of normalized permittivity or capacitance measurement at pixel or electrode combination i (nondimensional)

7.9 References

Chaplin, G., Pugsley, T., Winters, C., 2004a. *Application of chaos analysis to fluidized bed drying of pharmaceutical granule*, in ***Fluidization XI: Present and Future for Fluidization Engineering***. U. Arena, R.Chirone, M. Miccio and P. Salatino, (Eds.), Engineering Foundation, New York, pp. 419-426. [Chapter 2]

Chaplin, G., Pugsley, T., Winters, C., 2004b. *Application of chaos analysis to pressure fluctuation data from a fluidized bed dryer containing pharmaceutical granule*. Powder Technology 142(2-3), 110-120. [Chapter 3]

Chaplin, G., Pugsley, T., van der Lee, L., Kantzas A., Winters, C., 2004c. *The dynamic calibration of an electrical capacitance tomography sensor applied to the fluidized bed drying of pharmaceutical granule*. Submitted to Measurement Science and Technology. [Chapter 6]

Chaplin, G., Pugsley, T., Winters, C., 2004d. *The S-statistic as an early warning of entrainment in a fluidized bed dryer containing pharmaceutical granule.* Powder Technology 149(2-3), 148-156. [Chapter 4]

Diks, C., van Zwet, W.R., Takens, F., DeGoede, J., 1996. *Detecting differences between delay vector distributions.* Physical Review E 53(3), 2169-2176.

Dyakowski T. Edwards, R. B., Xie C. G., Williams, R. A., 1997. *Application of capacitance tomography to gas-solids flows.* Chemical Engineering Science 52(13), 2099-2110.

Dyakowski, T., Jeanmeure, L.F.C., Jaworski, A.J., 2000. *Applications of electrical capacitance tomography for gas-solids and liquid-solids flows-a review.* Powder Technology 112(3), 174-192.

Halow, J. S., Nicoletti, P., 1992. *Observations of fluidized bed coalescence using capacitance imaging.* Powder Technology 69(3), 255-277.

Isaksen, Ø, 1996. *A review of reconstruction techniques for capacitance tomography.* Measurement Science and Technology 7(3), 325-337.

Kühn, F.T., Schouten, J.C., Mudde, R.F., van den Bleek C.M., Scarlett, B., 1996. *Analysis of chaos in fluidization using electrical capacitance tomography.* Measurement Science and Technology 7(3), 361-368.

Kunii, D., Levenspiel, O., 1991. *Fluidization Engineering (2^{nd} Edition).* Butterworth-Heinemann, Toronto.

Makkawi, Y. T., Wright, P.C., 2002. *Fluidization regimes in a conventional fluidized bed characterized by means of electrical capacitance tomography.* Chemical Engineering Science 57(13), 2411-2437.

McKeen, T. R., Pugsley T. S., 2002. *The influence of permittivity models on phantom images obtained from electrical capacitance tomography.* Measurement Science and Technology 13(12), 1822-1830.

McKeen, T., Pugsley, T., 2003. *Simulation and experimental validation of a freely bubbling bed of FCC catalyst.* Powder Technology 129(1-3), 139-152.

Miller, R.W., Lee, W.F.Z., Gomez, C.J., 1990. *Measurement of fluid flow in pipes using orifice, nozzle and venturi.* ASME-MFC-3M-1989. New York.

Pugsley, T., Tanfara, H., Malcus, S., Cui, H., Chaouki, J., Winters, C., 2003. *Verification of fluidized bed electrical capacitance tomography measurements with a fibre optic probe.* Chemical Engineering Science 58(17), 3923-3934.

Tanfara, H, Pugsley T., Winters C., 2002. *Effect of particle size distribution on local voidage fluctuations in a bench-scale conical fluidized bed dryer.* Drying Technology 20 (6), 1273-1289.

van Ommen, J. R., Coppens, M.C., van Den Bleek, C.M., 2000. *Early Warning of Agglomeration in Fluidized Beds by Attractor Comparison.* AIChe Journal 46(11), 2183-2197.

van Ommen, J. R., 2001. *Monitoring fluidized bed hydrodynamics.* PhD. Thesis, Delft University of Technology.

Wang, S.J., Dyakowski, T., Xie, C.G., Williams, R. A., Beck, M.S., 1995. *Real time capacitance imaging of bubble formation at the distributor of a fluidized bed.* Chemical Engineering Journal 56(3), 95-100.

Yang, W Q, Peng, L., 2003. *Image reconstruction algorithms for electrical capacitance tomography.* Measurement Science and Technology 14(1), R1-R13.

Yang, W. Q., Spink, D. M., York, T. A., McCann, H., 1999. *An image reconstruction algorithm based on Landweber's iteration method for electrical-capacitance tomography*. Measurement Science and Technology 10(11), 1065-1069.

Table 7.1 Wet granulation ingredients

Component	Percentage by mass (dry basis)	Amount (g) for a 1 kg (wet) batch
Lactose Monohydrate (filler)	50%	375
Microcrystalline Cellulose (filler)	44%	330
Croscarmellose Sodium (disintegrant)	2%	15
Hydroxypropyl Methylcellulose (binder)	4%	30
Water (reverse-osmosis)	43%	315

Table 7.2 Particle size distribution of dry pharmaceutical granule

Particle Size (μm)	Mass percentage in range
<75	3.41
75-105	6.04
105-149	11.32
149-210	12.95
210-297	10.99
297-420	8.23
420-590	6.89
590-850	8.32
850-1190	9.6
1190-1680	10.41
1680-2380	7.96
2380-3360	3.71
>3360	0.17

Table 7.3 Optimum S-statistic algorithm parameters

Time window	0.1 seconds
Embedding (m)	10
Bandwidth (d)	0.5
Segment Length (L)	3 seconds

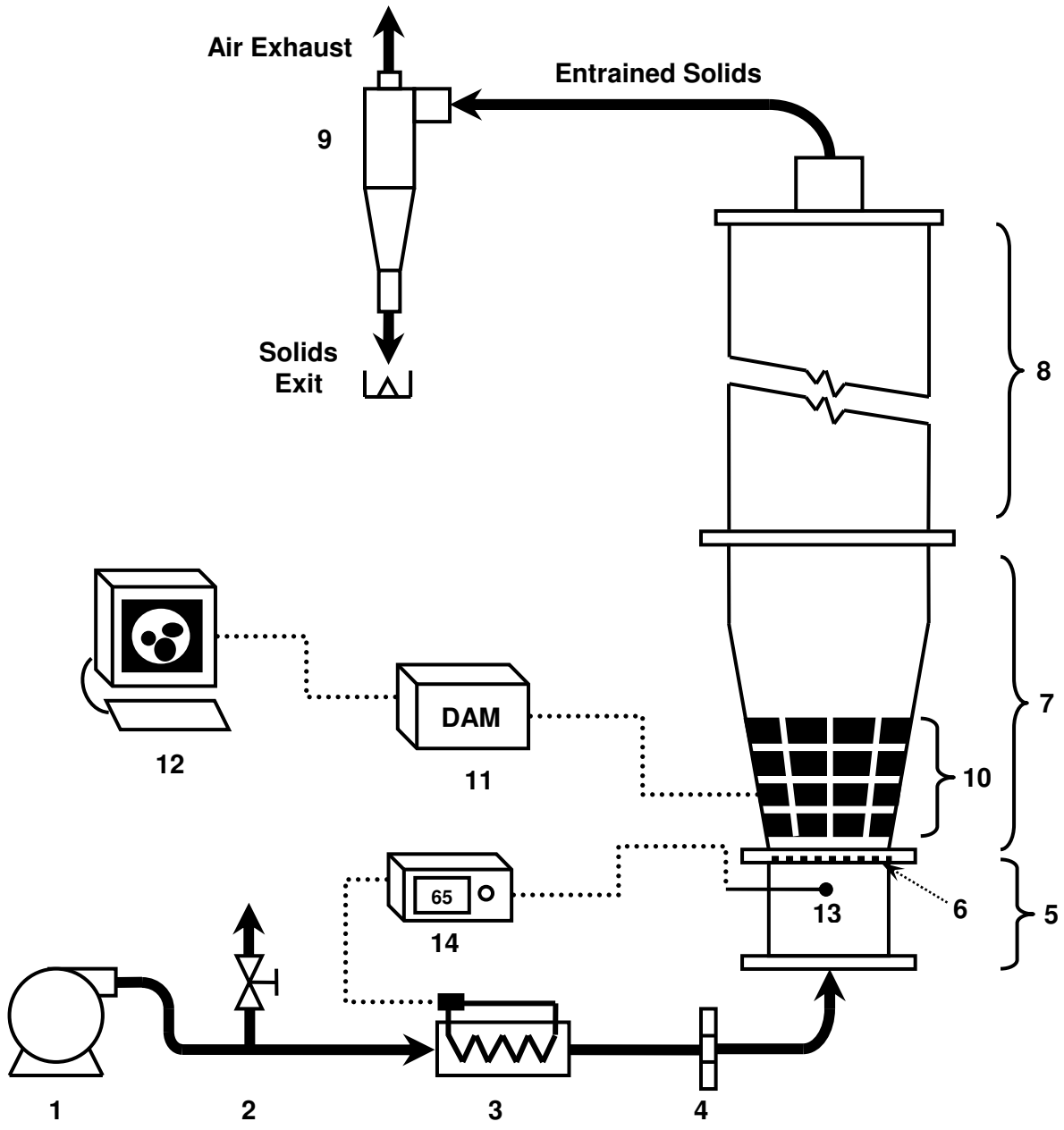

Figure 7.1 Fluidized bed dryer apparatus components and instrumentation. Blower (1), air bypass (2), air heater (3), orifice (4), windbox (5), distributor (6), product bowl (7), freeboard (8), cyclone (9), electrical capacitance tomography sensor (10), ECT data acquisition module (11), data acquisition computer (12), air-supply thermocouple (13), air heater controller (14).

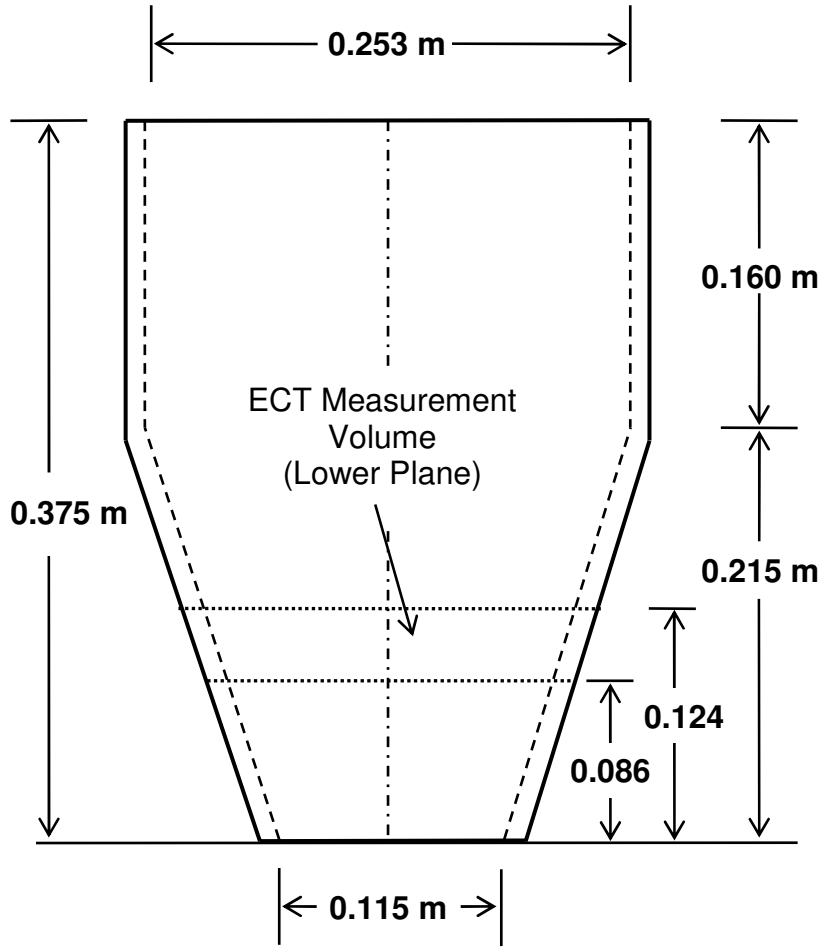

Figure 7.2 Internal dimensions for the acrylic ECT cone used in this study. All dimensions are given in metres. The tomographic measurement volume for the lower plane used in this study is also indicated.

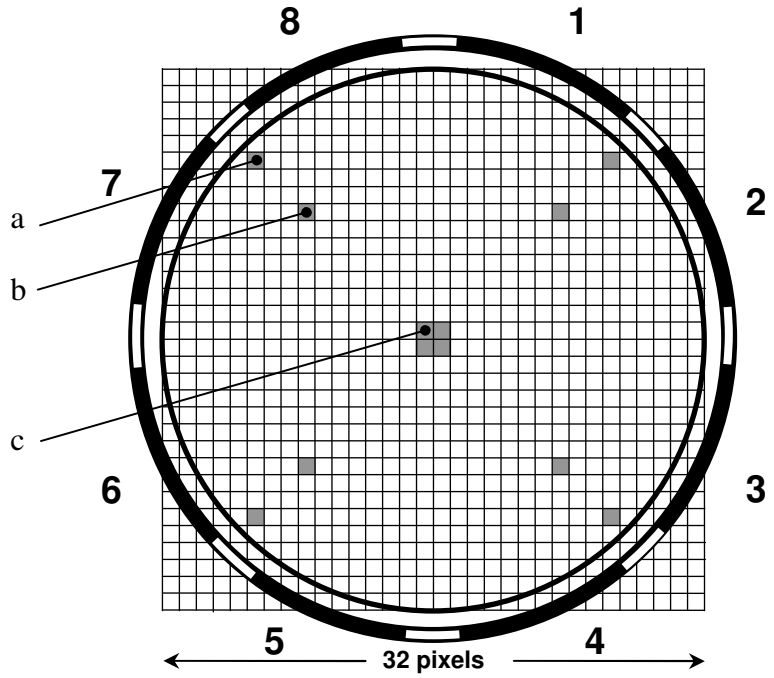

Figure 7.3 ECT electrode configuration and pixels used to describe the permittivity distribution within the measurement volume. Shaded pixels are those used for dynamic analysis of ECT data: wall pixel (a) intermediate pixel (b) and central pixel (c).

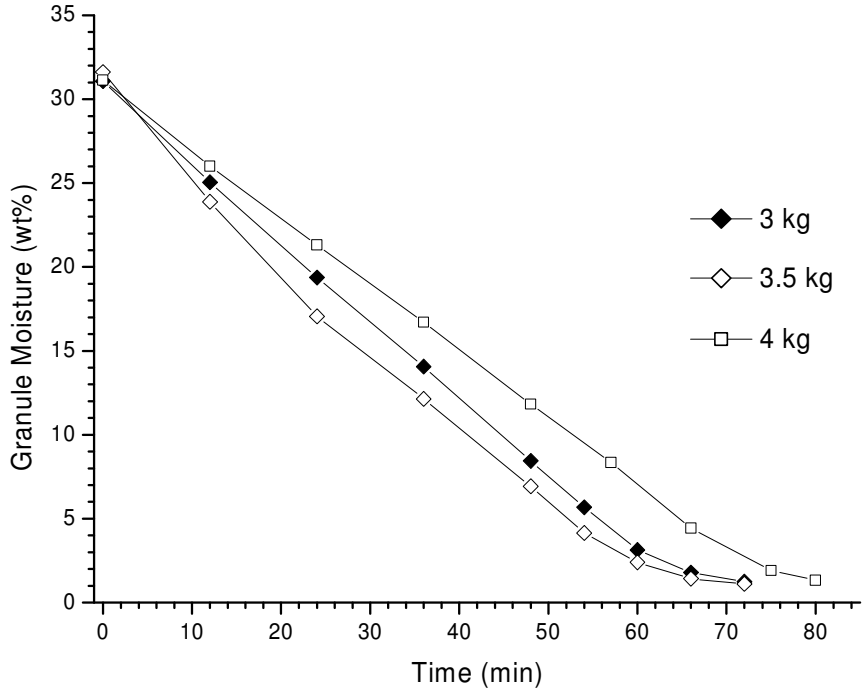

Figure 7.4 Drying curves for the three bed masses examined.

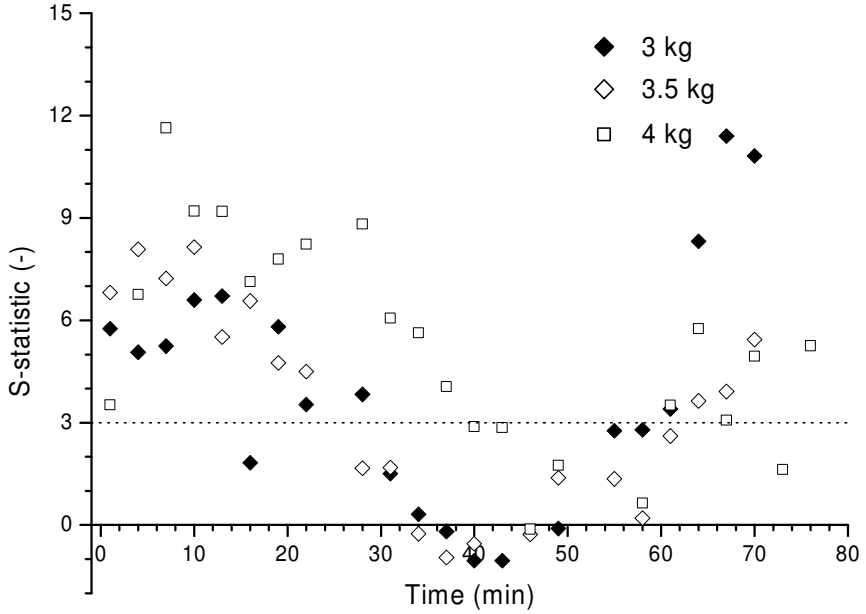

Figure 7.5 S-statistic analysis of permittivity data from the wall pixels. A reference state was chosen at 9-wt% moisture for all bed loadings.

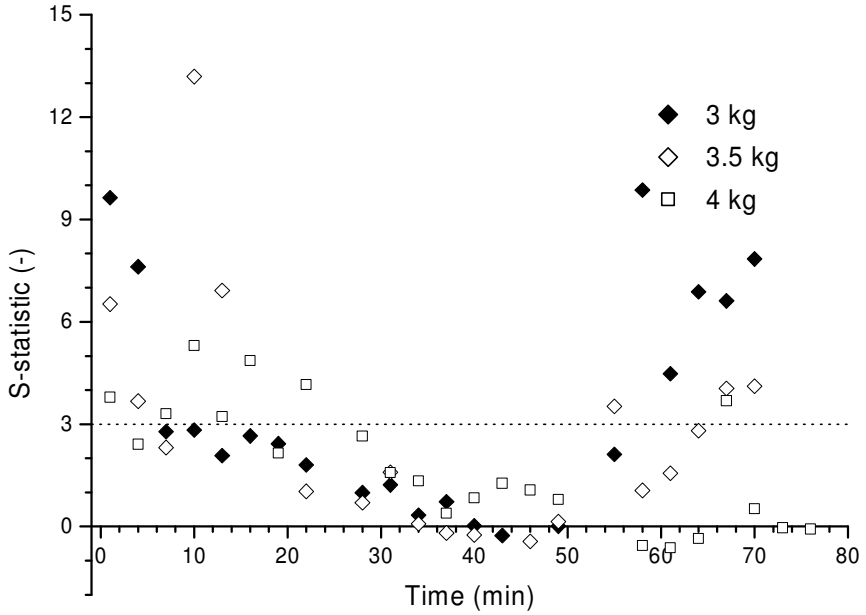

Figure 7.6 S-statistic analysis of permittivity data from the central pixels. A reference state was chosen at 9-wt% moisture for all bed loadings.

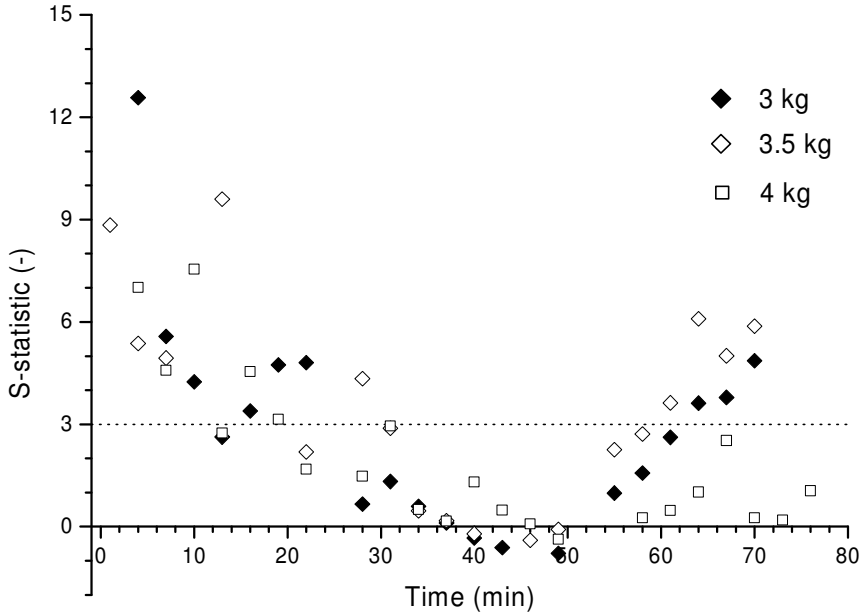

Figure 7.7 S-statistic analysis of permittivity data from the intermediate pixels. A reference state was chosen at 9-wt% moisture for all bed loadings.

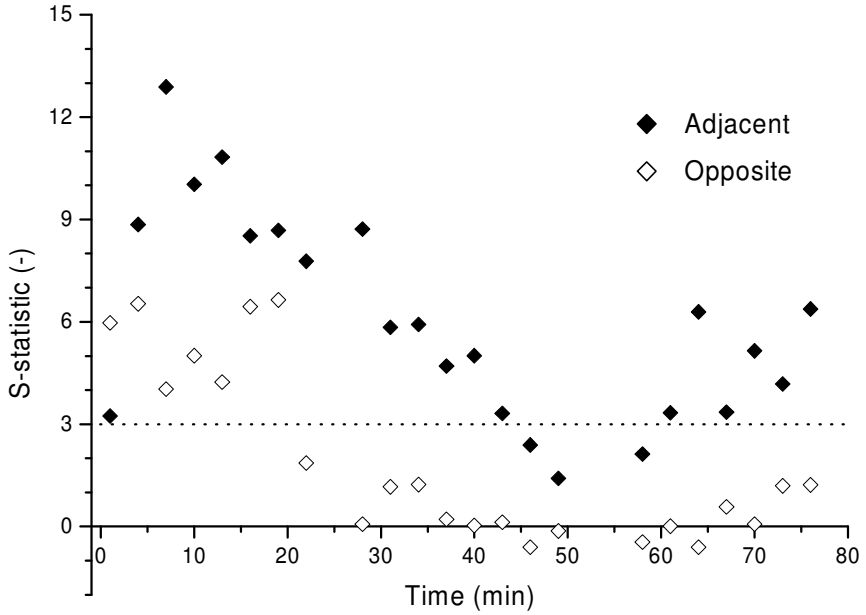

Figure 7.8 S-statistic analysis of the raw capacitance measurements made at the opposite and adjacent electrode pairs. A reference state was chosen at 9-wt% moisture for all bed loadings.

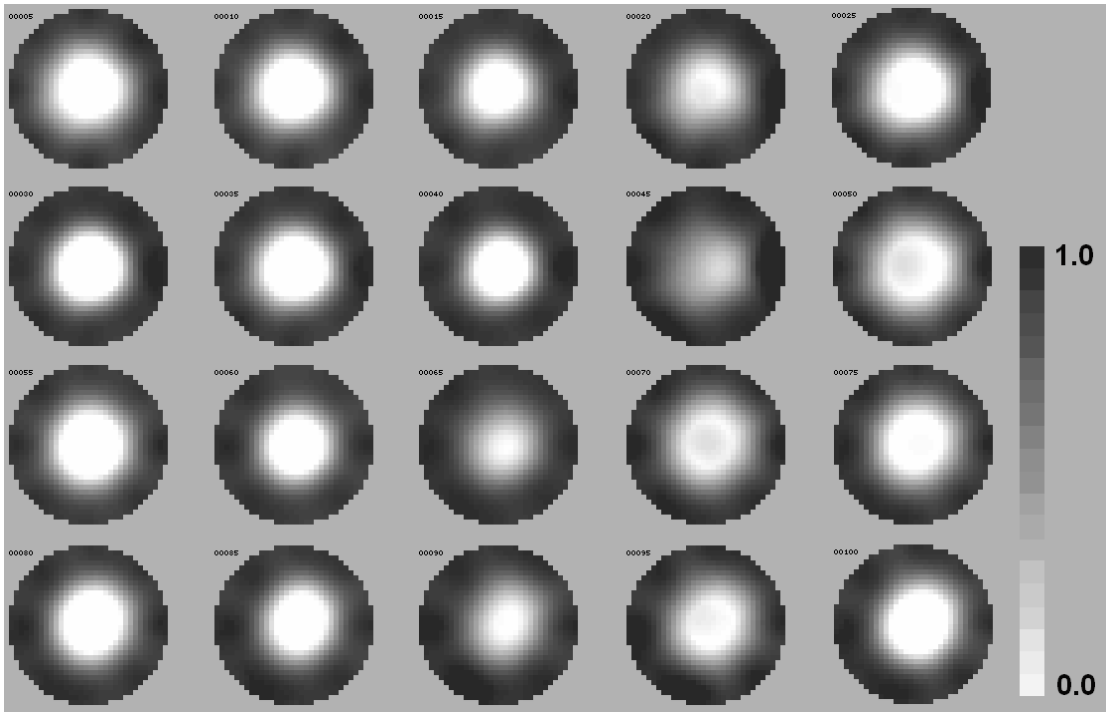

Figure 7.9 Tomographs collected in a 3.5 kg bed loading and a moisture of 28-wt%.

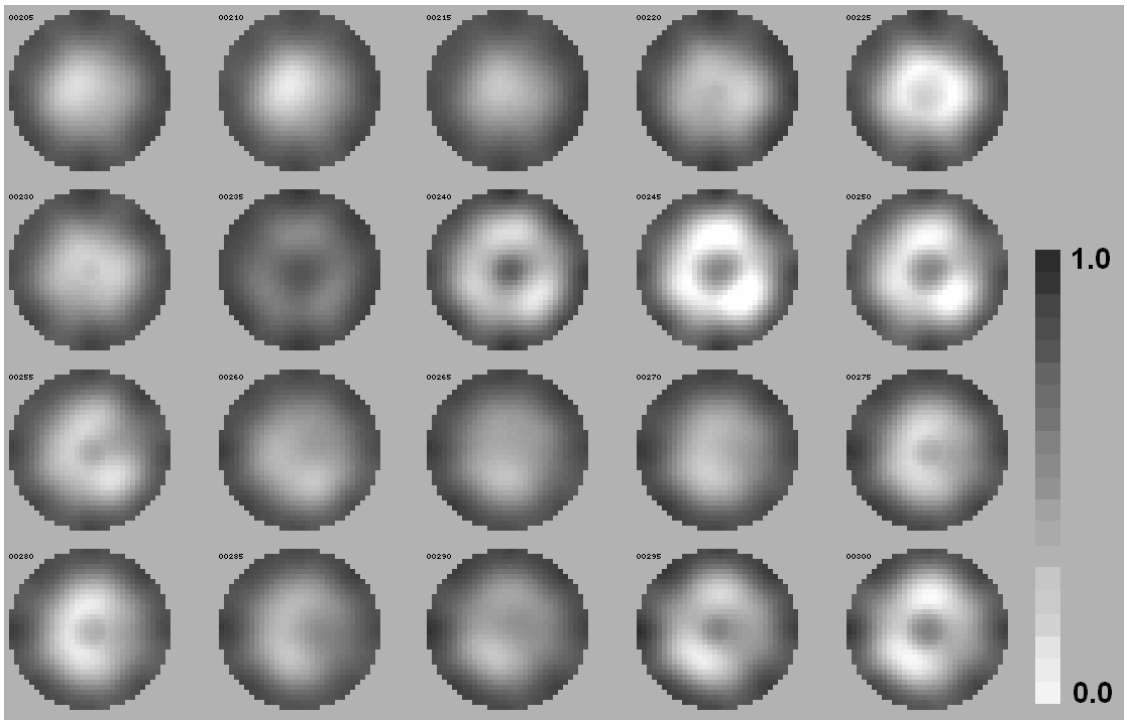

Figure 7.10 Tomographs collected in a 3.5 kg bed loading and a moisture of 18-wt%.

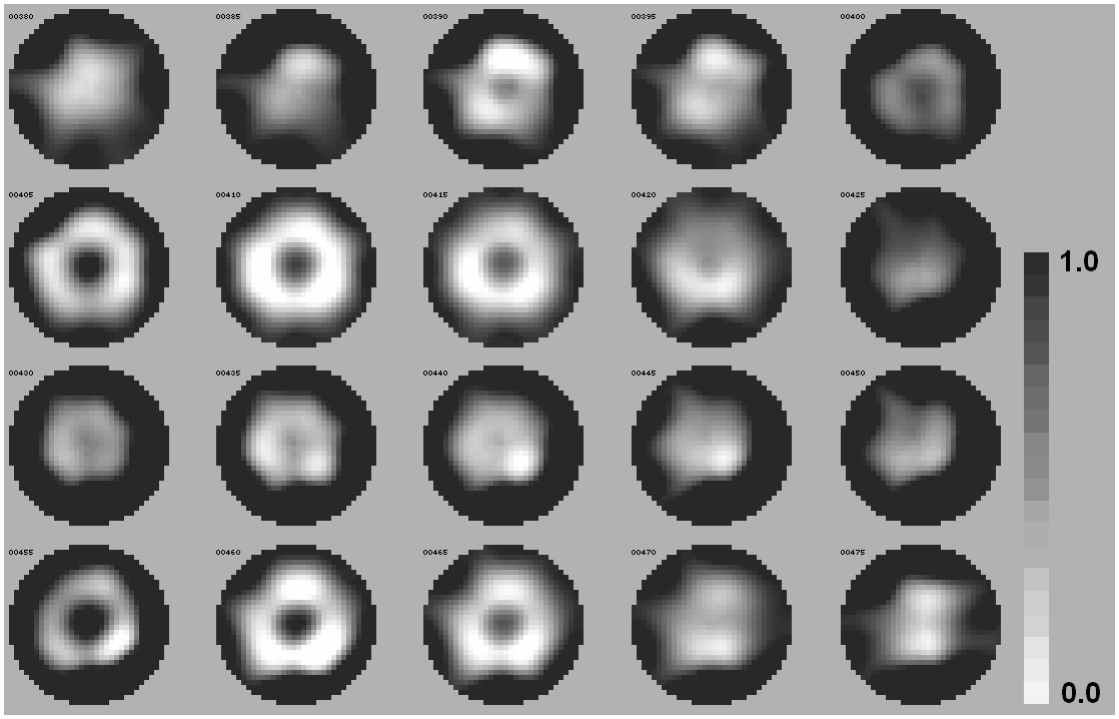

Figure 7.11 Tomographs collected in a 3.5 kg bed loading and a moisture of 10-wt%.

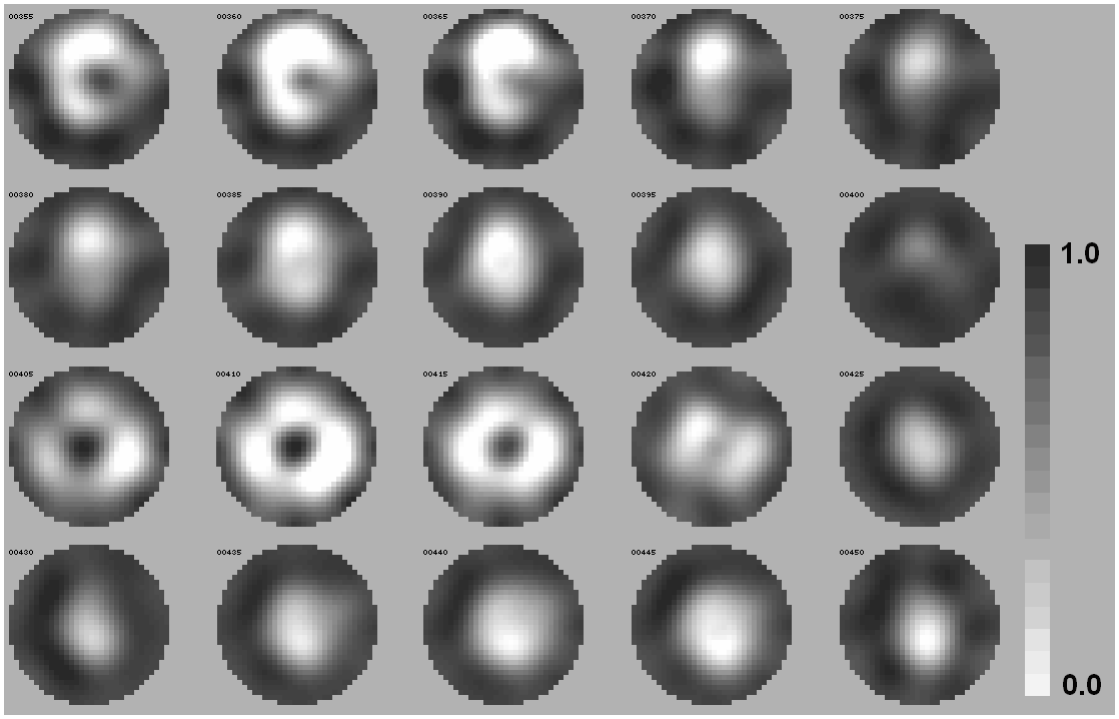

Figure 7.12 Tomographs collected in a 3.5 kg bed loading and a moisture of 1.5-wt%.

Chapter 8 - Conclusions and Recommendations

8.1 Conclusions

This study is divided into two sections. In chapter 2 to chapter 5, pressure fluctuations were used to identify the global changes in hydrodynamics of a fluidized bed dryer and granulator resulting from the changes in bed moisture. For this purpose, a chaotic attractor comparison, the S-statistic, was applied to these dynamic measurements. In the second section, chapters 6 and 7, ECT was applied to the dryer using a novel calibration technique which allowed for the determination of the localized changes in the voidage distribution accompanying the loss of moisture in a drying bed. This was accomplished through the investigation of the ECT tomograms as well as the S-statistic analysis of local voidage fluctuations in the bed.

The S-statistic has been applied to pressure fluctuations collected in an industrial bench-scale fluidized bed dryer at the Merck Frosst laboratories in Montreal. The influence of sensor positioning, inlet air temperature and bed mass were tested in a factorial experimental design. The results from these tests established a sensitivity of the S-statistic to changes in moisture. Since the S-statistic responds to changes in hydrodynamic state, this indicates that the effect of moisture on the bed hydrodynamics is significant. The hydrodynamic changes indicated by the S-statistic were not identified by amplitude and frequency analysis of the pressure fluctuations or by the monitoring of

bed and outlet air temperatures. Sensitivity of the S-statistic to variations in superficial velocity and particle size distribution were found to be not as significant as the response to moisture. Of the factorial variables examined, only bed mass was found to affect the performance of the S-statistic.

The S-statistic has also been shown to identify a hydrodynamic state associated with the onset of fines entrainment in a laboratory fluidized bed dryer at the University of Saskatchewan. The onset of entrainment was found to begin at a moisture content of 11-wt% for pharmaceutical granule and no entrainment was observed before this moisture. With the selection of an appropriate reference state (10-wt%), an 8-9 minute early warning for the onset of entrainment was identified. This hydrodynamic state occurred at consistent moisture for all bed masses tested.

In a preliminary investigation of the applicability of the S-statistic to pressure fluctuations collected in a bench-scale industrial fluidized bed granulator at Merck Frosst labs in Montreal, this technique has also been shown to respond to changes in moisture. As the moisture content of the granules increased during the granulation processes, a significant change in hydrodynamic state was identified. Upon drying of the granule, the state of the system returned to that consistent with a state identified early in the granulation process. Therefore, despite the growth of particles from an approximate volume mean diameter of 130 μm to 250 μm from beginning to end of this process, the S-statistic did not show a statistically significant change in hydrodynamic state. This confirmed findings from dry bed of pharmaceutical granule where insensitivity in the S-statistic to variation in particle size in the system was identified.

A calibration technique for Electrical Capacitance Tomography (ECT) which accounts for the significant change in bed permittivity occurring during the drying process has been developed. This calibration was based on a linear least-squares fit of ECT data collected in packed beds of pharmaceutical granule having several different moisture contents. For the first time, this calibration technique allows for the imaging of a drying fluidized bed of pharmaceutical granule using ECT. The verification of this calibration technique with x-ray tomography at the University of Calgary's Tomographic Imaging of Porous Media laboratory shows that the Böttcher permittivity model allows for the accurate reconstruction of time-averaged ECT data at bed moistures above 5-wt%. Below this value, the parallel capacitance model is more accurate.

Visual observations of the tomograms from the drying bed indicate a distinct centralized bubbling behaviour early in the drying process. This is consistent with visual observations of erupting bubbles from the centre of the bed. Divergence from the reference state was observed in the S-statistic at moisture contents below 5-wt% in both the pressure fluctuations and the ECT data. This divergence indicates that a rapid change in hydrodynamic behaviour occurs at low moisture. This change is possibly due to the increase in static charge or the significant entrainment of fine particles which has taken place at this time.

The application of the S-statistic to voidage data at a number of radial locations in the ECT tomograms shows that the S-statistic identifies changes similar to those seen in pressure fluctuations near the walls of the unit between moisture contents of 18-wt% and 10-wt%. At locations in the dryer closer to the centre, no statistically significant

change in hydrodynamic state can be identified during this period. Investigation of the tomograms shows that, during this period, there is a reduction in the area involved in fluidized behaviour. Therefore, the changes identified by the S-statistic analysis of the pressure fluctuations occur near the walls of the vessel and are a result of the reduction in this area.

The measurement of pressure fluctuations has the advantage of being non-intrusive, easy to implement and low in cost. This study has shown the potential of this measurement for the monitoring and control of fluidized bed dryers. The connection between bed state and moisture identified by the S-statistic could be utilized to determine the moisture content of the granules allowing for the precise determination of drying endpoint. Also, the S-statistic could be utilized to implement corrective action to mitigate effects harmful to product quality such as the onset of entrainment. Other parameters such superficial gas velocity, inlet temperature or humidity could also be controlled using this parameter based on a known or desired fluidized state. In a fluidized bed granulation process, control of binder addition rate could also be integrated into a control strategy.

ECT applied to the drying process allows for the determination of the voidage distribution in the dryer. As with pressure fluctuations, this information can be analyzed using the S-statistic for the determination of changes in hydrodynamic regime as moisture is lost. Furthermore, the voidage distribution information provided by the tomograms provides an on-line indication of the hydrodynamic regime which is currently not available for this process.

8.2 Recommendations

This study has shown that the measurement techniques of high-frequency pressure fluctuation measurements and ECT provide complimentary information about the hydrodynamic changes occurring within the fluidized system. For future investigations of fluidized bed dryers, these techniques should be used in conjunction to give a complete picture of both global and localized bed behavior. This is true for this and other fluidized systems.

This work has demonstrated that a change in hydrodynamic state, indicated by the S-statistic, accompanies the loss of moisture in the drying process. For each of the experiments performed, the reference state from the data set was utilized. For the use of this technique to a commercial process, a reference state collected from a test drying experiment must be compared with on-line data. This approach must be tested before this technique can be implemented for the industrial process for the monitoring of fluidized bed dryers and is a topic for future investigation.

In chapter 3, it was noted that variations in particle size distribution in a dry bed could be identified through the use of the S-statistic. Consequently, changes in this operating parameter identified utilizing the S-statistic may be provide important information allowing for tighter control of product quality.

The rapid divergence of the S-statistic toward the end of the drying process is an important topic for future research. Clearly, significant change in hydrodynamic behavior is occurring at this time in the drying process and control of this rapid change,

based on the unique information provided by the S-statistic, may be important for maintaining product quality during this period of rapid change in hydrodynamic state.

The effect of changes in dryer design was not investigated in this study. Investigations into the influence on dryer design on dynamic behavior using ECT images and the S-statistic analysis of pressure fluctuations would be beneficial for the design of fluidized bed dryers in the future.

The results from the fluidized bed granulation process presented in chapter 5 were limited to a single experiment. The results from this work, in conjunction with those results from the fluidized bed dryer presented in chapters 2, 3 and 4 demonstrate that the S-statistic can be utilized to determine the moisture content of a bed of pharmaceutical granule. This result can form the basis of a more rigorous experimental investigation of the changes seen in the S-statistic during the fluidized bed granulation process. In such an application, the S-statistic could be combined with a secondary moisture measurement technique, such as near infra-red (NIR).

For the application of ECT to the drying process, a more accurate ECT calibration is required. Here the effect of changes in voidage, which accompany the drying process, must be incorporated into any capacitance model used to describe non-linear trend seen the fit data at low values of permittivity.

The correction technique for ECT data developed in chapter 6 was implemented off-line. An on-line measurement of moisture using, for example, an NIR device could be utilized to correct for the influence of moisture on the capacitance readings through the calibration. This correction of the ECT data, combined with an on-line image

reconstruction algorithm would allow for the real-time imaging of a fluidized bed dryer using ECT. This information would be invaluable in a research or industrial setting for the determination of hydrodynamic changes allowing the operator to avoid undesirable fluidization regimes or more subtle changes in hydrodynamic state.

Appendix A : Computer Code for the S-statistic analysis of a Pressure Time Series

The following is the Matlab Code for the calculation of the S-statistic from the raw data which is read from an ASCII text file. The output from this file is a second ASCII text file containing the S-statistic value and the associated time index.

```
clear
close all
format long
cd([matlabroot '/S_Stat'])

 [filename,directory] =
uigetfile('c:\winnt\profiles\chapling\desktop\*.txt',...
   'Select Pressure Time Series for S-Statistic Evaluation')
input_path = strcat(directory,filename)
t_series = fopen(input_path,'r');

prompt = {'Reference time from beginning of data set (min):','Reference
Time Duration (min):','Evaluation Time Duration (min)','Time_window
(s)','embedding (m)','L (s)','d',};

gui_title = 'Input S-Statistic Parameters';
lines = 1;
def = {'10','2','2','0.1','20','3','0.7'};
user_input_matrix = inputdlg(prompt,gui_title,lines,def);

ref_offset_min = str2num(user_input_matrix{1})
ref_time_min = str2num(user_input_matrix{2})
eval_time_min = str2num(user_input_matrix{3})

m = str2num(user_input_matrix{5})

out_path = strrep(input_path,'.txt',strcat('_r-
',num2str(ref_offset_min),'_m-',num2str(m),'_S.txt'));
[filename2,directory2] = uiputfile(out_path,'Select Output File for S-
statistic');

out_path = strcat(directory2,filename2)
outfile = fopen(out_path,'w');

date = fgetl(t_series);
time = fgetl(t_series);
header_text = fgetl(t_series);
sample_rate = fgetl(t_series);
inter_chan_delay_base = fgetl(t_series);
header = fgetl(t_series);

freq = str2num(sample_rate)
data = fscanf(t_series,'%f',[2,inf]);

ref_offset = ref_offset_min*60*freq;
eval_time = eval_time_min*60;
ref_time = ref_time_min*60;

Num_eval = floor(length(data)/freq/eval_time);

t_window = str2num(user_input_matrix{4})
```

```
L_time = str2num(user_input_matrix{6})
d = str2num(user_input_matrix{7})

max_embedding = t_window*freq;
new_freq = freq*m /max_embedding

Np_X = ref_time*freq;
Np_Y = eval_time*freq;

data_ref = data([1:2],[ref_offset + 1 : (Np_X) + ref_offset]);
ref_set_rs = resample(data_ref(2,:),m,max_embedding);

N_X = ref_time * new_freq/m %data points
L = L_time * new_freq/m %data points

ref_set_rs = ref_set_rs([1:N_X*m]);
ave_ref = mean(ref_set_rs(:));
SDev_ref = std(ref_set_rs(:));

x_k = (ref_set_rs(:) - ave_ref)/SDev_ref;

N_Y = eval_time * new_freq/m;

for i = 1 : N_X
   for j = 1 : m
      X(i,j)= x_k((i-1) * m + j);
   end
end

fprintf(outfile,'S-Statistic Analysis\r\n');
fprintf(outfile,'\r\n');
fprintf(outfile,'File Processed:\t%s\r\n',input_path);
fprintf(outfile,'\r\n');
fprintf(outfile,'Experimental Run Parameters:\r\n');
fprintf(outfile,'Date:\t%s\r\nTime:\t%s\r\nHeader
Text:\t%s\r\nSampleing Freqency (Hz):\t%s\r\nInterchannel
Delay:\t%s\r\n%s\r\n',...
   date,time,header_text,sample_rate,inter_chan_delay_base)
fprintf(outfile,'%s\r\n',header);
fprintf(outfile,'\r\n');
fprintf(outfile,'S-Statistic Parameters:\r\n');
fprintf(outfile,'Embedding(m):\t%f\r\nSegment
Length(s):\t%f\r\nBandwidth:\t%f\r\n',m,L_time,d);
fprintf(outfile,'Effective Frequency (Hz):\t%f\r\n',new_freq);
fprintf(outfile,'Start of Reference Time Series from t = 0
(min):\t%f\r\n',ref_offset/freq/60);
fprintf(outfile,'Duration of Reference Time Series
(s):\t%f\r\n',ref_time);
fprintf(outfile,'Duration of Evaluation Time Series
(s):\t%f\r\n',eval_time);
fprintf(outfile,'\r\n');
fprintf(outfile,'Time(min)\tStandard Deviation\tS-Statistic\r\n');

for loop = 1 : Num_eval
   clear eval_set;
   eval_set = data([1:2],[(loop-1) * Np_Y + 1 : Np_Y * loop]);
   eval_set_rs = resample(eval_set(2,:),m,max_embedding);
```

```
   eval_set_rs = eval_set_rs([1:N_Y*m]);
   ave_eval(loop) = mean(eval_set_rs(:));
   SDev_eval(loop) = std(eval_set_rs(:));

   y_k = (eval_set_rs(:)-ave_eval(loop))/SDev_eval(loop);

   for i = 1 : N_Y
      for j = 1 : m
         Y(i,j)= y_k((i-1) * m + j);
      end
   end

   N_1 = floor(N_X / L);
   N_2 = floor(N_Y / L);
   N = N_1 + N_2;

   Z = [X ; Y];

   h_cross_sum  = 0;
   h_N1_sum = 0;
   h_N2_sum = 0;
   H_sum = 0;

   h_prime = s_stat(Z,N,L,d);

   for p = 1 : N
      for q = (p+1) : N
         if 1 <= p & q <= N_1
            h_N1_sum = h_N1_sum + h_prime(p,q);
         end
         if (N_1 + 1) <= p & q <= N
            h_N2_sum = h_N2_sum + h_prime(p,q);
         end
      end
   end

   for p =1 : N_1
      for q = (N_1+1) : N
         h_cross_sum = h_cross_sum + h_prime(p,q);
      end
   end


   H_sum = sum(sum(h_prime));
   H = h_prime - (2 / (N * (N-1))) * H_sum;

   Q_hat = h_N1_sum*(2/(N_1 * (N_1 - 1))) + h_N2_sum*(2/(N_2 * (N_2 -
1))) - h_cross_sum * (2/(N_1 * N_2));

   loop

   for p = 1 : N
      sum_Hpq = 0;
      for q = (p+1) : N
       sum_Hpq = H(p,q) + sum_Hpq;
      end
      g(p) = (1/(N-2)) * sum_Hpq;
```

```
   end

   phi_sum  = 0;
   for p = 1 : N
      for q = (p+1) : N
         phi(p,q) = H(p,q) - g(p) - g(q);
         phi_sum = phi_sum + (phi(p,q))^2;
      end
   end

   V_C = 4 * (N-1) * (N-2) * phi_sum / (N_1 * (N_1-1) * N_2 * (N_2-1) *
N * (N-3));
   S(loop,1) = eval_set(1,1)/60;
   S(loop,2) = Q_hat/sqrt(V_C)


fprintf(outfile,'%f\t%f\t%f\r\n',S(loop,1),SDev_eval(loop),S(loop,2));
   clear y_k Y Z;
   clear h_prime eval_set_rs;
   clear g H V_C Q_hat phi;
end

plot(S(:,1),S(:,2),'.')
three_line = line([0 max(S(:,1))],[3 3],'LineStyle',':');
set(three_line,'color','r');
title('S-statistic Response');
xlabel('Time (min)');
ylabel('S-Statistic (-)');
zoom on
hold on
fclose(t_series);
fclose(outfile);
```

The following is the supplementary C^{++} code for the calculation of the S-statistic. This code externally complied using the MEX function and is called from the above Matlab program through the s_stat function. This is highlighted in bold in the above program.

```
#include "mex.h"
#include "stdio.h"
#include "math.h"


void h_prime(double *Z, double *h, int rows, int L, int m,int N, double
d)
{
      int i, j, p, q, k, a = 0, b = 0, count=0;
      double Distsq = 0, E_dist = 0, h_pq_sum = 0;

      for (p=0; p<N; p++) {
      for (q=(p+1); q<N; q++) {
            h_pq_sum = 0;
            for (i=0; i<L; i++) {
                  a = p * L + i;
            for (j=0; j<L; j++) {
                  b = q * L + j;
                  Distsq = 0;
```

```
                  for (k = 0; k < m; k++) {
                        Distsq += pow((*(Z+a+k*rows) -
*(Z+b+k*rows)),2);
                        count++;
                        //printf("%f\r\n",Distsq);
                  }

                  E_dist = pow(Distsq,0.5);
                  h_pq_sum += exp(-Distsq/(4*pow(d,2)));
                  //printf("e equals == %f\r\n",E_dist);
            }
      //    printf("a = %i Za=%f  Za+1=%f Za+2=%f
\n",a,*(Z+a+0*rows),*(Z+a+1*rows),*(Z+a+2*rows));
            }
            *(h+p+q*N) = h_pq_sum/pow(L,2);
            //printf("p q count %i %i %f\r\n",p,q,*(h+p+q*N));
    }
      }
}

/* the gateway function */
void mexFunction( int nlhs, mxArray *plhs[],
                  int nrhs, const mxArray *prhs[])
{
  double *h,*Z;
  double  d;
  int     status,rows,cols,L,N,m;
  int p,q,c =0;

  /*  check for proper number of arguments */
  if(nrhs!=4)
    mexErrMsgTxt("Check number of inputs.");
  if(nlhs!=1)
    mexErrMsgTxt("One output required.");

  /*  create a pointer to the input matrix Z */
  Z = mxGetPr(prhs[0]);

  /* get the inputs */
  N = mxGetScalar(prhs[1]);
  L = mxGetScalar(prhs[2]);
  d = mxGetScalar(prhs[3]);

  /*  get the dimensions of the matrix input Z */
  rows = mxGetM(prhs[0]);
  m = cols = mxGetN(prhs[0]);

  /*  set the output pointer to the output matrix */
  plhs[0] = mxCreateDoubleMatrix(N,N, mxREAL);

  /*  create a C pointer to a copy of the output matrix */
  h = mxGetPr(plhs[0]);

  /*  call the C subroutine */
  h_prime(Z,h,rows,L,m,N,d);

}
```

Appendix B : Matlab Code for the Correction of ECT Signals

This program generates 28 calibration curves from the packed bed readings of capacitance made at discrete intervals in the drying process. The results of this linear least-squares fitting (slopes and intercepts) are written to an ASCII text file.

```
clear
close all
format long

VR1 = 9.9338
conv = 0.00365316

Meas = 28;
sample_freq = 100
delta_t = (1/sample_freq)

[newfile,newpath] = uiputfile('C:\Documents and
Settings\gareth\Desktop\ECT_moist_cal.txt',...
   'Save Moisture-Capacitance Calibration File Name');
output_path = strcat(newpath,newfile)
outfile = fopen(output_path,'w');

[filename,directory] = uigetfile('*.cal','Select Calibration File for
Data Set');
   cal_input_path = strcat(directory,filename);
   cal_file = fopen(cal_input_path,'r');

%read in Calibration file Parameters
Electrodes  = fscanf(cal_file,'%f',1);
M(:,3) = fscanf(cal_file,'%f',Meas); %M3 low
M(:,1) = fscanf(cal_file,'%f',Meas); %M1 offset
M(:,4) = fscanf(cal_file,'%f',Meas); %M3 high
M(:,2) = fscanf(cal_file,'%f',Meas); %M2 Atten coeff

M1L(:,1) = fscanf(cal_file,'%f',7); %Charge injection offset vals
M3_0 = fscanf(cal_file,'%f',1); %zero balence count
Gain_factor = fscanf(cal_file,'%f',1);

l = 0;
for k = 1 : Electrodes -1
   for g = (k+1) : Electrodes
     l=l+1;
     M1(l,1) = M1L(g-1,1);
   end
end

%Get C_low
M_1([1:Meas],1) = (M([1:Meas],3) - M3_0)./(Gain_factor * M([1:Meas],2))
+ M([1:Meas],1);
abs_cap_low([1:Meas],1) = (M_1([1:Meas],1) - M1([1:Meas],1)) * VR1 ./
(conv * 1023);
opp_elec_cap_low = (abs_cap_low(4,1) + abs_cap_low(11,1) +
abs_cap_low(17,1) + abs_cap_low(22,1))/4;

%Get C_high
M_1([1:Meas],1) = (M([1:Meas],4) - M3_0)./(Gain_factor * M([1:Meas],2))
+ M([1:Meas],1);
```

```
abs_cap_high([1:Meas],1) = (M_1([1:Meas],1) - M1([1:Meas],1)) * VR1 ./
(conv * 1023);

loop = 0
continue = 1;

while (continue==1)
   loop = loop + 1;
   [filename,directory] = uigetfile('*.cap','Capacitence File for
Averaging');
   input_path(loop) = {strcat(directory,filename)};
   cap_file = fopen(input_path{loop},'r');

   prompt = {'Moisture content of granule(%):','Duration of capacitance
readings for the average (sec):'};
   title = strcat(filename,' Properties');
   lines = 1;
   def = {'0.00','10'};
   user_input_matrix = inputdlg(prompt,title,lines,def);

   moisture(loop) = str2num(user_input_matrix{1});
   Number_of_averages(loop) = str2num(user_input_matrix{2})/delta_t;
   sum_cap = zeros(Meas,1);

   for t = 1:Number_of_averages(loop)
      time_ms(t,1) = fscanf(cap_file,'%f',1);
      sum_cap = sum_cap + fscanf(cap_file,'%f',Meas);
   end

   ave_cap(:,loop) = sum_cap/Number_of_averages(loop);

   button = questdlg('Continue Processing Cap
Files?','Continue','Yes','No','No');
   if strcmp(button,'Yes')
      continue = 1;
   elseif strcmp(button,'No')
      disp('End of file processing')
      continue = 0;
   end
   fclose(cap_file);
end

C(4,:) = (ave_cap(4,:) + ave_cap(11,:) + ave_cap(17,:) +
ave_cap(22,:))./4;

PR = C(4,:)./opp_elec_cap_low;

x0 = ones(size(moisture));
x = moisture;
phi = [x0' x'];
PI = inv((phi'*phi))*phi';

for 28 fit functions
   for loop2 = 1:28
      clear y_cap;
      y_cap = ave_cap(loop2,:)';
      theta(:,loop2) = PI * y_cap;
```

```
   end
end

theta2 = PI * PR';

%model output

xid = 0:.5:35;
x0id = ones(size(xid));

for loop3 = 1:28
   yid(loop3,:) = x0id*theta(1,loop3) + xid*theta(2,loop3);
end

%PRid = x0id*theta2(1) + xid*theta2(2) + x2id*theta2(3) +
x3id*theta2(4) + x4id*theta2(5) + x5id*theta2(6);
PRid = x0id*theta2(1) + xid*theta2(2);


fprintf(outfile,'Identified Models:\r\n');
fprintf(outfile,'Theta values-each row is the fit function for all
possible capacitence measuremnts ((adjacent(C1),C2,C3,C4)\r\n');
fprintf(outfile,'const\tx\tx2\tx3\tx4\tx5\r\n');
fprintf(outfile,'%10.8f\t%10.8f\r\n',theta);%1st order fit

fprintf(outfile,'\r\nTheta Values for Perm Ratio Fit\r\n');
fprintf(outfile,'const\tx\tx2\tx3\tx4\tx5\r\n');
fprintf(outfile,'%10.8f\t%10.8f\r\n',theta2);%1st order fit

fprintf(outfile,'\r\nFitted Data:\r\n');
fprintf(outfile,'Moisture\tPerm Ratio\tOne Apart\tTwo Apart\tThree
apart\tOpposite\r\n');
fprintf(outfile,'%10.10f\t%10.10f\t%10.10f\t%10.10f\t%10.10f\t%10.10f\r
\n',[moisture;PR;C]);

fprintf(outfile,...
'Moisture\tPerm
Ratio\tC1\tC2\tC3\tC4\tC5\tC6\tC7\tC8\tC9\tC10\tC11\tC12\tC13\tC14\tC15
\tC16\tC17\tC18\tC19\tC20\tC21\tC22\tC23\tC24\tC25\tC26\tC27\tC28\r\n')
;
fprintf(outfile,...
'%f\t%f\t%f\t%f\t%f\t%f\t%f\t%f\t%f\t%f\t%f\t%f\t%f\t%f\t%f\t%f\t%f\t%f
\t%f\t%f\t%f\t%f\t%f\t%f\t%f\t%f\t%f\t%f\t%f\t%f\t%f\r\n',...
   [moisture;PR;ave_cap]);

fprintf(outfile,...
'%f\t%f\t%f\t%f\t%f\t%f\t%f\t%f\t%f\t%f\t%f\t%f\t%f\t%f\t%f\t%f\t%f\t%f
\t%f\t%f\t%f\t%f\t%f\t%f\t%f\t%f\t%f\t%f\t%f\t%f\t%f\r\n',...
[xid;PRid;yid]);

fprintf(outfile,'\r\nAverage Capacitences From ECT
Meaurement:\r\n\r\n');
fprintf(outfile,'Data File\tNumber of Averages\tMoisture\t \t');
fprintf(outfile,'C12\tC13\tC14\tC15\tC16\tC17\tC18\t \t');
fprintf(outfile,'C23\tC24\tC25\tC26\tC27\tC28\t \t');
fprintf(outfile,'C34\tC35\tC36\tC37\tC38\t \t');
fprintf(outfile,'C45\tC46\tC47\tC48\t \t');
```

```
fprintf(outfile,'C56\tC57\tC58\t \t');
fprintf(outfile,'C67\tC68\t \t');
fprintf(outfile,'C78\r\n');

counter = 0;
start_index = 1;
fprintf(outfile,'Inital Moisture\txxx\t%f\t \t',moisture(1));
for i = 7:-1:1
   for j = 1:i
      fprintf(outfile,'%4.3f\t',ave_cap(counter+j,1));
   end
   counter = counter+j;
   fprintf(outfile,' \t');
end
fprintf(outfile,'\r\n');

for h = 2:loop
   fprintf(outfile,'%s\t%f\t%5.3f\t
\t',input_path{h},Number_of_averages(h),moisture(h));
   counter = 0;
   start_index = 1;
   for i = 7:-1:1
      for j = 1:i
         fprintf(outfile,'%4.3f\t',ave_cap(counter+j,h));
      end
      counter = counter+j;
      fprintf(outfile,' \t');
   end
   fprintf(outfile,'\r\n');
end


fclose(outfile);
```

This program reads in the ASCII text file containing the calibration information produced by the above program. This information is used to correct the capacitance measurements made by the ECT sensor off-line. The moisture of the bed when the measurements were made is inputted by the user. The program outputs an ASCII file containing a set of normalized capacitance reading which may be used by the image reconstruction software to generate tomograms.

```
clear
close all
format long

Meas = 28;
VR1 = 9.9338;
conv = 0.00365316;

[filename,directory] = uigetfile('C:\Documents and
Settings\gareth\Desktop\*.txt',...
      'Select ECT Capacitance vs. Moisture Calibration File (generated
from CalECT.m)');
input_path(1) = {strcat(directory,filename)};
theta_file = fopen(input_path{1},'r');

[filename,directory] = uigetfile('*.cap','Select ECT Capacitance File
for Correction');
input_path(2) = {strcat(directory,filename)};
cap_file = fopen(input_path{2},'r');

out_path = lower(input_path{2});
out_path = strrep(out_path,'.cap','_corr.ncp');
outfile = fopen(out_path,'w');

prompt = {'Average Moisture Content of Granule (%):'};
title = strcat(filename,'Average Moisture');
lines = 1;
def = {'0'};

user_input_matrix = inputdlg(prompt,title,lines,def);
moist_level = str2num(user_input_matrix{1})

[filename,directory] = uigetfile('*.cal','Select Calibration File');
input_path(3) = {strcat(directory,filename)};
cal_file = fopen(input_path{3},'r');

%read in Calibration file Parameters
Electrodes  = fscanf(cal_file,'%f',1);
M(:,3) = fscanf(cal_file,'%f',Meas); %M3 low
M(:,1) = fscanf(cal_file,'%f',Meas); %M1 offset
M(:,4) = fscanf(cal_file,'%f',Meas); %M3 high
M(:,2) = fscanf(cal_file,'%f',Meas); %M2 Atten coeff

M1L(:,1) = fscanf(cal_file,'%f',7); %Charge injection offset vals
M3_0 = fscanf(cal_file,'%f',1); %zero balence count
Gain_factor = fscanf(cal_file,'%f',1);

l = 0;
for k = 1 : Electrodes -1
```

```
   for g = (k+1) : Electrodes
     l=l+1;
     M1(l,1) = M1L(g-1,1);
   end
end

%Get C_low
M_1([1:Meas],1) = (M([1:Meas],3) - M3_0)./(Gain_factor * M([1:Meas],2))
+ M([1:Meas],1);
abs_cap_low([1:Meas],1) = (M_1([1:Meas],1) - M1([1:Meas],1)) * VR1 ./
(conv * 1023);

%read capacitance correction parameters
fgetl(theta_file);fgetl(theta_file);fgetl(theta_file);
theta = fscanf(theta_file,'%f',[2 Meas])';%1st order

fgetl(theta_file);fgetl(theta_file);fgetl(theta_file);fgetl(theta_file)
;
theta2 = fscanf(theta_file,'%f',[2 1])';%1st order
fclose(theta_file);

loop = 0;
t_temp = 0;
eof_query = 0;
C_low = abs_cap_low';

t_temp = fscanf(cap_file,'%f',1);
h = waitbar(0,'Generating ncp File...');
estimated_frames = 12000

C_high([1:Meas]) = theta([1:Meas],1) +
moist_level*theta([1:Meas],2);%1st order
PR = theta2(1) + moist_level*theta2(2);%1st order

fprintf(outfile,'Corrected NCP file:\t%s\r\n',input_path{1});
fprintf(outfile,'Calibration file:\t%s\r\n',input_path{2});
fprintf(outfile,'Capcitance vs. Moisture
file:\t%s\r\n\r\n',input_path{3});
fprintf(outfile,'Moisture:\t%f\r\n',moist_level);
fprintf(outfile,'Average Perm Ratio:\t%f\r\n\r\n',PR);

while eof_query ~= 1
   waitbar(loop/estimated_frames);

   loop = loop + 1;
   time_ms(loop) = t_temp;
   caps  = fscanf(cap_file,'%f',Meas)';
   counter = 0;
   start_index = 1;

   ncps(1) = (caps(1)-C_low(1))/(C_high(1)-C_low(1));
   ncps(7) = (caps(7)-C_low(7))/(C_high(7)-C_low(7));
   ncps(8) = (caps(8)-C_low(8))/(C_high(8)-C_low(8));
   ncps(14) = (caps(14)-C_low(14))/(C_high(14)-C_low(14));
   ncps(19) = (caps(19)-C_low(19))/(C_high(19)-C_low(19));
   ncps(23) = (caps(23)-C_low(23))/(C_high(23)-C_low(23));
   ncps(26) = (caps(26)-C_low(26))/(C_high(26)-C_low(26));
```

```
   ncps(28) = (caps(28)-C_low(28))/(C_high(28)-C_low(28));

   ncps(2) = (caps(2)-C_low(2))/(C_high(2)-C_low(2));
   ncps(6) = (caps(6)-C_low(6))/(C_high(6)-C_low(6));
   ncps(9) = (caps(9)-C_low(9))/(C_high(9)-C_low(9));
   ncps(13) = (caps(13)-C_low(13))/(C_high(13)-C_low(13));
   ncps(15) = (caps(15)-C_low(15))/(C_high(15)-C_low(15));
   ncps(20) = (caps(20)-C_low(20))/(C_high(20)-C_low(20));
   ncps(24) = (caps(24)-C_low(24))/(C_high(24)-C_low(24));
   ncps(27) = (caps(27)-C_low(27))/(C_high(27)-C_low(27));

   ncps(3) = (caps(3)-C_low(3))/(C_high(3)-C_low(3));
   ncps(5) = (caps(5)-C_low(5))/(C_high(5)-C_low(5));
   ncps(10) = (caps(10)-C_low(10))/(C_high(10)-C_low(10));
   ncps(12) = (caps(12)-C_low(12))/(C_high(12)-C_low(12));
   ncps(16) = (caps(16)-C_low(16))/(C_high(16)-C_low(16));
   ncps(18) = (caps(18)-C_low(18))/(C_high(18)-C_low(18));
   ncps(21) = (caps(21)-C_low(21))/(C_high(21)-C_low(21));
   ncps(25) = (caps(25)-C_low(25))/(C_high(25)-C_low(25));

   ncps(4) = (caps(4)-C_low(4))/(C_high(4)-C_low(4));
   ncps(11) = (caps(11)-C_low(11))/(C_high(11)-C_low(11));
   ncps(17) = (caps(17)-C_low(17))/(C_high(17)-C_low(17));
   ncps(22) = (caps(22)-C_low(22))/(C_high(22)-C_low(22));

   fprintf(outfile,'%4.0f\t\r\n',time_ms(loop));
   for i = 7:-1:1
     for j = 1:i
       fprintf(outfile,'%4.3f\t',ncps(counter+j));
     end
     counter = counter+j;
     fprintf(outfile,'\r\n');
   end

   t_temp = fscanf(cap_file,'%f',1);
   eof_query = feof(cap_file);
   clear caps;
   clear ncps;
end

actual_frames = loop

close(h)
fclose(cap_file);
fclose(outfile);
```

Appendix C : Matlab Code for S-statistic Analysis of Individual Pixels

Reconstructed ECT data is saved in an ASCII text file as a series of matrices at a sampling frequency of 100 Hz. The matrices are the tomograms and are saved as image (.img) files. The following program takes a set of ECT image files and outputs an ASCII text file containing a set of voidage signals (evaluation time series) for the S-statistic analysis. The four pixels where this data is collected are selected by the user.

```
clear
close all
format long
res = 32;

[filename1,directory1] = uiputfile('ECT.sig.4pix.txt','Select Output
File for img data');
out_path = strcat(directory1,filename1);
outfile = fopen(out_path,'w');

title = 'Input File Processing Parameters';
prompt = {'Sampleing Frequency','Number of Frames to Process'};
lines = 1;
def = {'100','12000'};
user_input_matrix = inputdlg(prompt,title,lines,def);

freq = str2num(user_input_matrix{1});
estimated_frames = str2num(user_input_matrix{2});

title2 = 'Input Pixel Locations (between 1 and 32)';
prompt2 = {'Row Pixel 1','Col Pixel 1','Row Pixel 2','Col Pixel 2','Row
Pixel 3','Col Pixel 3',...
      'Row Pixel 4','Row Pixel 4'};
lines2 = 1;
def2 = {'9','9','9','9','9','9','9','9'};
user_input_matrix2 = inputdlg(prompt2,title2,lines2,def2);

r_p1 = str2num(user_input_matrix2{1});
c_p1 = str2num(user_input_matrix2{2});
r_p2 = str2num(user_input_matrix2{3});
c_p2 = str2num(user_input_matrix2{4});
r_p3 = str2num(user_input_matrix2{5});
c_p3 = str2num(user_input_matrix2{6});
r_p4 = str2num(user_input_matrix2{7});
c_p4 = str2num(user_input_matrix2{8});

cont_button = 'Yes';
readloop = 0;
directory  = directory1;
guitext = 'ECT Data Set Path File';
[pathfile,pathdir] = uigetfile(directory,guitext);
path_path = strcat(pathdir,pathfile);
pathfile = fopen(path_path,'r');
eof_query1 = 0
readloop = 0

while eof_query1 ~= 1
   readloop = readloop + 1;
   t_index(readloop) = fscanf(pathfile,'%f',1);
   fgetl(pathfile);
```

```
   file_names(1,readloop) = cellstr(fgetl(pathfile));
  file_names(2,readloop) = cellstr(fgetl(pathfile))
  eof_query1 = feof(pathfile)
end

fclose(pathfile);
fprintf(outfile,'Number of files Processed:\t%i\r\n',readloop);
 fprintf(outfile,'Pixel\tRow\tColumn\r\n');
fprintf(outfile,'1\t%i\t%i\r\n',r_p1,c_p1);
fprintf(outfile,'2\t%i\t%i\r\n',r_p2,c_p2);
fprintf(outfile,'3\t%i\t%i\r\n',r_p3,c_p3);
fprintf(outfile,'4\t%i\t%i\r\n',r_p4,c_p4);
fprintf(outfile,'Time\t1\t2\t3\t4\r\n');

for i = 1 : length(file_names)
   input_path = strcat(file_names{1,i},file_names{2,i})
   img_file = fopen(input_path,'r');
   fprintf(outfile,'%s\r\nTime Index:\t%f\r\n',input_path,t_index(i));

   loop = 0;
   p_1 = fscanf(img_file,'%f',1);
   eof_query = 0;

   w_title = 'Processing file x of y';
   w_title = strrep(w_title,'x',num2str(i));
   w_title = strrep(w_title,'y',num2str(length(file_names)));

   h = waitbar(0,w_title);

   while eof_query ~= 1
      waitbar(loop/estimated_frames);
      loop = loop + 1;     t_step = loop/freq;
      pixels  = [p_1 ; fscanf(img_file,'%f',res^2-1)];
      frame = reshape(pixels,res,res);

      slice =
[frame(r_p1,c_p1),frame(r_p2,c_p2),frame(r_p3,c_p3),frame(r_p4,c_p4)];

      fprintf(outfile,'%f\t',t_step);
      fprintf(outfile,'%7.5f\t',slice(:));
      fprintf(outfile,'\r\n');

      clear frame pixels slice t_step p_1
      p_1 = fscanf(img_file,'%f',1);
      eof_query = feof(img_file);
      if loop >= estimated_frames
         eof_query = 1
      end
   end

   close(h)
   fclose(img_file);
end

fclose(outfile);
fclose(outfile2);
```

The following program takes the ASCII text file generated by the above program and a reference image file selected by the user to develop the S-statistic response of the combined pixels. The externally complied MEX function presented in Appendix A is also used in this program.

```
clear
close all
cd([matlabroot '/S_Stat'])
res = 32;
Meas = 28;

prompt = {'Sampleing Frequncy (Hz):','Reference Time Duration
(min):','Evaluation Time Duration (min)',...
      'Time_window (s)','embedding (m)','L (s)','d',};
title = 'Input S-Statistic Parameters';
lines = 1;
def = {'100','2','2','0.1','10','3','0.5'};
user_input_matrix = inputdlg(prompt,title,lines,def);

%enter files to process
[filename,directory] = uigetfile('C:\Documents and
Settings\gareth\Desktop\*.img','Select Reference Time Series')
input_path = strcat(directory,filename)
ref_file = fopen(input_path,'r');

%for all pixels
guitext = 'Time Index for xxx';
prompt2 = {'Reference Time Index (Min)'};
title2 = strrep(guitext,'xxx',filename);
lines2 = 1;
def2 = {'xxx'};
user_input_matrix_2 = inputdlg(prompt2,title2,lines2,def2);

Ref_TI = str2num(user_input_matrix_2{1})

[filename2,directory2] = uigetfile(strcat(directory,'*.txt'),'Select
Evaluation Time Series')
input_path2 = strcat(directory2,filename2)
eval_file = fopen(input_path2,'r');

out_path = strrep(input_path,'.img','_ECT_Sstat(4pix).txt');
[file3, dir3] = uiputfile(out_path, 'Save Output File As');
out_path = strcat(dir3,file3)
outfile = fopen(out_path,'w');

fscanf(eval_file,'%s',4);
num_eval = fscanf(eval_file,'%f',1);

freq = str2num(user_input_matrix{1})
ref_time_min = str2num(user_input_matrix{2})
eval_time_min = str2num(user_input_matrix{3})
eval_time = eval_time_min*60 %sec
ref_time = ref_time_min*60 %sec

eval_time = eval_time_min*60; %sec
ref_time = ref_time_min*60; %sec
```

```
t_window = str2num(user_input_matrix{4})
m = str2num(user_input_matrix{5})
L_time = str2num(user_input_matrix{6})
d = str2num(user_input_matrix{7})

max_embedding = t_window*freq;
new_freq = freq*m /max_embedding

Np_X = ref_time*freq;
Np_Y = eval_time*freq;

N_X = ref_time * new_freq/m %data points
N_Y = eval_time * new_freq/m;
L = L_time * new_freq/m %data points

%pixel Locations
fgetl(eval_file);fgetl(eval_file);

for p = 1:4
   fscanf(eval_file,'%f',1);
   pix_row(p) = fscanf(eval_file,'%f',1);
   pix_col(p) = fscanf(eval_file,'%f',1);
end

h = waitbar(0,'Loading Reference Data');

%comp_pix_ref = zeros(1,Np_X*4);
ref_pix = zeros(Np_X,4);

for i = 1:Np_X
   waitbar(i/Np_X);
   pixels  = fscanf(ref_file,'%f',res^2);
   frame = reshape(pixels,res,res);
   slice = frame(pix_row(1),pix_col(1));
   for p = 2:4
       slice = [slice,frame(pix_row(p),pix_col(p))];
   end
   for j = 1:4
      ref_pix(i,j) = slice(j);
   end
   clear slice pixels frame
end

close(h)
fclose(ref_file);

for k = 1:4
   ref_pix_rs(:,k) = resample(ref_pix(:,k),m,max_embedding);
   ave_ref(k) = mean(ref_pix_rs(:,k));
   SDev_ref(k) = std(ref_pix_rs(:,k));
   x_k_sigs(:,k) = (ref_pix_rs(:,k) - ave_ref(k))/SDev_ref(k);
   x_kc(:,k) = resample(x_k_sigs(:,k),freq/4,freq);
end

comp_x_kc = x_kc(1,:);
```

```
for j = 2:length(x_kc)
   comp_x_kc = [comp_x_kc x_kc(j,:)];
end

x_k = [x_k_sigs,comp_x_kc'];

for k = 1:5
   for i = 1 : N_X
      for j = 1 : m
         X(i,j,k)= x_k((i-1) * m + j,k);
      end
   end
end

fprintf(outfile,'S-Statistic Analysis of ECT Data (multiple
pixels)\r\n');
fprintf(outfile,'\r\n');
fprintf(outfile,'Reference File:\t%s\r\n',input_path);
fprintf(outfile,'\r\n');
fprintf(outfile,'Run Parameters:\r\n');
fprintf(outfile,'Reference Time Series Index (min):\t%f\r\n',Ref_TI);
fprintf(outfile,'Duration of Reference Time Series
(s):\t%f\r\n',ref_time);
fprintf(outfile,'Duration of Evaluation Time Series
(s):\t%f\r\n',eval_time);
fprintf(outfile,'\r\n');
fprintf(outfile,'S-Statistic Parameters:\r\n');
fprintf(outfile,'Embedding (m):\t%f\r\nSegment Length
(s):\t%f\r\nBandwidth (-):\t%f\r\n',m,L_time,d);
fprintf(outfile,'Effective Frequency (Hz):\t%f\r\n\r\n',new_freq);

fprintf(outfile,'Pixel\tRow\tColumn\r\n');
for p = 1:4
   fprintf(outfile,'%i\t%i\t%i\r\n',p,pix_row(p),pix_col(p));
end

fprintf(outfile,'\r\n');
fprintf(outfile,'Time(min)\tpixel 1\tpixel 2\tpixel 3\tpixel
4\tComposite Signal\r\n');

fgetl(eval_file);
for time_loop = 1:num_eval
   fgetl(eval_file);fgetl(eval_file);
   fscanf(eval_file,'%s',2);
   t_eval(time_loop) = fscanf(eval_file,'%f',1);

   wait_text = 'Processing xx of yy';
   wait_text = strrep(wait_text,'yy',num2str(num_eval));
   wait_text = strrep(wait_text,'xx',num2str(time_loop))

   %comp_pix_eval = zeros(1,Np_Y*4);
   eval_pix = zeros(Np_Y,4);

   h = waitbar(0,wait_text);
   for i = 1:12000
      waitbar(i/12000);
      t_index = fscanf(eval_file,'%f',1);
```

```
   slice = fscanf(eval_file,'%f',4);
   if i <= Np_Y
      for j = 1:4
         eval_pix(i,j) = slice(j);
      end
   end
   clear slice
end

close(h)

for k = 1:4
   eval_pix_rs(:,k) = resample(eval_pix(:,k),m,max_embedding);
   ave_eval(k) = mean(eval_pix_rs(:,k));
   SDev_eval(k) = std(eval_pix_rs(:,k));
   y_k_sigs(:,k) = (eval_pix_rs(:,k) - ave_eval(k))/SDev_eval(k);
   y_kc(:,k) = resample(y_k_sigs(:,k),freq/4,freq);
end

comp_y_kc = y_kc(1,:);

for j = 2:length(y_kc)
   comp_y_kc = [comp_y_kc y_kc(j,:)];
end

y_k = [y_k_sigs,comp_y_kc'];

for k = 1:5
   for i = 1 : N_Y
      for j = 1 : m
         Y(i,j,k)= y_k((i-1) * m + j,k);
      end
   end
end

N_1 = floor(N_X / L);
N_2 = floor(N_Y / L);
N = N_1 + N_2;

for loop = 1:5
%loop = 5;

   Z = [X(:,:,loop) ; Y(:,:,loop)];
   loop
   h_cross_sum  = 0;
   h_N1_sum = 0;
   h_N2_sum = 0;
   H_sum = 0;

   h_prime = s_stat(Z,N,L,d);

   for p = 1 : N
      for q = (p+1) : N
         if 1 <= p & q <= N_1
            h_N1_sum = h_N1_sum + h_prime(p,q);
         end
         if (N_1 + 1) <= p & q <= N
```

```
               h_N2_sum = h_N2_sum + h_prime(p,q);
            end
         end
      end

      for p =1 : N_1
         for q = (N_1+1) : N
            h_cross_sum = h_cross_sum + h_prime(p,q);
         end
      end


      H_sum = sum(sum(h_prime));
      H = h_prime - (2 / (N * (N-1))) * H_sum;

      Q_hat = h_N1_sum*(2/(N_1 * (N_1 - 1))) + h_N2_sum*(2/(N_2 * (N_2
- 1))) - h_cross_sum * (2/(N_1 * N_2));

      for p = 1 : N
         sum_Hpq = 0;
         for q = (p+1) : N
            sum_Hpq = H(p,q) + sum_Hpq;
         end
         g(p) = (1/(N-2)) * sum_Hpq;
      end

      phi_sum  = 0;
      for p = 1 : N
         for q = (p+1) : N
            phi(p,q) = H(p,q) - g(p) - g(q);
            phi_sum = phi_sum + (phi(p,q))^2;
         end
      end

      V_C = 4 * (N-1) * (N-2) * phi_sum / (N_1 * (N_1-1) * N_2 * (N_2-
1) * N * (N-3));
         S(time_loop,loop) = Q_hat/sqrt(V_C)
      clear Z,clear V_C,clear Q_hat;
   end
   clear Y;
end

for loop = 1:num_eval
   fprintf(outfile,'%f\t',t_eval(loop));
   fprintf(outfile,'%f\t',S(loop,:));
   fprintf(outfile,'\r\n');
end

fclose(outfile)
```